SCAVENGING MEASUREMENTS IN A DIRECT-INJECTION TWO-STROKE ENGINE

by

Hickory Zachariah Foudray

A thesis submitted in partial fulfillment of the

requirements for the degree of

MASTER OF SCIENCE

(Mechanical Engineering)

at the

University of Wisconsin–Madison

2002

Scavenging Measurements in a Direct-Injection Two-Stroke Engine

Hickory Zachariah Foudray

Under the supervision of Professor Jaal B. Ghandhi

At the University of Wisconsin–Madison

Abstract

The scavenging process in a direct-injection two-stroke research engine was examined. A physical model was developed to characterize scavenging based on known quantities. An electromagnetic valve was used to sample pre-combustion gases from the running engine. The valve proved to be very robust and was able to sample greater than 30mass under all test conditions. The concentration of either oxygen or carbon dioxide, the mass flow rate of the fuel, and the intake and exhaust temperatures were used to calculate the scavenging efficiency, trapping efficiency, trapped mass, and concentration of combustion products. A modified definition of delivery ratio, based on a reference trapped cylinder mass, was used for all scavenging calculations.

Good agreement was found between scavenging parameters calculated using the trapped oxygen concentration and those calculated using the trapped carbon dioxide concentration. Carbon monoxide was found to be a poor indicator of scavenging, because CO production continued after combustion. Oxides of nitrogen were theoretically good indicators of scavenging, but experimental problems with sampling were not resolved, and the NO_x data were

not considered to be reliable.

Tests were performed with a variable delivery ratio and: a constant air/fuel ratio, a constant fueling rate, or with fueling controlled by the engine control unit. Scavenging and trapping efficiency were shown to be strongly a function of delivery ratio. Scavenging efficiency increased with increasing delivery ratio, and trapping efficiency decreased. Tests were also run at constant delivery ratio with a variable air/fuel ratio or a variable engine speed. Scavenging efficiency decreased slightly with increasing air/fuel ratio, and with decreasing speed. Trapping efficiency did not seem to be affected by either parameter. Scavenging and trapping efficiency were near the non-isothermal perfect mixing model for all test cases.

Dedicated to Angie, the love of my life,

and in memory of Deborah, my mother.

Acknowledgements

I would like to thank all the people who made the completion of my degree possible, and everyone who made my time in the Engine Research Center so interesting and enjoyable.

First, I would like to thank my parents, Rod and Deborah, who never doubted my ability to do anything I set out to do. Their love and support never flagged, even in the worst of times. Also, my wonderful wife, Angela (the rocket scientist), who's example kept me from taking the easy route (lest I be beaten by a girl).

Jaal Ghandhi, my advisor, greatly deserves my thanks for all his involvement, which helped keep the project moving when it hit hurdles. He was always available for questions and to talk about new ideas, and his broad knowledge was always a boon.

I would also like to thank Mark Ruman, Brian McGuire, and all the other people at Mercury Marine for their support in getting the sampling valve working, and for the financial assistance of the Brunswick Fellowship.

There are also several other people at the Engine Research Center whom I would like to thank for their assistance with the project, or just keeping me sane. For all his help machining parts, or finding experimental equipment wherever it might be, I would like to sincerely thank Ralph Braun. He was always available and willing to help in whatever way he could. My time spent at the Engine Research Center was made more enjoyable and beneficial by the group of intelligent and knowledgable graduate students that also made it their home. I would like to give a hats off to Karen Bottom, Dave Rothamer, Brian

Albert, Jared Cromas, Matt Wiles, Dan Probst, Steve Ciatti, and William Church. It's hard to imagine working with a better group of people.

Contents

List of Tables

List of Figures

Chapter 1

Introduction

1.1 Two-Stroke Overview

Today, reduction of polluting trace emissions is a major concern for manufacturers of automotive, recreational, and other internal combustion engines. Two-stroke cycle spark-ignition engines have largely fallen out of use in the automotive sector, despite their favorable power-to-weight ratio and mechanical simplicity, largely due to the inherent difficulty in controlling the composition of their emissions.

The two-stroke engine benefits from a power stroke for every crankshaft rotation, as opposed to one power stroke every two crankshaft rotations for a four-stoke cycle engine, by using piston porting to overlap the exhaust and intake portions of the cycle. This also means the two-stroke engine does not require the added complexity and weight of a valve system, unlike it's four-stroke counterparts. The gas exchange process, where combustion products are replaced by a fresh charge of air and fuel, or just air, is controlled by complex fluid dynamics. The efficiency with which the fresh charge replaces the combustion products, called scavenging, can vary greatly with different combustion chamber, cylinder,

head, and port geometries, as well as with different running conditions. Figure 1.1 depicts several common port configurations and the direction of flow through the cylinder during the scavenging event.

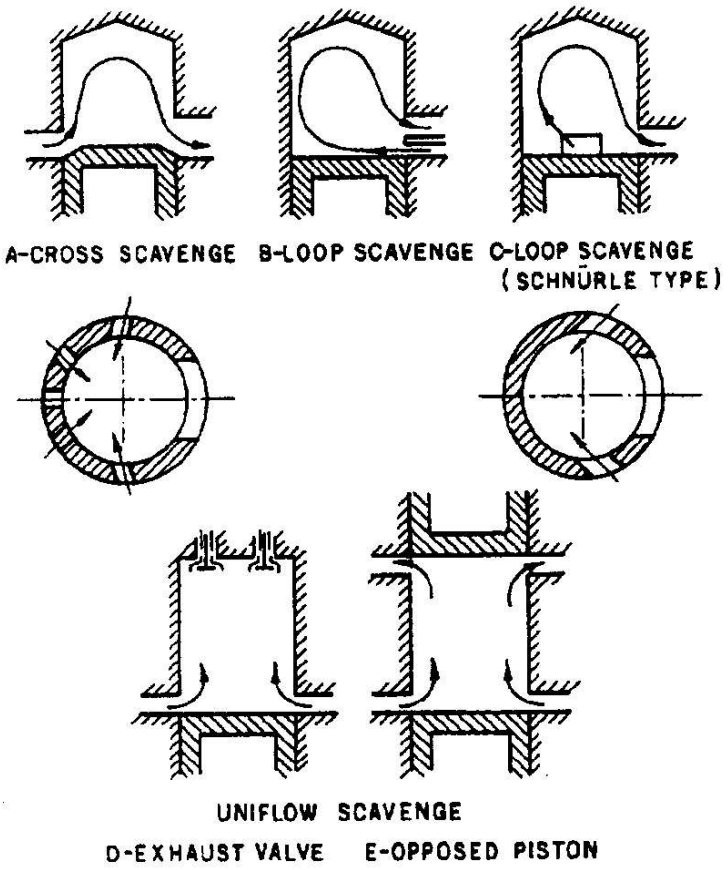

Figure 1.1: Common scavenging port configurations [28].

1.2 Motivation for the Study of Scavenging

One of the greatest problems facing carburated or port injected two-stroke engines is that of fresh charge ”short-circuiting”. This occurs when some amount of intake air and fuel flows directly out the exhaust port during the scavenging process. This is clearly undesirable because it causes both increased hydrocarbon emissions, and lower fuel efficiency. With the

advent of electronic direct-injection systems suitable for use in gasoline direct-injection (GDI) engines, short-circuiting of fuel can be largely eliminated.

Reduction of harmful emissions to levels mandated for future production will require more than simply eliminating short circuited fuel. An improved knowledge the pre-combustion contents of the combustion chamber is necessary to optimize two-stoke engine emissions.

1.3 Objectives

The focus of the research presented in this thesis was to estimate the scavenging and trapping efficiency of a two-stroke engine by measuring the trapped pre-combustion cylinder charge during fired engine operation. Initially, both pre-combustion and exhaust samples were to be used to determine scavenging parameters [3]. However, after further analysis, pre-combustion samples, temperature and pressure measurements were used to determine those parameters, with exhaust gas concentrations used as a check of the results.

A sampling valve was designed and built to be threaded into an auxiliary sparkplug hole in the cylinder head. The valve was designed to sample as large a fraction of the cylinder mass as possible, such that the extracted sample would be representative of the entire cylinder contents. It was also designed to be robust and portable, since eventually a similar design is to be used to sample gas from production marine engines running in the field.

An improved understanding of the cylinder contents prior to combustion should aid engine designers in optimizing engine calibrations for fuel economy, power, and low emissions.

Chapter 2

Literature Review

2.1 Scavenging Terminology

To facilitate open discourse of two-stroke engine-related research and design, a large body of standard terminology has been created. This section will give a summary of the standard definition of terms that will be used to describe experimental configurations and results later in this text.

The equivalence ratio, Φ, is defined as the ratio of the actual fuel-air mass ratio to the fuel-air mass ratio at stoichiometric conditions [13].

$$\Phi \equiv \frac{(F/A)_{actual}}{(F/A)_{stoich}} \tag{2.1}$$

A set of standard terminology for mass-based scavenging relations has been laid out by the Society of Automotive Engineers(SAE) [25]. The delivery ratio, Λ, relates delivered charge to engine geometry. It is defined as the ratio of the mass delivered to the mass the displaced volume of air has at ambient conditions,

$$\Lambda \equiv \frac{m_{deliver}}{V_{swept} \cdot \rho_{amb}} \tag{2.2}$$

where $m_{deliver}$ is the mass of air delivered, V_{swept} is the volume swept by the piston each crankshaft revolution, and ρ_{amb} is the density of air at ambient conditions. A similar term to delivery ratio is the scavenge ratio, r_s:

$$r_s \equiv \frac{m_{deliver}}{V_{cyl} \cdot \rho_{amb}} \tag{2.3}$$

where V_{cyl} is the sum of the combustion chamber volume (cylinder volume at TDC) and the volume swept by the piston. Charging efficiency, η_c, relates the retained portion of the delivered charge to the swept mass. It is defined as:

$$\eta_c \equiv \frac{m_{retain}}{V_{cyl} \cdot \rho_{amb}} \tag{2.4}$$

where m_{retain} is the mass of the delivered charge that is retained in the cylinder after the scavenging process. Scavenging efficiency, η_s, is defined as:

$$\eta_s \equiv \frac{m_{retain}}{m_{trap}} \tag{2.5}$$

where m_{trap} is the total mass trapped in cylinder after the scavenging process, including the exhaust residual and the trapped portion of the delivered charge. The trapping efficiency, η_t, is defined as the mass fraction of the delivered charge that is retained. It can also be expressed as the ratio of the charging efficiency to the deliver ratio:

$$\eta_t \equiv \frac{m_{retain}}{m_{deliver}} = \frac{\eta_c}{\Lambda} \tag{2.6}$$

Further terminology will be introduced later in the text, but this will provide a basis for understanding the various quantities discussed in scavenging analysis.

2.2 Theoretical Models of Scavenging

One of the earliest major papers on scavenging was by Hopkinson [15], and the theoretical models he laid out are still used as references today. Two simple single-phase models

define the scavenging process. The models are known as the perfect displacement model, and the perfect mixing model. These were later combined with short-circuiting in multi-zone models. Both perfect scavenging and perfect displacement assume that scavenging process occurs at constant temperature and pressure, and that there is no heat transfer between the gas and the cylinder walls.

2.2.1 Perfect Displacement Model

In the perfect displacement model it is assumed that all of the fresh charge entering the cylinder is retained, and that it displaces the exhaust gas with no mixing. This means the amount of charge delivered is the same as the amount of charge retained for delivered charges less than or equal to the cylinder volume. Therefore:

$$0 < \Lambda \leq 1 \Rightarrow \eta_s = \Lambda,\ \eta_t = 1 \tag{2.7}$$

$$\Lambda > 1 \Rightarrow \eta_s = 1,\ \eta_t = 1/\Lambda \tag{2.8}$$

2.2.2 Perfect Mixing Model

The perfect mixing model assumes that the intake charge instantaneously mixes with the exhaust gas in cylinder. Therefore, at a given instant, the gas leaving the exhaust port has the same composition as what is in the cylinder. Perfect mixing requires a more complex derivation of scavenging parameters than perfect displacement, and reduces to:

$$\eta_s = 1 - e^{-\Lambda} \tag{2.9}$$

$$\eta_t = \frac{1 - e^{-\Lambda}}{\Lambda} \tag{2.10}$$

for all scavenging ratios.

Figure 2.1 and Figure 2.2 depict scavenging and trapping efficiency for the perfect displacement and perfect mixing models. Efficiencies in the perfect displacement case are always the maximum theoretical values for a particular scavenge ratio. Usually experimentally derived scavenging and trapping efficiencies lie between the two models, nearer to perfect mixing. However, due to short circuiting, it is possible for actual efficiency values to be lower than those predicted by the perfect mixing model.

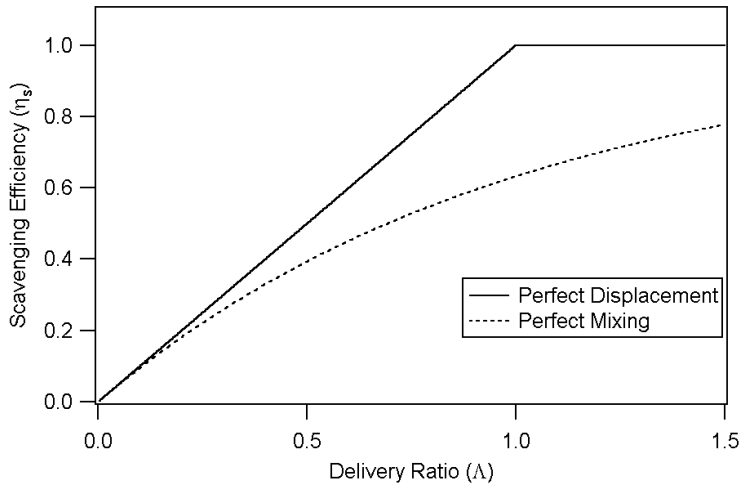

Figure 2.1: Scavenging efficiency for perfect displacement and perfect mixing.

Relating scavenging and trapping efficiency to the delivery ratio, as it is defined above, is inherently flawed. The delivery ratio relates the delivered mass to a trapped mass calculated from swept volume and ambient density, which is not representative of running conditions. A more meaningful quantity to use in the place of delivered ratio would be the ratio of delivered mass to the mass in cylinder at exhaust port closing, m_{trap}. However, m_{trap} is not a trivial quantity to measure.

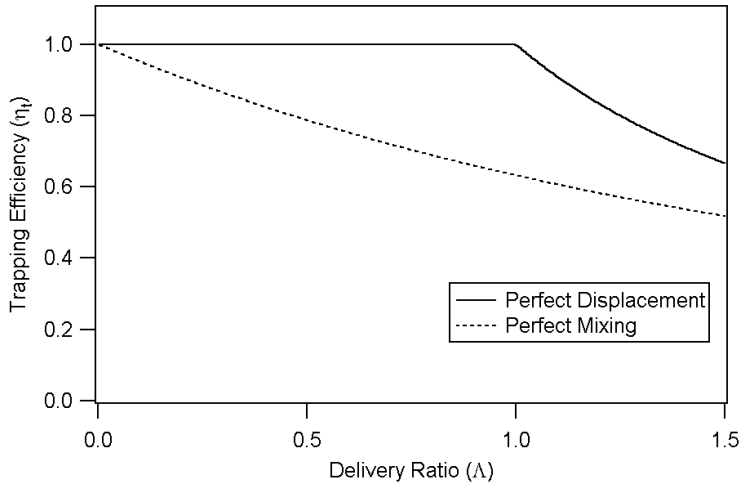

Figure 2.2: Trapping efficiency for perfect displacement and perfect mixing.

2.2.3 Multi-Zone Models

While the single-phase models are easy to use and present effective checks for scavenging measurements, they are not realistic. A more accurate representation of the scavenging process can be found in multi-zone models. These models divide the cylinder into multiple zones and apply the single-phase models to the gas interactions between the zones. The scavenging process is divided up into different phases, in which different gas interactions take place.

The multi-zone models generally assume [28]:

1. Uniform in-cylinder pressure.

2. Temperature within each zone is uniform, but may vary between zones.

3. No heat transfer between zones.

One example of a multi-zone model is Benson's three-zone model [2]. This model divides the chamber into three zones and divides the scavenging process into three phases.

The three zones are: a fresh charge zone, a zone of burned gas, and a zone made up of a mixture of both. The phases describe different zone interactions. During phase I the fresh charge enters the cylinder and displaces the burned gas. The exiting charge does not contain any of the fresh charge, and mixing occurs on the boundaries of the fresh charge. In phase II short-circuited fresh charge is the only gas to exit the cylinder. Mixing still occurs between the fresh charge and the mixing zone. In phase III a homogeneous mixture of fresh charge and burned gas exits the cylinder. The composition of this mixture varies with time, as mixing is still occurring.

In addition to the general assumptions above, this model assumes:

4. Fresh charge entering the mixing zone is a fixed portion of the instantaneous fresh charge flow rate entering the cylinder.

5. Instantaneous proportions of burned gas and fresh charge entering the mixing zone are constant.

6. Both gases are of the same specific heat and molecular weight.

Figure 2.3 depicts the gas distribution for the phases this model describes, and simplified representations of the zones and gas flows.

The three phases of the Benson model were assigned to different crank-angle ranges. Figure 2.4 shows charging efficiency, delivery ratio, and the fraction of residual gas remaining in the cylinder as a function of crank angle. The two sets of lines are versions of the model in which the values of assumed parameters were changed.

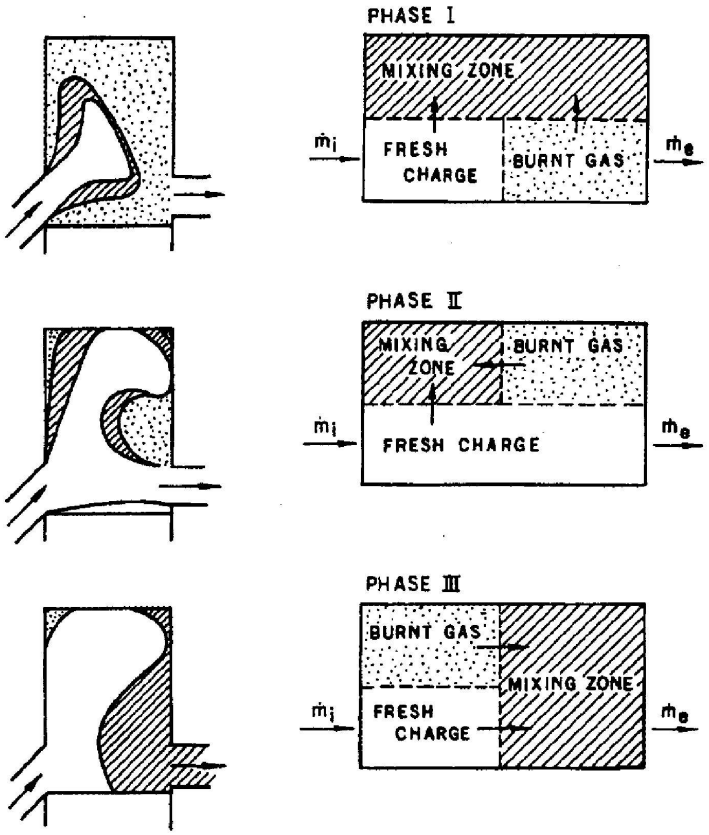

Figure 2.3: Diagram of Benson's [2] three-zone model.

2.3 Scavenging Measurement Methods

The fluid dynamics of the scavenging process are very complex, and the influence that measurement apparatus has on those dynamics is often hard to estimate. Consequently, many varied methods have been used to characterize scavenging. Each has its strengths and weaknesses. The following is a brief overview of these methods.

2.3.1 2-D Velocimetry (Jante Method)

One of the simplest methods for modeling air flow during the scavenging process is the Jante test, developed by Alfred Jante [19]. This test uses a bank of pitot tubes mounted

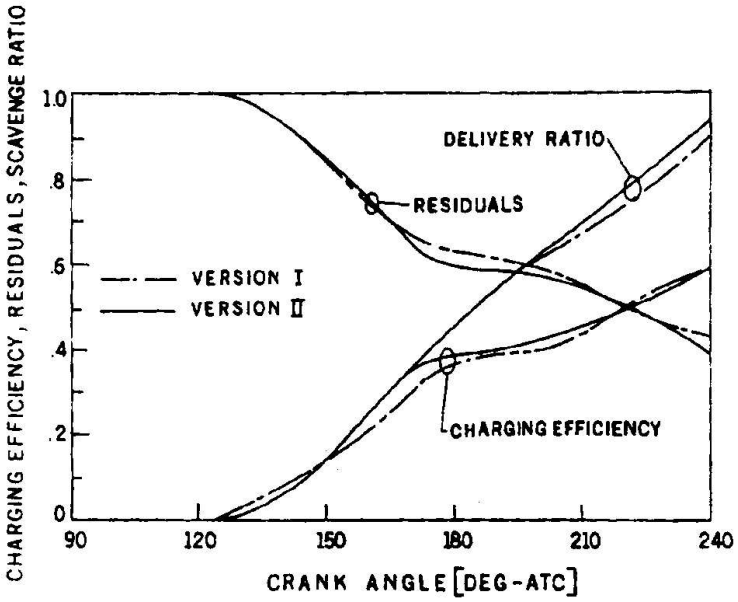

Figure 2.4: Instantaneous η_c and Λ for Benson's [2] three-zone model.

in place of the cylinder head to acquire a two-dimensional map of pressure in the cylinder. Originally a steady flow test, the Jante test rig has been adapted for use in motored engines as well. Subsequent research [20] has discredited the stationary piston method.

Although this method is simple and inexpensive to implement, it does suffer from several drawbacks. Because it is a motored test, it does not take into account any of the combustion dynamics. By replacing the cylinder head with an arrangement of pitot tubes, the gas flow in that area can be changed. In terms of scavenging efficiency, this test is qualitative, since there is no way to directly correlate the velocity fields with scavenging efficiency numbers. Its main use lies in evaluating the merits of a given port design based on previous correlations between flow fields and engine performance.

Figures 2.5 and 2.6 show a typical Jante test rig, and four common velocity countour maps, respectively. According to Jante [19], only the velocity contour pattern (a) is indica-

tive of good scavenging. The ”tongue” pattern, (b), shows high velocity across the cylinder head to the exhaust port, leading to high short-circuiting losses. The ”wall” pattern, (c) and the ”unsymmetrical” pattern, (d), would lead to high entrainment of exhaust gases in the fresh charge.

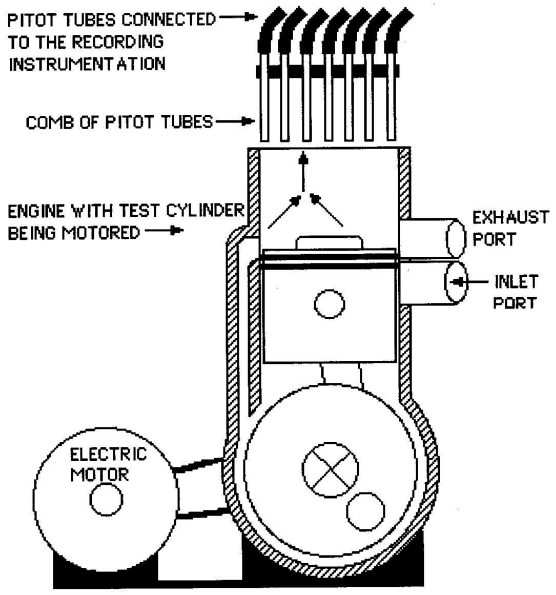

Figure 2.5: Motored Jante test rig [5].

2.3.2 In-Cylinder Velocity Measurements

Several methods are available for obtaining fluid velocity measurements inside the cylinder. Three methods which require optical access to the engine are Laser-Induced Photochemical Anemometry (LIPA), Laser Doppler Velocimetry (LDV), and Particle Image Velocimetry (PIV). Each of these methods is able to interrogate flow fields in most locations and orientations inside the cylinder. However, setting up optical access is expensive and time consuming, compared to most of the other methods described here.

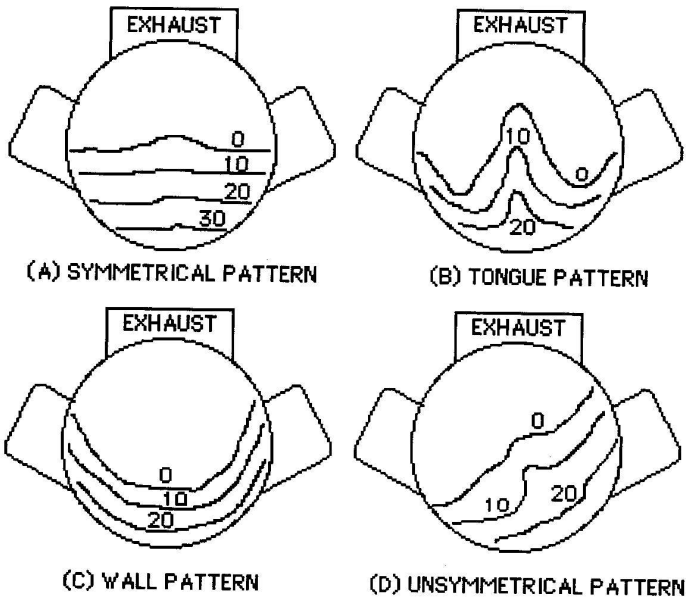

Figure 2.6: Common velocity contour results from Jante tests [5].

2.3.2.1 Laser Induced Photochemical Anemometry

Laser-induced photochemical anemometry is a technique where a phosphorescent gas is seeded in the intake air. A laser beam is directed through the cylinder, causing the gas to phosphoresce for a time, during which two or more consecutive pictures are taken.

In a study by Hilbert and Falco [14], biacetyl (2,3-Butanedione) was evaporated into nitrogen. The resulting fluid was used to scavenge their test engine. Biacetyl was chosen because its gaseous density is near to that of air, and it has a low vapor pressure. Nitrogen was used as a carrier gas because the phosphorescence of biacetyl is quenched by oxygen. An array of laser beams were passed through optical access ports in the engine cylinder walls, forming a grid. One pulse was given per cycle to excite the biacetyl. Two consecutive pictures were then taken of the grid through a window in the head. Velocity and vorticity could be derived from the translation and deformation of the grid lines.

This method can produce quite detailed maps of the velocities in whichever plane in the cylinder is chosen for analysis. Because oxygen quenches phosphorescence, however, it cannot be used in a fired engine.

2.3.2.2 Laser Doppler Velocimetry

Several experiments [8, 12, 21, 22] used Laser Doppler Velocimetry (LDV) to measure velocity in several points in the cylinder, as well as in the intake and exhaust ports. The principal of LDV is that a single laser beam is split into two beams of equal intensity which are focused at a chosen point. An interference pattern is formed at the point where the beams intersect. Particles moving through the intersection point scatter light of varying intensity. A photodetector is placed so as to collect some of the scattered light, and its output frequency is directly related to velocity. LDV can only measure velocity at one point at a time for each wavelength of laser light. While mapping the single-point measurements over the full chamber provides useful insights, it is not possible to quantitatively assess scavenging in this manner.

2.3.2.3 Particle Image Velocimetry

Ghandhi and Martin [11] used particle image velocimetry (PIV) to map the flow velocities in a two-stroke engine. In PIV the intake charge is seeded with particles, and two successive pictures are taken of the particle positions in cylinder. The particles are illuminated by a sheet of light from a puled laser. Flow velocity data can be derived by comparing the positions of the particles in the first picture to the positions in the second. PIV is generally limited to two-dimensional analysis of a single event, unless multiple wavelengths of laser light are used to illuminate the particles. Also, like LIPA and LDV, PIV does not give

a quantitative representation of the scavenging process.

2.3.3 Single-Cycle Models

One way to isolate the scavenging event is to create an apparatus which operates for one complete scavenging cycle and stops at its conclusion.

In a simple piston ported two-stroke cycle engine, the scavenging process can be divided into three phases [26]. The first is a blow-down through the exhaust port, with possible blow-back into the intake transfer ports. The second is the actual scavenging phase, in which there is simultaneous inflow and outflow. The third is the final exhaust flow, which may include some backflow depending on the exhaust system gas dynamics. The use of a single-cycle model with a constant volume cylinder can be useful for eliminating the first and third phases, and evaluating just the scavenging phase. The cylinder is kept at a constant volume because a second piston, which is attached to the normal piston by a connecting arm, is used in place of a cylinder head.

Although this method greatly simplifies data collection, it has several drawbacks. Because combustion does not occur, in-cylinder temperatures, pressures and fluid flow do not represent those seen in a running engine. Also, the constant volume cylinder may not produce the same flow results as the real engine.

2.3.3.1 Liquid-Based Single-Cycle Model

The use of a liquid in place of a gas for scavenging measurements is possible through the use of dimensionless parameters [26]. By matching the density ratio of the intake to cylinder charges with that of the intake and cylinder gases in a fired engine, the scavenging parameters derived from the liquid-based tests can be meaningful. Reynolds number ($Re =$

$u \cdot L/\nu$) is fairly unimportant as long as it indicates flow in the turbulent regime.

Several studies have used liquids in place of a gases for single-cycle simulation of the scavenging event. In order to account for the incompressibility of the liquid, a double-piston arrangement was used. Instead of a stationary head, a second piston moved at the same rate as the first to keep the cylinder volume constant. Figure 2.7 [26] is a sketch of liquid-flow scavenging test equipment. In each study, one liquid was used to simulate the intake charge, and a similar, but quantifiably different, fluid was used for the exhaust charge. Most of the studies use water for the exhaust charge.

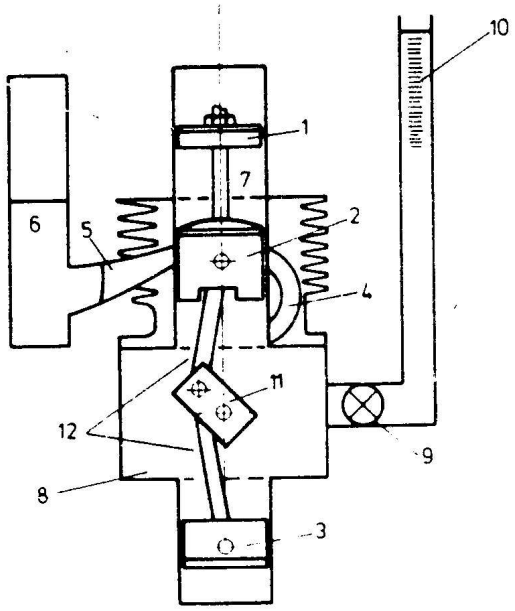

Figure 2.7: Liquid flow scavenging test rig [26].

Sanborn [26] used a sugar solution of a known specific gravity, and measured scavenging efficiency using the specific gravity of the cylinder charge after scavenging. Oka and Ishihara [23] measured the change in temperature and specific gravity of a salt solution. They also added a dye to allow for visualization of the scavenging process through

the transparent cylinder walls of the test rig. Other studies have used fluids with different conductivities [27], or different absoptivities of some light spectra [24].

Figure 2.8 is a graph of scavenging efficiency versus delivery ratio from Sanborn's liquid scavenging experiments. It includes curves for six cylinder configurations as well as curves for the perfect displacement (perfect scavenging) and perfect mixing models.

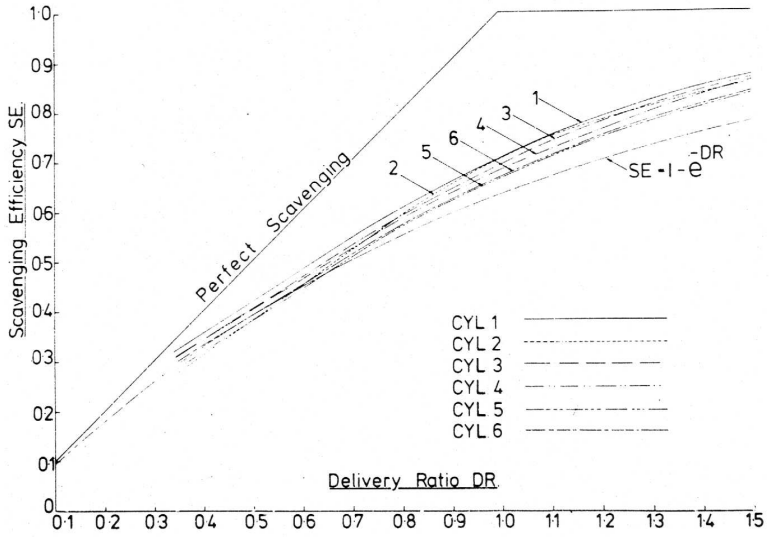

Figure 2.8: Scavenging efficiency results from a liquid-scavenging rig [26].

2.3.3.2 Gas-Based Single-Cycle Model

Sweeny [29] used the same setup as for a liquid-based single-cycle method, but used carbon dioxide for the intake charge and air for the exhaust gas. Using a gas allowed pressurization of the constant-volume crankcase to more nearly simulate the variation of intake pressure over the course of the scavenging event. Because the cylinder is of constant volume, the test can still be used to separate the scavenging event from the initial exhaust blowdown and final exhaust flow.

2.3.4 Sampling Cylinder Gas

A very straightforward method of ascertaining the composition of the pre-combustion charge is taking a direct sample using some sort of a valve mounted in the engine head. Scavenging and trapping efficiencies can be directly ascertained by sampling pre- and post-combustion charge as well as exhaust gas [1]:

$$\eta_s = \frac{Y_1 - Y_2}{Y_0 - Y_2} \tag{2.11}$$

$$\eta_t = \frac{Y_0 - Y_3}{Y_0 - Y_2} \tag{2.12}$$

Y_0, Y_1, Y_2, and Y_3 are mass percent concentrations of a particular gas species in fresh air, pre-combustion charge, post-combustion charge, and exhaust gas, respectively.

Asanuma [1] used two electromagnetic valves, a needle and a poppet-type, to sample pre- and post-combustion gases. He found that the needle valve was unsuitable for high engine load operation. The high chamber pressure during combustion could force the valve open and contaminate the sample. The poppet valve was not susceptible to this problem, since higher chamber pressure simply forces the valve against its seat. The larger flow area of the poppet valve also resulted in greater sample volume. However, Asanuma's poppet valve was unable to open against chamber pressure after combustion during high speed, high load operation of the engine.

Blair and Ashe [6] used a mechanical poppet valve to extract gas from a high speed engine. An electromagnetic valve was thought to be inadequate for extracting a large sample from an engine running at high speed (about 6% of the trapped charge at 5000 RPM and 3% at 8000 RPM for the electromagnetic valve). The mechanical valve was able to extract 18% to 35% of the cylinder volume for speeds ranging from 4000 to 9000 RPM.

The mechanical valve was actuated by a cam. The cam was chain driven by the

crankshaft, with a 1:11 gear ratio. This meant there were ten cycles of normal combustion between every sampled cycle. Although the mechanical valve has apparent benefits over electromagnetic valves in terms of sample size at high speed, the large mechanism reduces it's portability. The mechanical valve also lacks the ease of adjustment of its electromagnetic counterpart.

Figure 2.9 shows scavenging efficiency and engine performance data as a function of engine speed. Although the air/fuel ratio was held constant for these tests, delivery ratio was not.

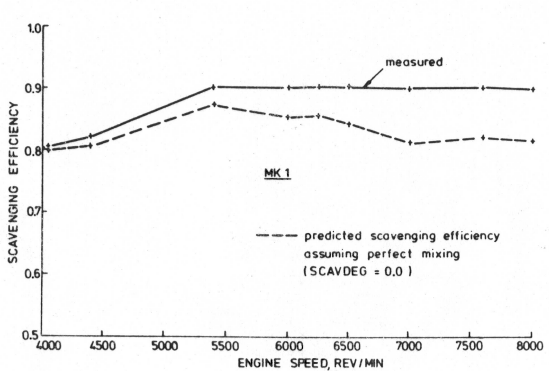

MK1 ENGINE TEST DATA

Speed (rpm)	bhp	bmep	delivery ratio	bsfc	Air/fuel ratio
4000	9.86	65.3	0.672	0.978	11.08
4400	11.38	68.5	0.594	0.811	11.25
5000	15.80	83.7	0.857	0.995	10.82
5500	20.87	100.5	0.930	0.855	11.40
6000	26.28	116.0	0.932	0.754	11.22
6250	27.40	116.1	0.923	0.747	11.25
6500	28.58	116.5	0.927	0.763	10.98
7000	28.22	106.8	0.889	0.796	11.00
7600	26.23	91.4	0.820	0.847	11.15
8000	25.45	84.3	0.752	0.854	10.98

Figure 2.9: η_s and engine data for tests with a mechanical sampling valve [6].

A study by Tobis, *et al.* [30] used a poppet-type electromagnetic valve to extract samples of the cylinder contents. The electromagnetic valve has the advantage of variable timing and open-duration. It also is more portable than the mechanical valve. However, due to limitations of the solenoid actuation force, the maximum speed at which it can extract a sizeable sample was limited. Also, because a solenoid does not instantly apply or remove force, it was difficult to calibrate without a direct lift sensor. Finally, the poppet-style solenoid-actuated valve may have difficulties opening against cylinder pressure for

sampling post-combustion gases.

In Figure 2.10 scavenging and trapping efficiency are plotted against delivery ratio for a range of engine speeds. Although the scavenging curve follows the general shape seen in other tests, the numerical values exceed the values calculated by the perfect displacement model, the theoretical maximum, for most of the points. This does not necessarily denote inaccuracy in the measurement method, however, since the standard definition of delivery ratio (Equation 2.2) may not be representative of the delivered fraction of the maximum possible cylinder mass.

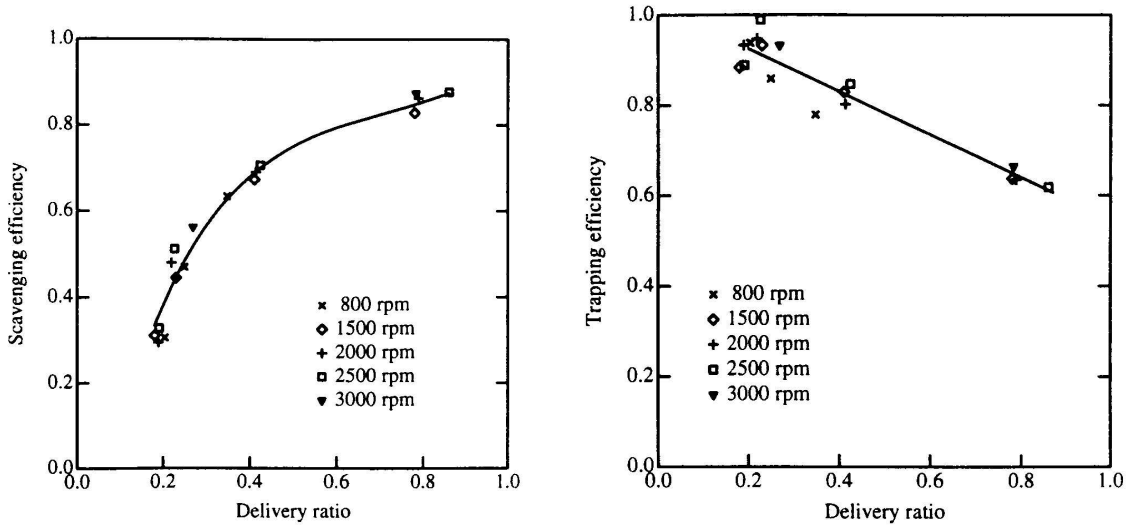

Figure 2.10: η_s and η_t results for tests with a solenoid sampling valve [30].

2.3.5 Skip Firing

The skip firing technique [7] works by allowing the engine to motor for a number of cycles before each fired cycle. The idea is that the indicated mean effective pressure (IMEP) of the fired cycle just after the motored cycle(s) will be greater than that of a normal fired cycle with the same delivered air/fuel (A/F) ratio. Each successive scavenging event,

in motored operation, brings the A/F ratio in the cylinder closer to the delivered A/F ratio, while increasing the total amount of air and fuel available for combustion. The IMEP is related to the exhaust residual by:

$$\frac{IMEP_n}{IMEP} = \frac{1 - Y_{res}^n}{1 - Y_{res}} \tag{2.13}$$

where $IMEP_n$ is the IMEP of the skip-fired cycle, and $IMEP$ is the IMEP when the engine is run normally, not skip-fired. Y_{res} is the mass fraction of the exhaust residual, and the engine is fired once every n cycles.

The skip fired method is easy to implement on a fired engine, as it requires only a means of determining IMEP, such as a pressure transducer and a shaft encoder. Its main disadvantage is that relies on the assumption that scavenging occurs with the same efficiency after non-fired cycles as after fired cycles. Data from Tobis, *et al.* [30] suggests that this is not necessarily a valid assumption. Also, this method only works on a port-injected or carburated engine, since it requires the scavenging of exhaust residual with an air/fuel mixture.

2.3.6 Tracer Gas

A fairly simple, non-intrusive method of measuring trapping efficiency involves introducing a tracer gas into the fresh charge. Booy [7] cites four requirements for a tracer gas:

1. It must behave identically with the other components with regard to distribution and scavenging.

2. It must not affect the combustion reactions, even when present in small concentrations.

3. The portion of the tracer trapped with the cylinder charge should be completely destroyed by the combustion process, while the short circuited portion must remain intact in the exhaust gases.

4. The tracer gas should be easily analyzed quantitatively by some analytical means.

Tracer concentrations can be compared from any two of the following locations: intake charge, pre-combustion charge, and exhaust gas. For simplicity, usually the intake charge and exhaust gas are measured. Isigami [18] gives the following relation between trapping efficiency and tracer gas concentration:

$$\eta_t = 1 - \frac{X_{tracer,exhaust}}{X_{tracer,intake}} \tag{2.14}$$

where $X_{tracer,exhaust}$ and $X_{tracer,intake}$ are the tracer concentration in the exhaust and the fresh charge, respectively.

If a tracer gas is available that meets all of these requirements for a particular application, then the implementation of the tracer gas method is straightforward. This method can suffer inaccuracies due to incomplete combustion, and tracer gas destruction in the exhaust. This makes the tracer gas method unsuitable for use in a direct-injection engine operating under stratified combustion, because the air in the retained charge, which the tracer would be seeded in, is not completely burned.

2.3.6.1 Oxygen as a Tracer Gas

For fuel-rich combustion of a premixed charge, where it can be reasonably assumed that all of the oxygen in the combustion chamber is consumed during the combustion event, oxygen can be used as a tracer gas. Under these conditions, all of the oxygen in the exhaust must come from short-circuited air. The calculation of trapping efficiency from the oxygen

concentration in the exhaust gas is straightforward [16]:

$$\eta_t = 1 - \frac{X_{O_2,exhaust}}{X_{O_2,air}} \tag{2.15}$$

Inaccuracies may arise if exhaust temperatures are too high, causing the oxygen from the fresh charge to react in the exhaust. Also, a certain amount of oxygen comes from the exhaust charge due to incomplete combustion. Huber's tests on four-stroke engines [16] suggest that for $1.05 \leq \Phi \leq 1.25$, the concentration of oxygen in the exhaust charge is between 0.1% and 0.3%. This method is very simple to implement, but is not useful for stratified direct-injection operation. This is because lean operation is necessary to prevent misfiring under such operating conditions.

2.3.7 Computational Methods

Computational fluid dynamics (CFD) should be briefly mentioned as an analysis method. The level of detail CFD can offer is unparalleled. All relevant properties of the fluid can be solved for at any point and time that the simulation encompasses. There is no interference from the measuring equipment, since it doesn't exist. The deficiencies of the CFD method include concerns with the validity of the models, especially turbulence models, its questionable prediction value for an engine without experimental data for correlation and "tweaking", and its massive requirements in terms of computation time. Fortunately all these disadvantages can be reduced as computational power becomes greater.

Chapter 3

Experimental Setup

3.1 Test Cell Overview

The test cell and engine were designed to facilitate a range of experimental configurations and conditions. The major components of the test cell are the engine, dynamometer, fuel and air delivery systems, cooling system, and engine controller unit. Additional instrumentation is available to measure airflow, fuel flow, engine load and speed, cylinder pressure, and the concentration of species in sampled gas.

3.2 Single Cylinder Research Engine

The Single Cylinder Research Engine (SCRE) is based on the geometry and port configuration of a Mercury Marine 2.5-liter V-6 two-stroke outboard motor, and was designed and built by Mercury Marine. The engine is liquid-cooled and loop-scavenged with a geometric displacement of 389 cm^3. The SCRE is capable of being configured with several cylinder heads, but the production head design was used for these tests. Rated power is 20 kW at 5000 RPM. Detailed specifications are shown in Table 3.1.

Table 3.1: Mercury SCRE Specifications.

Bore	85.8 *mm*
Stroke	67.3 *mm*
Connecting Rod Length	139.7 *mm*
Combustion Chamber Volume	34.4 cm^3
Volume at Top Dead Center	41.48 cm^3
Total Volume Swept by the Piston	389.11 cm^3
Volume Swept from EPC to TDC*	234.57 cm^3
Geometric Compression Ratio	10.4:1
Actual Compression Ratio	6.8:1
Exhaust Port Opening	95° ATDC**
Intake Transfer Port Opening	117° ATDC
Intake Boost Port Opening	117° ATDC

*EPC to TDC = Exhaust port closing to top dead center. **ATDC = after top dead center.

3.3 Engine Dynamometer

A Froude Engineering eddy-current dynamometer was used to control engine load. It was mounted below the engine and coupled to the crankshaft by a vertical shaft. The dynamometer is only capable of resisting the rotation of the crankshaft, and cannot be used to motor the engine. Engine torque was measured by a load cell, which was calibrated prior to testing using a dead weight on an arm of fixed length. The dynamometer was controlled by a Digalog dynamometer controller. The controller was able to automatically adjust the load to keep the engine at a set speed, or could be used to control absolute load. The dynamometer temperature was regulated by water cooling.

3.3.1 Fuel Delivery System

The fuel delivery system was capable of delivering fuel at low or high pressure. The air-assist fuel injectors used in this test required only low pressure fuel. The low-pressure

fuel system pulled fuel from the tank with the first-stage pump. The fuel then passed through a filter and a Micro-Motion flow meter to a float bowl. Fuel from the float bowl was pumped to the fuel rail. Excess fuel was passed through a cooler back to the float bowl.

The fuel used in all the tests was Amoco brand Indolene. Indolene is a standardized version of gasoline. Its composition is much more consistent from batch to batch than a comparable gasoline product sold at a gas station. A summary of its relevant properties are shown in Table 3.2.

Table 3.2: Properties of BP-Amoco Indolene.

Research Octane Number (RON)	97.3
Motor Octane Number (MON)	87.5
Hydrogen/Carbon Mole Ratio	1.845
Net Heating Value	42966 kJ/kg
Sulfur Content	$<$10 ppm
Reid Vapor Pressure	62.74 kPa

3.4 Air Delivery System

Airflow to the engine originated as either filtered room air, or filtered pressurized air. Both sources passed through an inlet surge tank (of 440 times the cylinder volume) and an electronic throttle control (ETC) before entering the engine crankcase through reed valves.

The air mass flow rate into the engine was measured by an array of orifices and a pressure regulator. By ensuring choked flow through one or more of the orifices, the mass flow rate could be calculated as a linear function of the pressure upstream of the orifices.

3.5 Air-Assist Fuel-Injection System

The fuel injection system use in all the tests was an Orbital air-assist direct injection system. The Orbital system consisted of a fuel injector and an air injector which were mounted on a fuel rail. The fuel injector delivered a metered amount of fuel to a pre-injection chamber. The air-injector would then inject the pressurized fuel-air mixture directly into the cylinder. Compressed air was supplied to the air-injector after passing through a filter-drier and a regulator. A differential fuel regulator in the rail controlled the fuel pressure. The fuel regulator maintained the fuel pressure at 70 kPa above the air pressure, which was set to 650 kPa absolute pressure.

3.6 Cooling System

The cooling system included a heat exchanger, which used tap water to cool a 50/50 mixture of water and ethylene glycol (automotive antifreeze). The antifreeze was used to cool the head of the engine and then flowed through the heat exchanger to a reservoir. The flow of tap water through the heat exchanger was regulated by a solenoid switch located at the exit of the heat exchanger. For all test runs, the solenoid switch was set to maintain engine temperature below 50°C. An emergency shutoff circuit would stop the engine if the coolant temperature were ever to exceed 70°C.

3.7 Engine Control Unit

The engine control unit (ECU) used for these experiments was a Mototron model PCM-555, which included a Motorola MPC555 microcontroller and a ProSAK knock control chip. This ECU was similar to that used on production Mercury Marine engines, except that the calibration maps could be modified while the engine was running. The ECU

controlled spark, fuel and air injection, and the ETC. It received inputs from coolant and intake-air temperature sensors, as well as an intake-air pressure sensor and a Hall-effect crank-angle/speed sensor. It was capable of monitoring intake-air mass flow, and knock, and controlling oil injection, but these capabilities were not utilized.

The software interface for this ECU was the Mototron Mototune program. It ran on a x86 compatible computer and interfaced with the ECU through a serial port. With this program, ignition and injection timings could be locked and adjusted, as could the quantity of fuel injected per cycle. Because an electronic throttle controller was used, throttle angle could also be set.

Since the controller was designed for a six-cylinder engine, it had several unused outputs, one of which was used to supply a control signal to the sampling valve driver circuit. A special operating mode was programmed into the ECU for cylinder sampling operations. In this mode the ECU would send a TTL signal to the valve driver and disable spark and fuel for a single cycle every twenty normal cycles. The number of normal cycles between sampled cycles was variable.

3.8 Pressure Transducer

An AVL model QC42D-E C109 water-cooled piezoelectric pressure sensor was mounted flush with the cylinder head. The output signal from it was amplified by a Kistler model 5010 charge amplifier and sent to a Hi-Techniques HT-600 data-acquisition and analysis instrument. The HT-600 was also connected to the A- and Z-pulse outputs from a shaft encoder attached to the crankshaft. Resolution of the shaft encoder was 360 A-pulses (and one Z-pulse at TDC) per crank revolution, and a pressure reading was taken on every A-pulse.

3.9 Emissions Bench

The emissions bench consisted of a delivery system and five individual analyzers for measuring oxygen (O_2), carbon monoxide (CO), carbon dioxide (CO_2), oxides of nitrogen (NO_x), and hydrocarbons (HC). The HC analyzer required a heated sample delivery line, to prevent the more massive hydrocarbon molecules from condensing, and was not used for these tests. The other four analyzers received dry samples. The O_2 analyzer was a Beckman OM11-EA polarographic analyzer and had a full range of 1-100% oxygen concentration by mass. The CO and CO_2 analyzers were Horiba PIR-2000 non-dispersive infrared analyzers. The NO_x analyzer was a ThermoElectron 10A chemiluminescent analyzer, and was capable of measuring NO or NO_x. All analyzers were calibrated with zero-gas (nitrogen) and span-gas (gas of a known concentration with the balance being nitrogen) before each experiment to minimize sensor drift.

When dry samples were taken from the exhaust or the cylinder, the sample passed through two filters and then a condenser. The condenser consisted of a coil submersed in an ice-water mixture. The condenser removed water and heavy hydrocarbon molecules from the sample, making it what is referred to as a ”dry” sample. Numeric correction factors, discussed later, can be applied to a dry sample to find the corresponding emissions values if the sample were ”wet”. The temperature of the sample was decreased while passing through the condenser, typically to near 10°C.

The delivery system is a set of valves, toggles and pumps used to transport the sample to the analyzers and control the flow rate through each analyzer. It also allows bottled gases to be sent to the analyzers for calibration purposes. Some modifications had to be made to the delivery system to accommodate the flow from the sampling valve.

Each analyzer output a voltage corresponding to the concentration of the measured gas in the sample. These voltages were read by a National Instruments NI-6024E data-acquisition card in a x86 compatible computer (also used to interface with the ECU). A LabVIEW Virtual Instrument (VI) was used to transform the voltages to meaningful concentration values and average samples over a desired interval. The VI also collected torque data from the engine dynamometer. All data for these tests were averaged over a two minute interval to filter out transient noise.

Chapter 4

The Sampling Valve

The purpose of this project was to obtain an understanding of scavenging by examining the contents of the combustion chamber. In order to extract a portion of the cylinder contents for examination, a sampling valve was designed and built.

4.1 Design

The initial design of the valve was completed by students in a technical design course at UW-Madison. Subsequent design changes were made to enhance durability, machineability, and to allow easier replacement of worn parts.

4.1.1 Objectives and Constraints

Previous sampling experiments [3] with the single-cylinder research-engine (SCRE) had shown that a small sample was not adequate to characterize cylinder contents, especially during stratified running conditions. Therefore the first requirement was that the valve be able to sample a large fraction of the cylinder mass.

The eventual goal of this project is to have a system that can be attached to a produc-

tion engine and carried in a boat for field-testing. Because of this, the valve needed to be driven by a simple, portable mechanism. Also, the size of the valve was constrained so that it could be attached to a production engine without any major modification.

4.1.2 Final Design

The final valve design was a poppet-style, solenoid-actuated valve. The poppet-style valve was chosen for two reasons. The primary reason was its large flow area. The second was that cylinder pressure serves to press the valve against the seat. In the case of a needle-type valve, the cylinder pressure would push the valve away from the seat, requiring a stronger spring and thus higher actuation force.

In previous tests with the SCRE [3], elevated valve temperature was a problem, thus stainless steel was chosen as the valve body material because its low thermal conductivity significantly reduced heat transfer to the solenoid. Because the fit between the valve and valve guide was looser than expected, leakage of ambient air past the valve guide was considered a possible problem. To avoid contamination of the sample, flow through the valve was driven entirely by cylinder pressure. Thus, the pressure inside the valve was always greater than, or equal to, atmospheric pressure. A bypass of the vacuum pump in the emissions bench was installed for this purpose.

The actuator chosen was a Ledex-Dormeyer low-profile linear solenoid, model 5SF-2x. This solenoid was selected because of its high rated actuation force. An unregulated 48V power supply was used to drive the solenoid. The voltage rating of the power supply was about three times the manufacturer's suggested supply voltage for a ten percent duty cycle. This was acceptable because the valve would be run at no more than a one percent duty cycle. Engine testing showed that the solenoid withstood the higher supply voltage

well and did not overheat. A simple circuit was used to supply voltage to the solenoid according to a square wave input.

Drawings of the valve assembly and the individual parts, as well as a circuit diagram of the driver, are available in Appendix C.

4.2 Characterization

In order to gain a better understanding of how the valve would perform in the engine, several tests in which the conditions could be more easily controlled were performed. This allowed for fine-tuning of the valve that would not have been possible under running conditions. On a more pragmatic note, it gave the valve a chance to break before doing so could harm the research engine.

4.2.1 Steady Flow Tests

To determine the effective area for flow through the valve, a series of steady flow tests were performed. In these tests, compressed air flowed in through a mass flow meter to a pressure regulator. The valve was mounted a short distance downstream of the regulator and vented to the atmosphere.

4.2.1.1 Test Apparatus

The valve assembly was modified slightly to allow the valve to be locked open at a desired lift. A bolt was threaded into the top of the assembly, where the displacement transducer would normally go. This bolt had a dial attached to its head, and the lift of the valve was determined by the thread pitch and the number of degrees it had been turned.

Compressed air was supplied at about 600 *kPa* from a general purpose supply. A Rosemount orifice flow meter, model 3095, was used to measure mass flow through the

valve. Pressure upstream of the valve was measured by a high-resolution pressure gauge mounted just downstream of the pressure regulator.

4.2.1.2 Equations

The steady flow tests were performed in order to determine the effective area of the valve, the cross-sectional area the valve would be if it were a round orifice. The gas flow was approximated as an isentropic ideal gas flow, and the valve was modelled as a nozzle. Equation 4.1 [9] was used to calculate the ratio between the upstream pressure, P_0, and the critical pressure (pressure at the throat in choked flow), P^*. The specific heat ratio for air is $k = c_p/c_v = 1.4$.

$$\frac{P_0}{P^*} = \left[1 + \frac{k-1}{2}\right]^{\frac{k}{k-1}} = 1.893 \tag{4.1}$$

In these tests, pressure in the throat cannot be lower than ambient. Therefore, the upstream pressure must be at least 1.893 times ambient pressure for the flow to be choked.

Equations 4.2 and 4.3 allow the choked temperature and density ratios, respectively, to be calculated. The upstream temperature and density are T_0 and ρ_0 respectively, and T^* is the critical temperature and ρ^* the critical pressure.

$$\frac{T_0}{T^*} = \left[1 + \frac{k-1}{2}\right] = 1.20 \tag{4.2}$$

$$\frac{\rho_0}{\rho^*} = \left[1 + \frac{k-1}{2}\right]^{\frac{1}{k-1}} = 1.577 \tag{4.3}$$

The sonic velocity is a function of temperature, so velocity at the throat can be calculated from the throat temperature and Equation 4.4.

$$V^* = \sqrt{k \cdot R \cdot T^*} \tag{4.4}$$

By dividing the measured mass flow rate, $\dot{m}_{measured}$, by the density at the throat, the volumetric flow at the throat is acquired. The effective area, A_{eff}, of the valve is then the

volumetric flow rate divided by the velocity in the throat, the sonic velocity.

$$A_{eff} = \frac{\dot{m}_{measured}}{\rho^* \cdot V^*} \tag{4.5}$$

4.2.1.3 Results

The steady flow tests were performed over a range of pressure ratios, from 2 to 6. However, the compressed air supply was not adequate to maintain the highest pressure ratio over the entire range of valve lift. Effective areas were calculated for all test points and are shown in Figure 4.1.

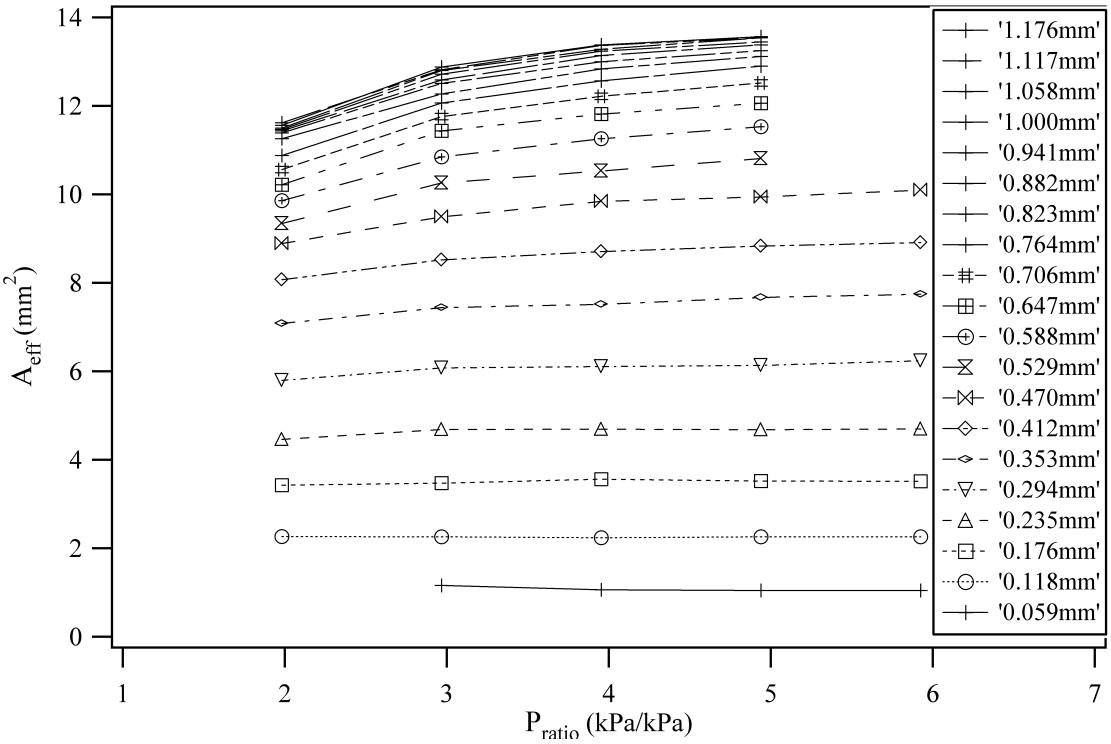

Figure 4.1: Effective area of the valve for steady choked flow

There was no significant difference in effective area for valve lift above 0.94 mm.

Because the valve is solenoid-actuated, a lower lift profile can result in significantly better response times. With that in mind, mica shims were placed under the solenoid to restrict the maximum lift imparted on the valve to 1.0 mm.

Ideally, A_{eff} would be a function of valve lift only. However, Figure 4.1, shows a trend toward higher effective area at higher pressure ratio, especially at high lift. The greatest difference in A_{eff} for a given lift condition is on the order of ten percent over the range of pressure ratios tested. For the purpose of sample size approximation, this is a difference small enough that it can be neglected. Equations 4.6 and 4.7 give polynomial curve fits (R^2=0.9996) of A_{eff} vs. lift (L) for pressure ratios of 2.97 and 4.94 respectively. For these curve fit equations, units of A_{eff} are mm^2 and units of L are mm.

$$A_{eff} = 35.5 \cdot L^4 - 80.2 \cdot L^3 + 43.8 \cdot L^2 + 14.4 \cdot L \tag{4.6}$$

$$A_{eff} = 33.2 \cdot L^4 - 71.6 \cdot L^3 + 35.4 \cdot L^2 + 15.8 \cdot L \tag{4.7}$$

Figure 4.2 is a plot of those curve fits over the experimental data points. The calculated physical flow area between the valve and seat is included for reference.

The physical flow area, A_{calc} was approximated by:

$$A_{calc} = L \cdot cos(\alpha) \cdot \pi \cdot D_{seat} \tag{4.8}$$

where D_{seat} is the inner diameter of the valve seat and α is the angle of the valve seat. This calculation diverges from the measured effective area at high lift because flow restriction elsewhere in the valve assembly is becoming more important than the restriction at the valve face.

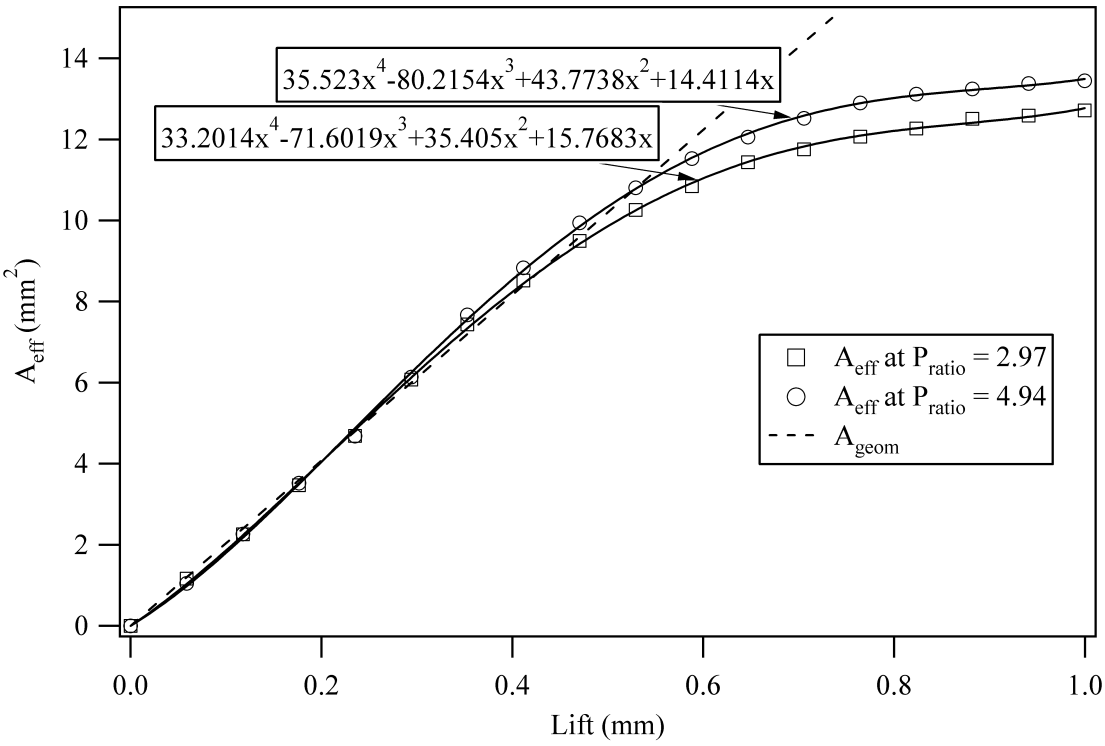

Figure 4.2: Effective area curve-fits for two pressure ratios

4.2.2 Transient Valve Lift

In order to approximate the gas quantities sampled from the engine, the valve lift profile is required for the sampling period. Due to the initial lack of a displacement transducer that could be attached to the back of the solenoid and measure the entire range of the solenoid movement, valve lift profiles were first made with the valve not installed in the engine.

4.2.2.1 Test Apparatus

For the valve lift profile tests, the valve was configured such that the greatest lift imparted on the poppet by the solenoid would be 1.0 *mm*. The valve was mounted in a stationary bracket, such that the poppet portion of the valve was visible. A digital camera

with a fast shutter speed was used to capture images of the valve as it was actuated. The camera was set with an incrementing delay timer, which was triggered by the rising edge of the signal that drove the valve. This produced one image per actuation, in which the series of images appeared to step through a single valve actuation. Lift values were obtained by counting pixels from the edge of the valve head, in the closed position, to the edge in a given image. A pixel-to-millimeter conversion was obtained by taking a picture of a machinists scale next to the valve head.

Figure 4.3 is a sample valve image. Lift variability in the axial direction was minimal for most of the stroke, suggesting that this method gave a reasonably representative picture of any given valve actuation.

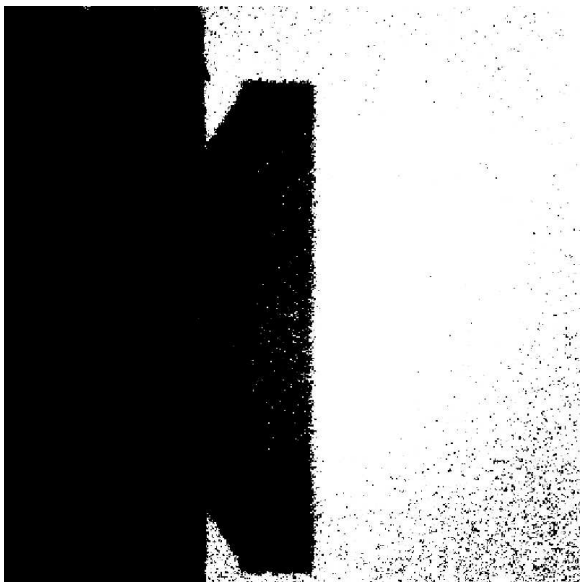

Figure 4.3: The valve head at full lift.

4.2.2.2 Results

Lift profiles were measured as a function of the pulse width supplied to the driver circuitry. The driver always applied full available power to the solenoid to charge it as quickly as possible. Lift profiles were acquired for a range of pulse widths from 2.40 to 4.0 *ms*. Figures 4.4, - 4.6 include three ranges of pulse widths. In the first range, from 2.40 to 2.50 *ms*, the open duration of the valve increased consistently, but at a much greater rate than the driving signal. During the second range, 2.50 to 2.60 *ms*, the profiles and their corresponding open durations were all very similar. Like the first range, the third range exhibited a consistent relationship between open duration and pulse width. However, the increase in open duration was less, for a given pulse width increase, in the third range than in the first range.

The open duration is not necessarily representative of the flow possible through the valve. A more useful quantity is the integral of A_{eff} over the open duration. Figure 4.7 shows the relation between $\int A_{eff}$ and pulse width for the valve. The three ranges depicted in Figures 4.4 - 4.6 are clearly visible in this graph as regions of different slope.

4.2.3 In-Cylinder Valve Actuation

For a poppet-style valve, the delay between issuing an actuation signal and the actual opening of the valve can vary according to the pressure in the cylinder. For this reason, a linearized driver circuit was not built for this valve. Instead, a displacement transducer was mounted on the valve, and driver signal timing and duration were determined for each running condition based on the lift measurements.

A Kaman Instruments model .5U sensor was mounted in the damper bolt and attached to a model KD-2300 displacement transducer. To increase the operational range of the

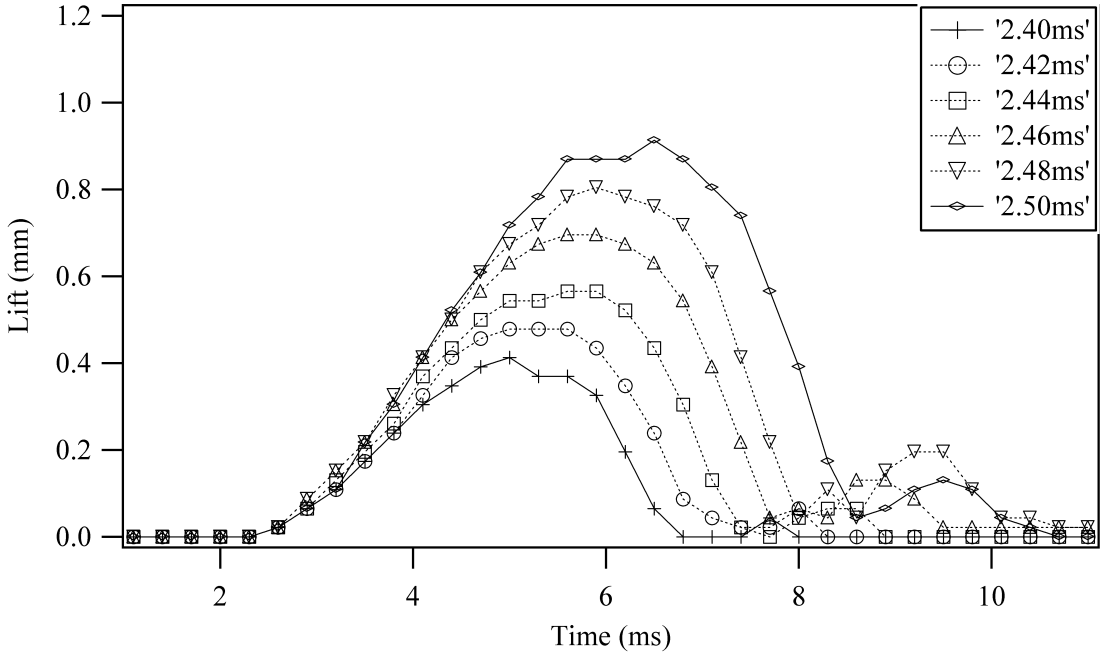

Figure 4.4: Valve lift profiles for input signals 2.40 - 2.50 *ms*.

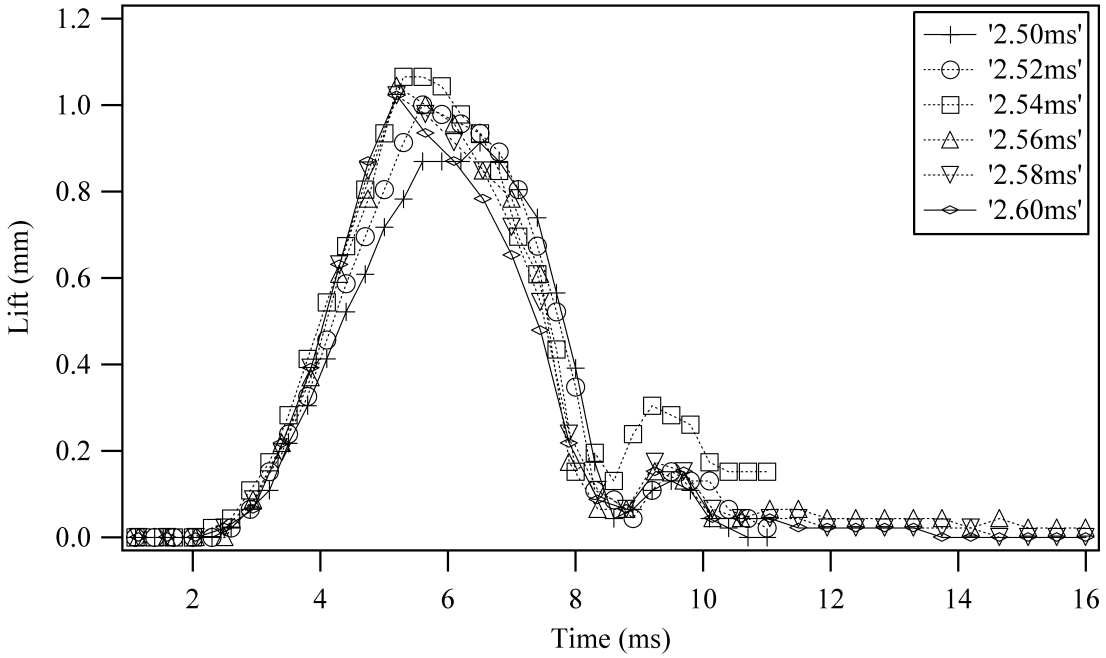

Figure 4.5: Valve lift profiles for input signals 2.50 - 2.60 *ms*.

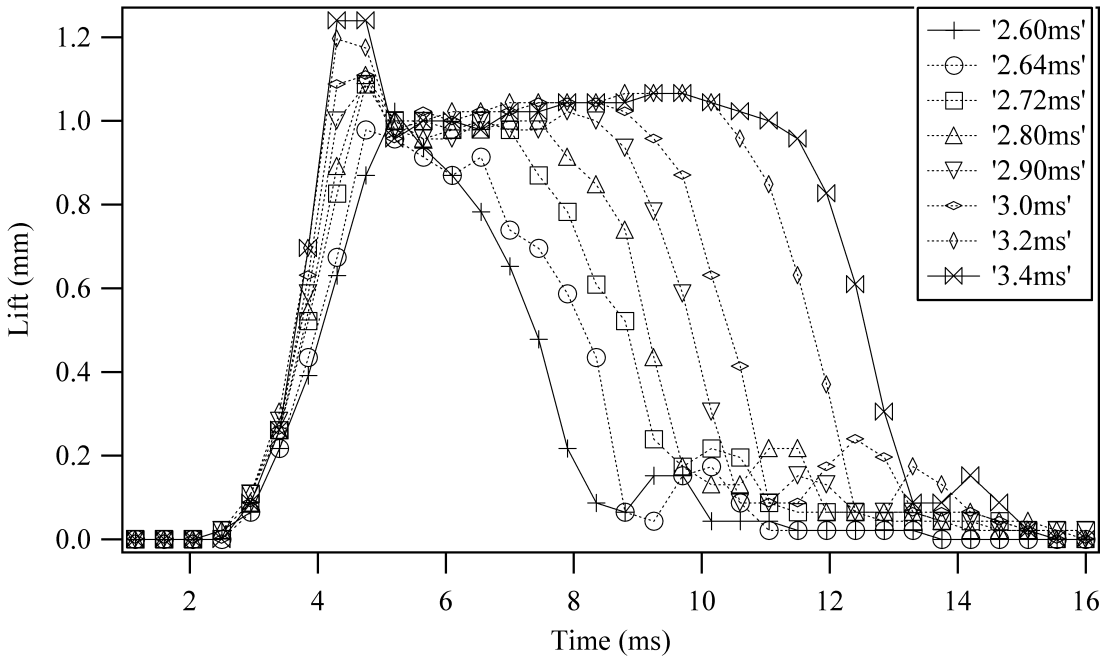

Figure 4.6: Valve lift profiles for input signals 2.60 - 3.40 *ms*.

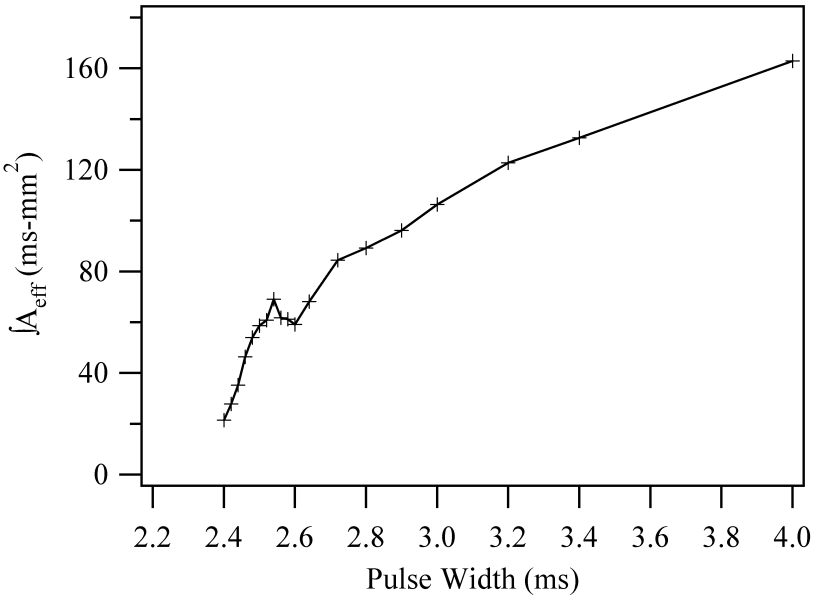

Figure 4.7: $\int A_{eff}$ for a range of pulse widths.

sensor, a steel fob was attached to the top of the solenoid plunger. Even with the addition of the steel fob, the sensor was only able to measure plunger lift up to 0.5 *mm*. While this did not give the complete lift profile, it was enough to determine when the valve was opening and closing.

The signal from the displacement transducer was monitored with a Hi-Techniques HT-600 data acquisition instrument, along with the signals from a shaft encoder attached to the crankshaft, enabling single-crankangle-degree resolution of the movement of the valve. By analyzing the crank angles at which the valve opened and closed, a start angle and duration for the valve control signal were empirically determined. The valve was intentionally closed well before exhaust port opening (EPO) because of valve bounce, and because the in-cylinder pressure reached sub-atmospheric levels in the region prior to EPO.

4.2.4 Sampled Flow From a Running Engine

The preceding tests showed that the valve should have been capable of extracting a large quantity of the cylinder contents. The only true test of the sample size, however, is to measure the flow rate of sampled gas from the SCRE.

The sample flow rate was determined by attaching a bellows flow meter downstream of the valve. A 30 foot length of 1/4" Teflon tube was attached between the valve and the bellows meter to simulate the ice bath and other tubing through which the sample must travel before reaching the emissions bench. Ideal gas behavior and a molecular weight equivalent to air were assumed for the volume to mass convertion. Also, the pressure at the bellows meter was assumed to be atmospheric, and the temperature was assumed to be 30° C.

Another important factor to be determined was the rate at which cylinder gas leaked past the valve-seat interface while the valve was not being actuated. In order to determine

this value, a high-resolution volumetric soap-bubble flow meter was constructed. Leakage rate was based on a sampling rate of one sample for every thirty fired cycles, and was expressed as a mass-percent of the sample size leaked over thirty cycles. Because the valve was not actuated during the leakage tests, combustion chamber deposits slowed down the rate of leakage. Based on qualitative observations, the actual leakage rates for the thirty cycles after sampling were approximately double the recorded values.

Figures 4.8 and 4.9 depict sample size, and the corresponding leakage rate, as a function of load, at 2000 RPM, and as a function of engine speed, respectively.

A method of estimating trapped mass is derived as part of the scavenging calculations in Chapter 5. The calculated trapped mass ranged from 0.19 to 0.23 g/cycle for the variable demand sample flow rate tests, yielding sample sizes of about 50% of the cylinder mass for that range of tests. For the variable speed tests, sample size ranged from a maximum of 66% at 1400 rpm to 33% of the cylinder mass at 3000 rpm. Past studies [1,3,6,30] implementing sampling valves have suggested that, at a minimum, between 10% and 25% of the cylinder contents must be extracted for the sample to be representative of the entire cylinder contents. Linearly extrapolating the sample data to 4000 rpm yields a sample size of 0.039 g/cycle, or 18% of the cylinder volume.

4.2.5 Effect on In-Cylinder Pressure

One other method of determining the amount of cylinder gas removed is comparing cylinder pressure of a sampled cycle to that of a motored cycle. However, determining the actual mass of gas removed based on the pressure data would require an instantaneous average cylinder temperature at some point after valve closing and before EPO.

Figure 4.10 shows fired, motored, and sampled pressure traces, as well as the valve

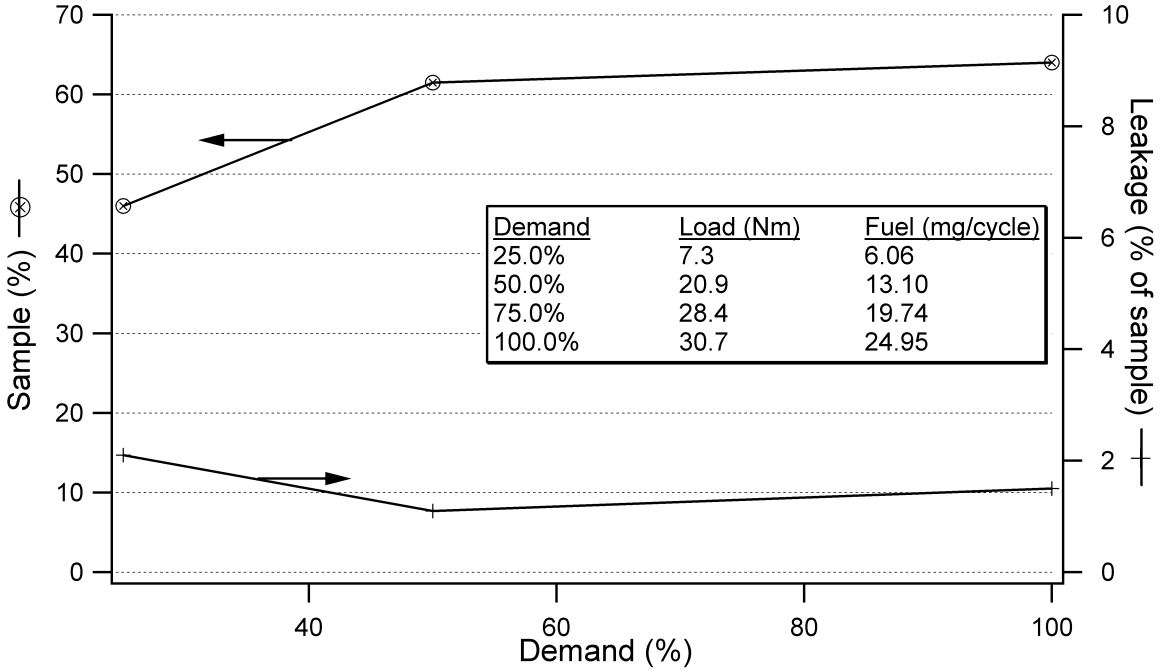

Figure 4.8: Sample size and leakage rate for variable load at 2000 rpm.

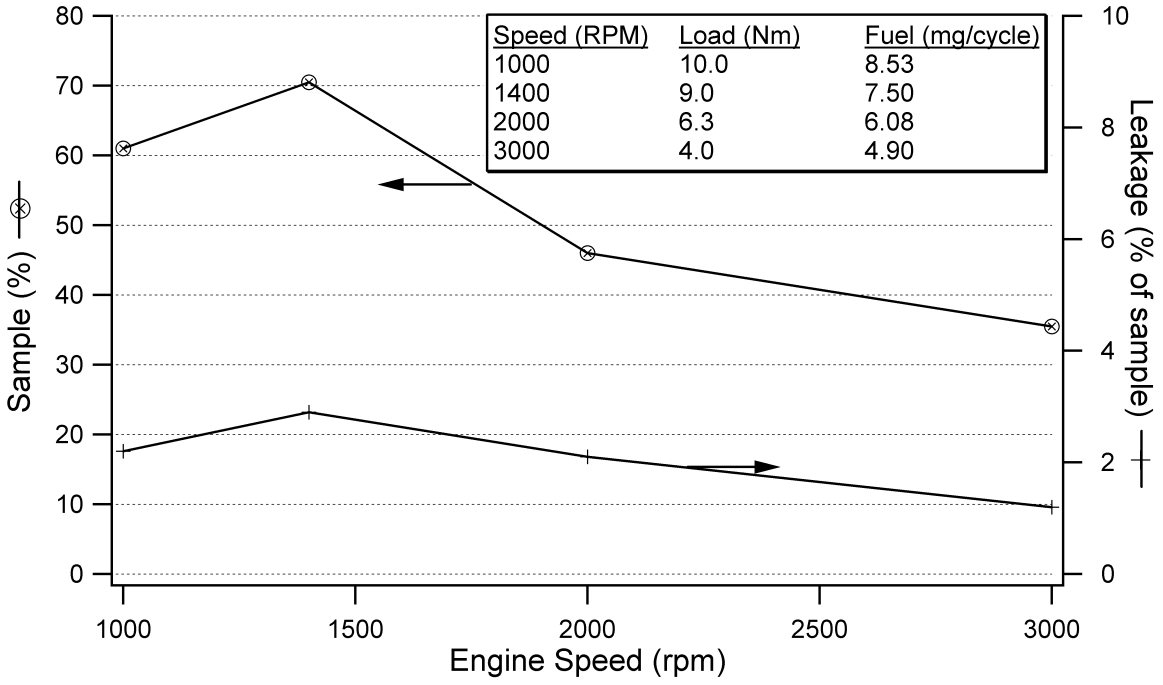

Figure 4.9: Sample size and leakage rate for variable speed.

lift profile from the displacement transducer. The lift shown is only useful for determining the beginning and end of the valve lift profile because of the limited range of the sensor. In Figure 4.10, the engine was running at 2000 RPM, with 6 *mg* of fuel being injected each cycle. The peak pressure of the sampled cycle is approximately 60% of that of the motored cycle. The location of the peak is at an earlier crank angle because the removal of gas continually lowers the cylinder pressure. Also, in the sampled cycle the pressure goes below atmospheric late in the cycle, before exhaust port opening.

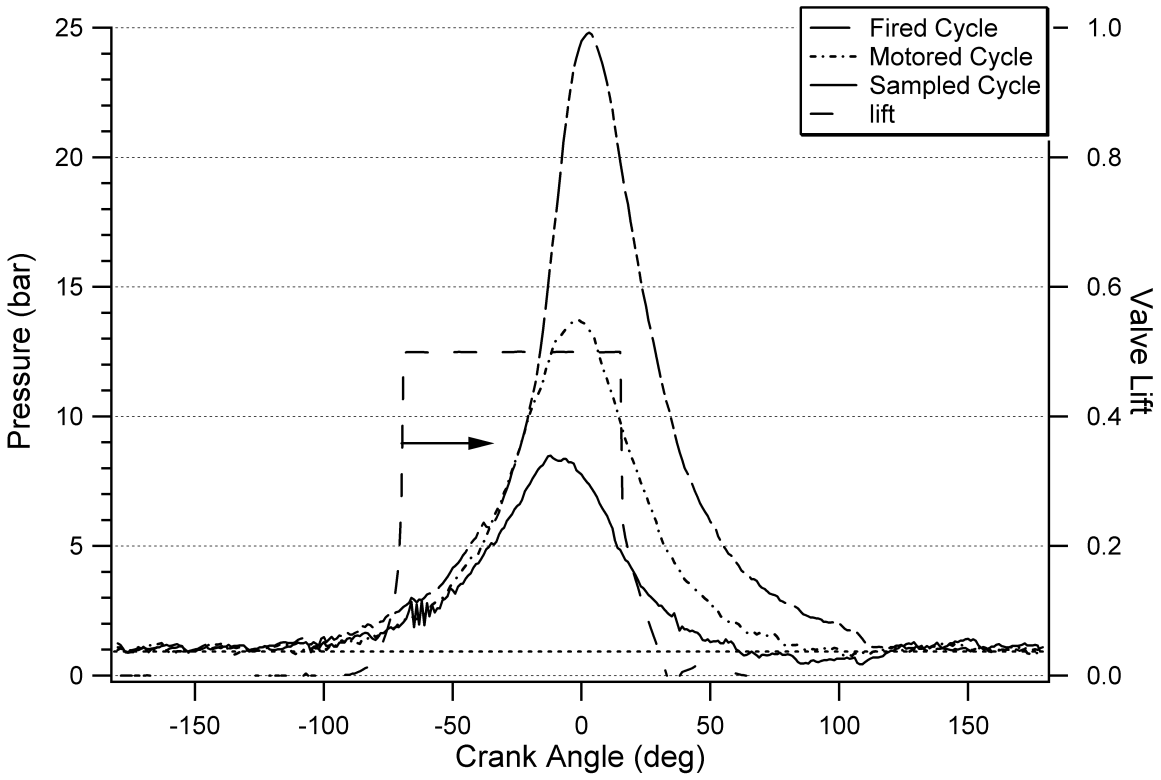

Figure 4.10: Pressure traces for fired, motored, and sampled cycles.

4.3 Conclusions

There is not necessarily a set minimum fraction of the cylinder mass which must be extracted to acquire a representative sample. The valve was able to sample between 33% and 66% of the cylinder mass, with a maximum measured leakage rate of 3% of the sample size. Past studies [1, 3, 6, 30] have suggested that between 10% and 25% of the cylinder volume is adequate to characterize the cylinder contents. This allows confidence that this valve is extracting a sample that is representative of the cylinder contents. Furthermore, the trends in the data shown in chapter 5 suggest that at the very least, this valve was not collecting some random part of a stratified mixture.

Chapter 5

Results and Discussion

This chapter discusses the results of the different experiments that were performed, as well as the experimental matrix. The investigated method for analysis of the experimental results will be discussed, as will possible reasons for trends observed in the processed data.

5.1 Engine Operating Conditions

To isolate the effect of operating parameters on the scavenging process, parameters were varied independantly while keeping as many other parameters as possible constant. Many of the parameters of concern were under direct control through either the ECU or the air-flow rate metering system. These included: delivery ratio (Λ), air/fuel (A/F) ratio, and speed. Delivery ratio was based on the definition in Equation 2.2, and A/F ratio was calculated based on delivered air. Other parameters not under direct control included the torque output of the engine, the indicated mean effective pressure (IMEP), and the coefficient of variation (COV) of IMEP. Generally these parameters were governed by fuel injection and ignition timing as well as the other controllable parameters mentioned above.

All tests were limited such that fuel injection would not occur before exhaust port

closing (EPC) because the spray from the air-assist fuel injector may interact with the scavenge flow field.

5.1.1 Variable Delivery Ratio

In general, each running condition in a set of tests proceeded as follows. The air flow rates required to maintain the desired delivery ratios were calculated before running, and set by the regulator on the orifice mass-flow metering system. For each test condition, the fuel flow rate would be set first. The injection and ignition timings were set by the ECU calibration maps, except in cases where injection was retarded to reduce the COV of IMEP. Once the fuel and ignition parameters were locked, the air delivery system was switched from drawing room air to the metered-flow system. The intake and exhaust throttle valves were then adjusted simultaneously to achieve the desired intake and exhaust pressures.

There were three variable delivery ratio (Λ^*, which is defined in Section 5.2.1) test types, one in which A/F ratio was held constant, one where fuel per cycle (FPC) was constant, and one where the fueling was controlled by the ECU. In the constant A/F ratio tests, ignition and fuel injection timings were allowed to shift to achieve the lowest COV of IMEP. In the constant FPC tests, the ignition and fuel injection parameters were held constant for all tests. Fuel was injected late in the cycle for these tests, meaning combustion was stratified. This made combustion much more likely to occur at the high Λ^* test points, where overall A/F ratio was high.

5.1.2 Variable Air/Fuel Ratio

When running tests with variable A/F ratio, speed and Λ^* were held constant. Because of this, intake air flow rate was constant. Intake and exhaust throttles were adjusted

between operating points to maintain constant surge tank and exhaust pressures. A/F ratio was adjusted based on pre-calculated air-flow and fuel-flow rates.

5.1.3 Variable Speed

For the variable speed tests, the air-flow rate was set such that the air delivered per cycle would always be the same. This meant Λ^* would be constant if the intake temperature was constant. The amount of fuel injected per cycle was also kept constant, so the A/F ratio calculated from the delivered air would, therefore, also be constant. The injection and ignition timings were allowed to float when changing speed, to prevent the COV of IMEP from changing drastically. Once a speed was selected by adjusting the dynamometer control, the fuel injection and ignition timings were locked for the duration of that test. The intake air was then switched to metered flow, and the intake and exhaust throttles adjusted to provide the desired inlet and exhaust pressures.

5.2 Analysis Methods

Although knowledge of the contents of the pre-combustion charge is very useful for engine calibration purposes, more general information about the scavenging process can be derived from pre-combustion samples and other concentrations. Scavenging and trapping efficiency are widely used generic parameters, which allow simple and straightforward comparison between different engines and port designs.

To make the scavenging parameters more meaningful, they were based on a modified delivery ratio, described below. The equations used to calculate the scavenging parameters are shown below and derived more fully in Appendix A.

5.2.1 Modified Scavenging Parameters

Delivery ratio is not a numerically meaningful quantity as defined in Equation 2.2 because the swept volume typically exceeds the trapped volume. Because of this it would be possible for the experimental scavenging efficiency, η_s, to that of perfect mixing.

If delivery ratio is defined with respect to a reference mass in the cylinder at EPC, then it is not theoretically possible to exceed η_s of the perfect displacement model without changing the density. This modified delivery ratio, Λ^*, is thus defined as:

$$\Lambda^* \equiv \frac{m_{del}}{\rho_{del} \cdot V_{EPC}} \tag{5.1}$$

where m_{del} is the mass of fresh charge delivered, ρ_{del} is the density of the delivered charge, and V_{EPC} is the cylinder volume at exhaust port closing. The delivered charge density is approximated based on the measured crankcase air temperature and the cylinder pressure at exhaust port closing. Therefore, the delivery ratio used in the analysis of all the experimental data will be Λ^*.

5.2.2 Zero-Dimensional Analysis Using Pre-Combustion Gases and Non-Isothermal Models

In order to quantify the scavenging event for comparison purposes, scavenging and trapping efficiencies are derived. Originally, data were taken with the supposition that some kind of comparison between the concentrations of the constituents in the pre-combustion charge and the exhaust could be used to calculate these parameters [3]. However, that form of analysis was flawed because it relied on dilution equations for the two constituents, which described the same physical process. So another approach was derived which only used one of the dilution equations. To close the set of equations, a two-zone non-isothermal method

for estimating trapped mass was derived, and relative concentrations of O_2, CO_2, and H_2O in the products were calculated by assuming complete stoichiometric combustion. This set of equations can be solved using either the concentration of O_2 or one of the combustion products measured from the unburned sample.

This method of calculating the scavenging parameters relies on several assumptions:

1. The sample of pre-combustion gas is representative of the total in-cylinder mixture.
2. The molecular weights of the burned gas, pre-combustion gas, and exhaust gas are equal to that of air.
3. No fuel is injected during the scavenging while the intake or exhaust ports are open.
4. The fuel reacts completely to form only CO_2 and H_2O, before the exhaust port opens.
5. The scavenging process occurs under constant pressure (P=101.5 kPa).
6. Density of the delivered charge is at pressure P and measured crankcase temperature.
7. Density of the residual charge is at pressure P and measured exhaust gas temperature.

5.2.2.1 Dilution

The first set of equations describe scavenging as a dilution process. The cylinder contents are assumed to be well mixed at EPC and EPO. Figure 5.1 illustrates the distribution of gas charges before and after the scavenging event. The retained portions of the intake charge and the combustion products are $n_{air,ret}$ and $n_{prod,ret}$ respectively, and the exhaust portions are $n_{air,ex}$ and $n_{prod,ex}$ respectively.

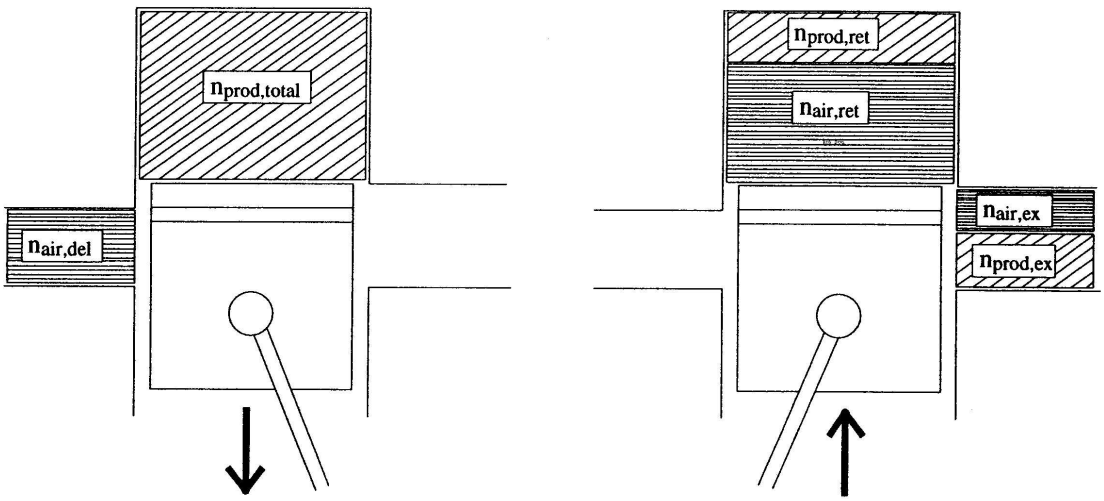

Figure 5.1: Schematic of charge division [10]

Equations 5.2 and 5.3 are mole balances for the intake charge and combustion products. $n_{air,del}$ is the molar quantity of air delivered during the scavenging process, and $n_{prod,total}$ is the molar quantity of post-combustion gases.

$$n_{air,del} = n_{air,ret} + n_{air,ex} \tag{5.2}$$

$$n_{prod,total} = n_{prod,ret} + n_{prod,ex} \tag{5.3}$$

where $n_{prod,total}$ is the content of the cylinder after combustion, and $n_{air,del}$ is the delivered charge of intake air.

Scavenging and trapping efficiency (Equations 2.5 and 2.6) can be converted to molar quantities:

$$\eta_s = \frac{m_{retain}}{m_{trap}} = \frac{MW_{air} \cdot n_{air,ret}}{MW_{air} \cdot n_{air,ret} + MW_{prod} \cdot n_{prod,ret}} \tag{5.4}$$

$$\eta_t = \frac{m_{retain}}{m_{deliver}} = \frac{MW_{air} \cdot n_{air,ret}}{MW_{air} \cdot n_{air,del}} = \frac{n_{air,ret}}{n_{air,del}} \tag{5.5}$$

where MW_{air} and MW_{prod} are the molecular weights of air and the combustion products, respectively. The scavenging equation can be further simplified if it is assumed that the molecular weight of the combustion products is approximately equal to the molecular weight of air ($MW_{prod} \approx MW_{air}$).

$$\eta_s = \frac{n_{air,ret}}{n_{air,ret} + n_{prod,ret}} \tag{5.6}$$

The molar concentration of a species in the unburned gas can be related to the retained portions of the combustion products and intake charge by the following equation:

$$X_{O_2,u} = \frac{n_{air,ret}}{n_{air,ret} + n_{prod,ret}} X_{O_2,air} + \frac{n_{prod,ret}}{n_{air,ret} + n_{prod,ret}} X_{O_2,prod} \tag{5.7}$$

where $X_{O_2,u}$, $X_{O_2,air}$, and $X_{O_2,prod}$ are the molar concentrations of oxygen in the unburned charge, intake air, and combustion products respectively. For any gas which is not present in significant quantities in atmospheric air, equation 5.7 is simplified. This is shown below for CO_2:

$$X_{CO_2,u} = \frac{n_{prod,ret}}{n_{air,ret} + n_{prod,ret}} X_{CO_2,prod} \tag{5.8}$$

where $X_{CO_2,u}$ and $X_{CO_2,prod}$ are the molar concentrations of CO_2 in the unburned charge and intake charge, respectively.

By substituting equation 5.6 into equations 5.7 and 5.8, dilution equations can be obtained with respect to scavenging efficiency.

$$X_{O_2,u} = \eta_s X_{O_2,air} + (1 - \eta_s) X_{O_2,prod} \tag{5.9}$$

$$X_{CO_2,u} = (1 - \eta_s) X_{CO_2,prod} \tag{5.10}$$

However, equations 5.9 and 5.10 describe the same physical process (dilution), so only one can be used in a set of equations.

5.2.2.2 Combustion Chemistry

By assuming complete stoichiometric combustion, the quantities of O_2 and CO_2 in the products can be related to the quantities in the unburned charge, knowing the mass of fuel delivered and the trapped mass. For high A/F ratios, this is a reasonable assumption. The following equations describe these relations for O_2 and CO_2:

$$X_{O_2,u} - \frac{m_f\left(1+\frac{n}{4}\right)}{m_{tr}}\frac{MW_{air}}{MW_{CH_n}} = X_{O_2,prod}\frac{m_{tr}+m_f}{m_{tr}} \tag{5.11}$$

$$X_{CO_2,u} + \frac{m_f}{m_{tr}}\frac{MW_{air}}{MW_{CH_n}} = X_{CO_2,prod}\frac{m_{tr}+m_f}{m_{tr}} \tag{5.12}$$

where m_f is the mass of fuel, m_{tr} is the mass of the trapped charge, and n is the hydrogen/carbon mole ratio of the fuel (see Table 3.2). See Appendix A.2 for more details.

5.2.2.3 Trapped Mass Calculation

Because post-combustion gas samples were not taken, a calculation of the trapped cylinder mass is required to solve for scavenging efficiency. Trapped mass was calculated by:

$$m_{tr} = \frac{\rho_{res}\cdot V_{EPC}}{1-\eta_s(1-\tilde{\rho})} \tag{5.13}$$

where

$$\tilde{\rho} \equiv \frac{\rho_{res}}{\rho_{del}} \tag{5.14}$$

and ρ_{del} and ρ_{res} are the densities of the delivered charge and the residual portion of the post combustion charge, respectively. This estimate is based on a two-zone non-isothermal model of the scavenging process. See Appendix A.3 for more details.

5.2.2.4 Dry to Wet Conversion

Because all emissions measurements are taken dry, a dry-to-wet conversion must be performed to derive the corresponding in-cylinder concentrations. For the purposes of this conversion, it was assumed that:

$$\frac{X_{H_2O,prod}}{X_{CO_2,prod}} = \frac{n}{2} \tag{5.15}$$

where $X_{H_2O,prod}$ is the molar concentration of water in the combustion products. This assumption is valid for complete combustion of a stoichiometric or fuel-lean mixture.

$$K \equiv \frac{n_{dry}}{n_{wet}} = 1 - (1 - \eta_s)\left(\frac{n}{2}\right) X_{CO_2,prod} \tag{5.16}$$

Sample concentrations for equations 5.9 - 5.12 are derived from:

$$X_{i,u} = K(X_{i,u})_{measured} \tag{5.17}$$

where $X_{i,u}$ is the molar concentration of the desired species. This is usually a small correction factor, on the order of three percent. This method tends to overestimate the concentration of water in the sample, because if only takes into account the concentration in the products, and neglects that of the fresh charge, which is always lower in steady-state running.

Values of η_s, m_{tr}, and $X_{O_2,prod}$ can be determined using the unburned concentration of O_2 (Equations 5.9, 5.11, 5.13, and 5.17). Also, using the unburned concentration of CO_2, values of η_s, m_{tr}, and $X_{CO_2,prod}$ can be determined (Equations 5.10, 5.12, 5.13, and 5.17). Having two sets of equations which determine scavenging efficiency and trapped mass provides a check for the solution.

5.2.3 Inclusion of Post-Combustion Gases

Previous studies [1,6] have derived scavenging efficiency by comparing pre-combustion and post-combustion cylinder concentrations (Equation 2.11), and trapping efficiency by comparing post-combustion and exhaust concentrations (Equation 2.12). This is a straightforward application of the definitions of scavenging and trapping efficiency, and relies only on the accuracy of the concentration readings.

Post-combustion samples were not taken in this set of tests with the SCRE. This was because the necessary control scheme for the ECU, which would allow the valve to be actuated without interrupting firing of the engine, has not yet been implemented. The sampling valve should be capable of opening and closing after combustion and before exhaust port opening. Follow-up testing will likely be done to correlate the results from the non-isothermal models with those from this proven method.

5.2.4 Perfect Mixing and Perfect Displacement Models

It is standard practice to compare experimental scavenging and trapping efficiencies with the perfect mixing and perfect displacement models (Equations 2.7 - 2.10). However, since the scavenging and trapping efficiencies here were calculated using non-isothermal models and Λ^*, they should not be compared with standard isothermal perfect mixing and perfect displacement models, or two-zone non-isothermal models based on Λ. Instead, the following derivations of the perfect displacement and perfect mixing models will be used (see Appendix A.4):

Perfect Displacement:

$$0 < \Lambda^* \leq 1 \quad \Rightarrow \quad \eta_s = \frac{1}{1 + \tilde{\rho}\left(\frac{1}{\Lambda^*} - 1\right)}, \quad \eta_t = 1 \tag{5.18}$$

$$1 < \Lambda^* \quad \Rightarrow \quad \eta_s = 1, \quad \eta_t = \frac{1}{\Lambda^*} \tag{5.19}$$

Perfect Mixing:

$$\eta_s = \frac{1 - e^{-\Lambda^*}}{1 - (1 - \tilde{\rho})\, e^{-\Lambda^*}} \tag{5.20}$$

$$\eta_t = \frac{\eta_{s,PM} \cdot \tilde{\rho}}{\Lambda^* \left[1 - \eta_{s,PM}\,(1 - \tilde{\rho})\right]} \tag{5.21}$$

where $\eta_{s,PM}$ is scavenging efficiency for perfect mixing.

Figure 5.2 illustrates the difference between the standard perfect displacement and perfect mixing models, and those derived above. The experimental scavenging efficiency data shown is from an experiment with a constant delivered A/F ratio of 27.5. Scavenging efficiency for perfect mixing and perfect displacement and trapping efficiency for perfect mixing may vary between experiments, because the density ratio, $\tilde{\rho}$, varies with intake and residual temperatures. In general, $\tilde{\rho}$ was between 0.33 and 0.5 for all tests.

5.3 Emissions Sampling Procedure

Because the analyzers, particularly the oxygen analyzer, were sensitive to sample flow rate, care had to be taken to ensure that the sample flow rate always matched the flow rate of span gas used to calibrate the analyzers. When sampling from the exhaust, a vacuum pump was used to draw the sample to the bench. The exhaust sample was taken from a mixing tank that was assumed to be homogeneous. Because of this, sample size was irrelevant and the flow rate of the sample could be controlled by a needle valve in the flow path.

When sampling from the cylinder, flow was driven entirely by cylinder pressure. Due to concerns of leakage past the valve guide, the sample was not drawn out of the valve

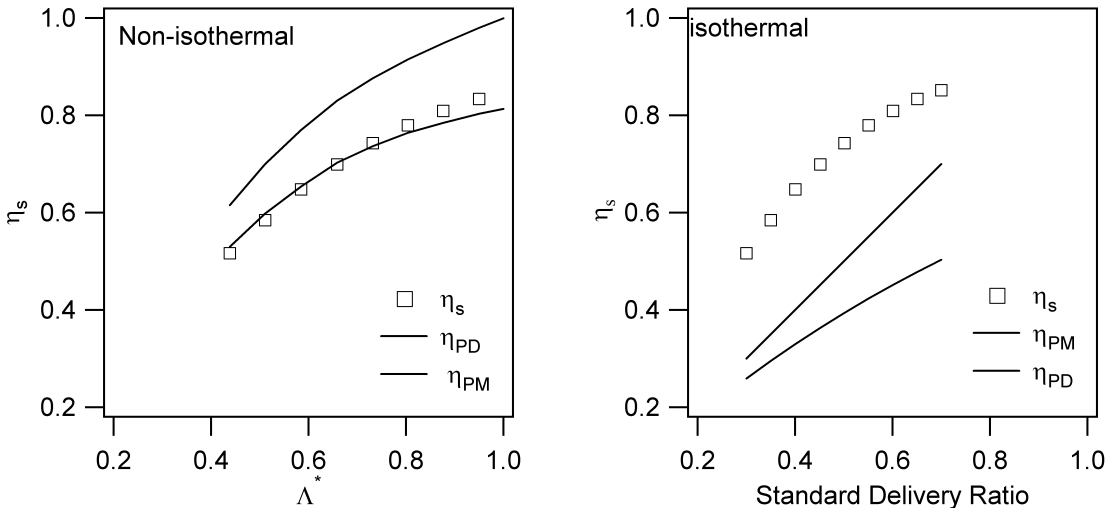

Figure 5.2: Comparison of perfect displacement and mixing models based on Λ^* to the standard models.

by vacuum. Also, the contents of the cylinder were considered inhomogeneous, so a large sample was required. Once the sample was out of the cylinder and had travelled through a filter and several feet of tubing, it was assumed to be homogeneous. A needle valve could not be used in the flow path because it would restrict the size of the sample that could be removed from the cylinder. Instead, an adjustable bypass was placed after the ice bath. A needle valve in the bypass allowed adjustment of the fraction of flow that was diverted to an exhaust, thereby controlling the flow rate through the analyzers.

5.4 Error Analysis and Reduction

The following sections will talk about some of the considerations necessary to obtain useful data from the raw data. Some checks of the analysis method will be discussed with their results.

5.4.1 Emissions Mechanisms

When sampling exhaust and pre-combustion gases for the basis of scavenging efficiency calculations, the concentrations of four gases were measured. Those gases were carbon monoxide (CO), carbon dioxide (CO_2), nitrous oxides (NO_x), and oxygen (O_2). The mechanisms by which they are formed or destroyed can help discern which may be useful for the calculation of scavenging parameters.

The formation of CO can occur at low temperatures relative to combustion temperatures. This means that the production of CO can continue in the cylinder even during and after the scavenging event. Fuel that impinged on the cylinder walls, and was not consumed during combustion due to wall quenching, may be entrained in the air during the scavenging process and react to form CO. Due to the low initial concentration of CO, this effect can cause a very significant change to the concentration of CO in the pre-combustion sample. In practice, quantities of CO in the exhaust and the pre-combustion sample were often nearly equal. For CO_2, the concentrations in the exhaust and pre-combustion sample generally differed by a factor of about three.

Carbon dioxide is one of the primary products of combustion, and as such its formation mechanisms are well known. The majority of carbon contained in the fuel molecules before combustion will be part of CO_2 by EPO. Because the reaction rate for converting CO to CO_2 at low temperatures is very slow, very little CO_2 will be produced after combustion is complete. This makes CO_2 a good choice for scavenging efficiency measurements.

While there are three main NO_x formation mechanisms, by far the predominant mechanism seen in internal combustion is thermal NO_x [13]. Thermal NO_x is generated at temperatures in excess of about 1300° C. This means NO_x formation should occur almost en-

tirely in or near the combustion products, similar to CO_2. However, a previous study [17] with the SCRE indicated that the location of NO_x in cylinder may not correlate with the location of CO_2. In this study emissions measurements were taken at the exhaust port, and were time resolved over the duration of the scavenging event. The study showed that the concentrations of NO_x, CO, and CO_2 in the sample decreased over the course of the scavenging event, as fresh charge diluted these gases. However, the concentration of NO_x consistently decreased at a rate much greater than that of the other gases. For the study of scavenging, this translated to a high concentration ratio between NO_x in the exhaust to NO_x in the pre-combustion sample.

Unlike the above gases, O_2 is consumed in the combustion reaction. During overall lean combustion, the extent of its reaction is directly related to how much fuel is injected, assuming the concentrations of unburned hydrocarbons and CO are relatively low. For stratified combustion, the existence of locally rich regions in an overall lean reaction can cause less fuel to react with the oxygen, but this generally has a small effect on the concentration of O_2. Also, because the experimental running conditions were always fuel-lean, the concentration of excess O_2 after combustion is not greatly affected by the continuing formation of CO. Therefore, O_2 concentration is another good choice for scavenging efficiency calculations.

5.4.2 Sensitivity of Scavenging Equations to Temperature and Pressure

Calculation of the mass trapped in cylinder, m_{tr}, required temperature measurements of the fresh charge and residual gas, as well as the pressure at exhaust valve closing. For the purpose of simplification, the inlet temperature is taken to be the measured crankcase

temperature. The residual temperature is approximated by the equation:

$$T_{ex} = T_{res} \cdot \eta_s \left(\frac{2 \cdot Cp_{res}}{Cp_{res} + Cp_{air}} \right) + T_{air} \left(1 - \eta_s\right) \left(\frac{2 \cdot Cp_{air}}{Cp_{res} + Cp_{air}} \right) \tag{5.22}$$

where Cp_{air} and Cp_{res} are the specific heat values of the intake air and the residual charge, respectively. The specific heat of the residual charge is estimated by:

$$Cp_{res} = X_{CO_2,prod} \cdot Cp_{CO_2} + X_{O_2,prod} \cdot Cp_{O_2} + X_{H_2O,prod} \cdot Cp_{H_2O} + \left(1 - X_{CO_2,prod} - X_{O_2,prod} - X_{H_2O,prod}\right) Cp_{N_2} \tag{5.23}$$

where the values of Cp for the in-cylinder gases are evaluated at the residual temperature. When solving for the residual temperature, several iterations are required to converge on a solution. The computer program EES (Engineering Equation Solver) greatly simplified this task. The pressure at exhaust port closing was approximated as atmospheric pressure because all tests were run with no exhaust backpressure.

The crankcase temperature is probably a good approximation of the fresh charge temperature, but the relation between the exhaust temperature and the residual temperature varies with the amount and temperature of the short-circuited charge. Also, in-cylinder pressure traces suggest that the cylinder pressure begins increasing just after intake port closing (IPC), well before exhaust port closing (EPC). For this reason it is necessary to test the sensitivity of the scavenging equations to changes in temperature and pressure. Figure 5.3 shows calculated scavenging and trapping efficiency versus Λ^* for a delivered A/F ratio of 27.5. Pressure at EPC, intake temperature, and residual temperature were all varied independently by the magnitude of their estimated error. Judging by the disparity from baseline, inlet temperature has the smallest effect on scavenging efficiency while pressure exhibited an effect several times greater than that of either of the temperature variations.

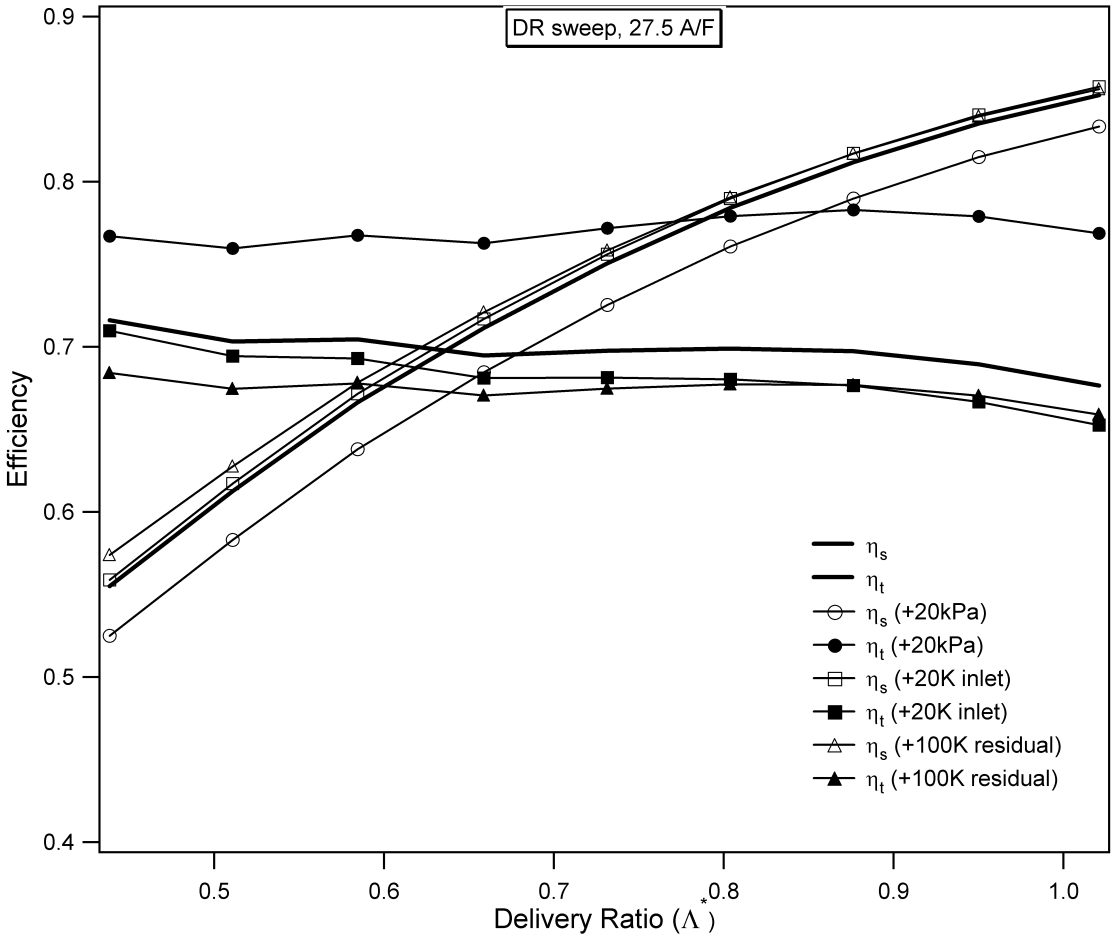

Figure 5.3: Scavenging and trapping efficiencies vs. delivery ratio for multiple inlet and residual temperatures and cylinder pressures.

5.4.3 Correlation Between Sampled Gases

The analysis of scavenging parameters has been accomplished using the concentration of CO_2 in the unburned charge. Oxygen concentration should also be a good indicator of the scavenging performance of the engine. Figure 5.4 compares scavenging and trapping efficiency calculated using the concentration of CO_2 to those calculated using the concentration of O_2. Figure 5.5 plots η_s calculated from the concentration of O_2 against η_s calculated

using CO_2, as well as the trapped mass to fuel mass ratio (m_{tr}/m_f) calculated using O_2 against m_{tr}/m_f calculated using O_2. A line of slope=1 is included to reference where the points should be for perfect agreement.

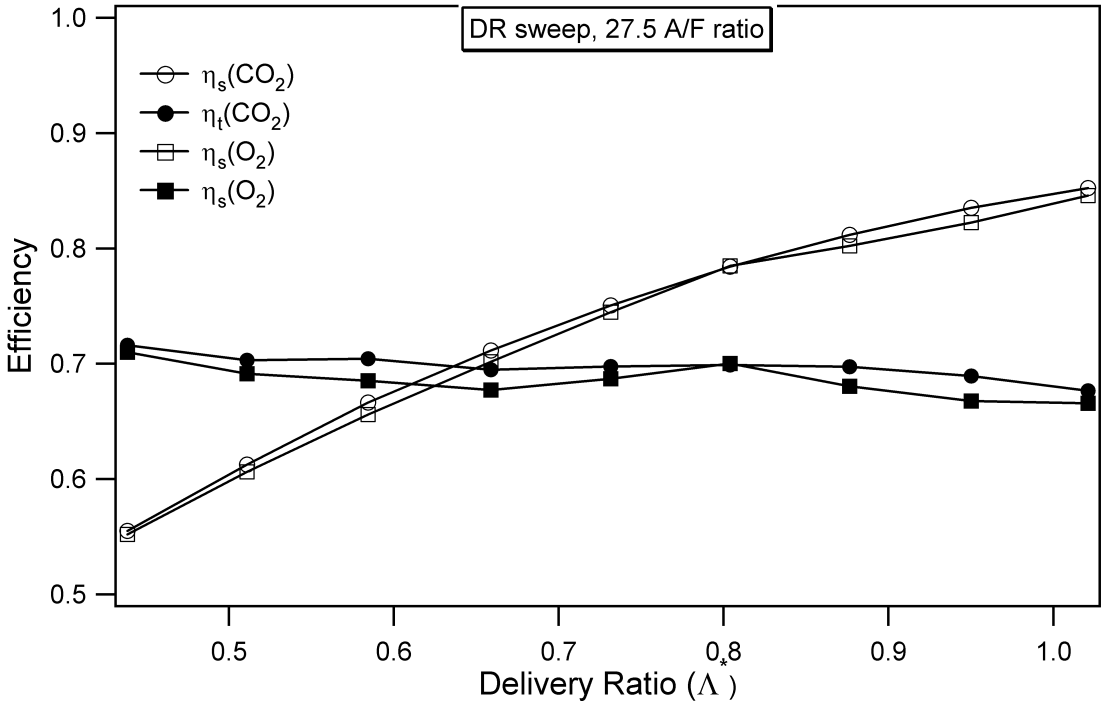

Figure 5.4: Comparison between scavenging and trapping efficiencies calculated using concentrations of CO_2 and O_2 in the pre-combustion charge.

Generally, the calculated scavenging efficiencies from the two gases were within about one percent of one another, and the trapping efficiencies were within two percent. This lends credence to the assumption that the sampled gas is representative of the cylinder contents.

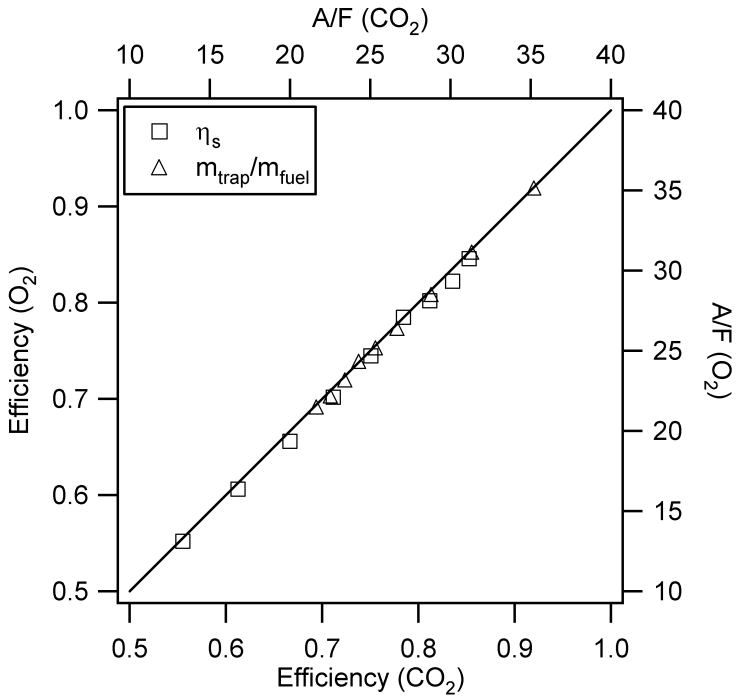

Figure 5.5: Comparison between scavenging efficiencies and trapped mass to trapped air ratios calculated using concentrations of CO_2 and O_2 in the pre-combustion charge.

5.4.4 Correlation With Measured Exhaust Gas Concentrations

The validity of the scavenging equations can be further tested by comparing the calculated concentration of the exhaust constituents to the measured values. Calculation of exhaust composition is possible through a second set of dilution equations (see Appendix A.1)

$$X_{O_2,ex} = \frac{1-\eta_t}{1+\phi_{del}} X_{O_2,air} + \frac{\eta_t+\phi_{del}}{1+\phi_{del}} X_{O_2,prod} \tag{5.24}$$

$$X_{CO_2,ex} = \frac{\eta_t+\phi_{del}}{1+\phi_{del}} X_{CO_2,prod} \tag{5.25}$$

where ϕ_{del} is the delivered fuel/air ratio, and $X_{O_2,ex}$ and $X_{CO_2,ex}$ are the concentrations of oxygen and carbon dioxide in the exhaust gas. Figure 5.6 illustrates this comparison with experimental data from a variable delivery ratio, constant A/F ratio test.

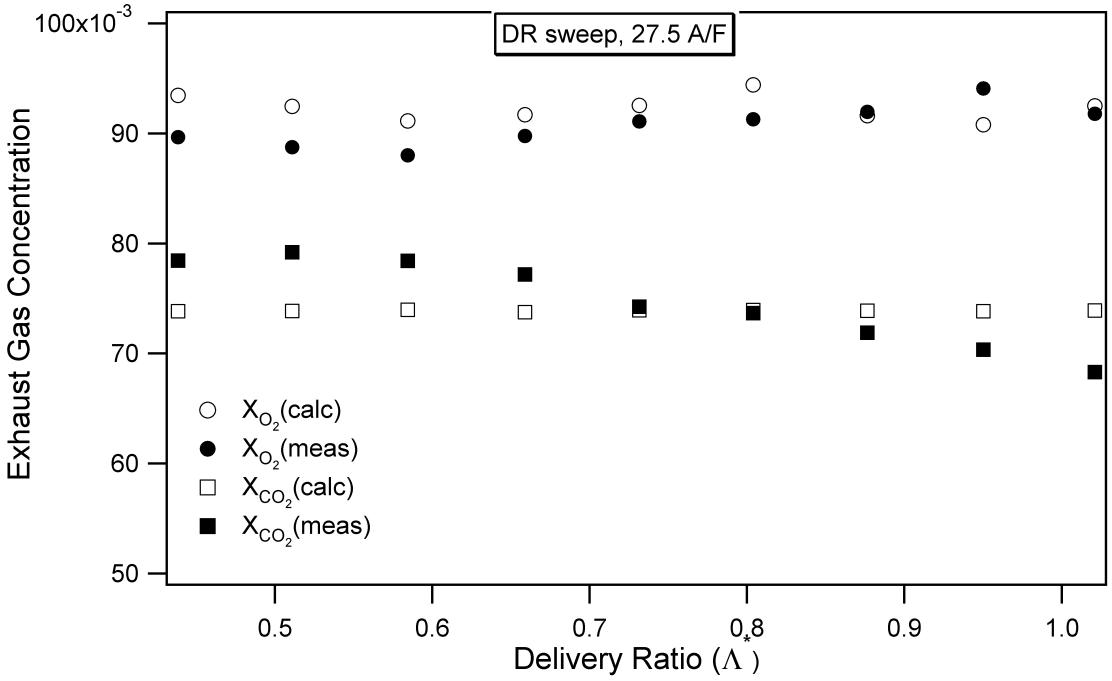

Figure 5.6: Comparison between the calculated and measured concentrations of O_2 and CO_2 in the exhaust.

The difference between the the results for O_2 are all small (less than 5% difference), while the CO_2 predicted values had slightly greater error (up to 8%). The lower accuracy of the calculated CO_2 concentration may be due in part to the fact that CO concentration was assumed to be neglegible. In this set of tests, the CO concentration in the exhaust was as high as 0.835%, 11.6% of the CO_2 concentration. Because CO requires one less oxygen atom than CO_2, the CO concentration, which has been assumed to all go to CO_2, may also effect the accuracy of the calculated oxygen concentration.

5.5 Discussion of Results

5.5.1 Scavenging and Trapping Efficiency

Several sets of tests were set up with the purpose of isolating variables for analysis. Previous scavenging studies have suggested that delivery ratio is the most important factor in the scavenging process. For this reason several test runs were designed to iterate delivery ratio while keeping other factors constant. The experiments were run based on delivery ratios calculated using the original definition (Equation 2.2), but all calculated efficiencies will be plotted against Λ^* for consistency.

Other factors of interest included A/F ratio, fueling rate, and engine speed. When varying these factors, it was important to keep delivery ratio constant. A/F ratio was calculated based on the intake air flow rate and the fuel flow rate. With the exception of the variable speed tests, all tests were run at an engine speed of 2000 RPM. With the exception of the variable delivery ratio test with constant fueling rate, all the tests were completed on the same day in which they were started. Raw data from all tests is included in Appendix B. Because the scavenging parameter equations were not formulated until after most of the data were taken, crankcase temperature data were not taken for most of the sets. For these calculations, the intake temperature was assumed to be 40°C.

5.5.1.1 Variable Delivery Ratio

The variable Λ^* with constant fuel delivery rate tests were performed over two days to check the consistency of the emissions data. The first set of data was taken for delivery ratios of 0.44, 0.59, 0.74, 0.88, 1.03, and 1.11 and the second set was taken for delivery ratios of 0.52, 0.67, 0.81, 0.96, 1.04, and 1.11. Figures 5.7 and 5.8 show the calculated scavenging

and trapping efficiencies for both sets of data, as well as the corresponding perfect mixing and perfect displacement models.

The scavenging efficiency curve is generally close to that of the perfect mixing model. This is logical, because an increased delivered charge should displace more of the post-combustion gases from the cylinder, unless the intake charge short-circuits directly to the exhaust. The perfect mixing model exceeds the experimental values at low delivery ratios, suggesting that a significant quantity of the intake charge may be short-circuiting to the exhaust early in the scavenging cycle. The downward slope of the trapping efficiency indicates that a smaller percentage of the delivered charge was being trapped in-cylinder as the delivery ratio increased. Both of these trend were expected and have been cited in previous experiments [4, 28].

The variable Λ^* constant A/F ratio tests were run for two A/F ratios, 27.5 and 41.3, as shown in Figures 5.9 - 5.10, and 5.12 - 5.12 respectively. The high A/F ratio test was not run at low delivery ratios because the amount of fuel, which required to keep the A/F ratio constant, was too low to maintain the engine running speed.

Both these tests exhibit efficiency trends similar to the constant fuel-delivery-rate tests. For each Λ^* which is run in both sets of tests, the lower A/F ratio test exhibits lower scavenging and trapping efficiencies.

The A/F ratio for these tests was estimated by dividing the mass of delivered air by the mass of delivered fuel. While the mass of delivered fuel should be indicative of the mass of fuel in-cylinder, but the mass air retained in-cylinder is dependent on the η_t as well as the mass of delivered air. After running the scavenging efficiency calculations, a more accurate representation of the overall A/F ratio in cylinder can be determined. Figures 5.13 and 5.14 compare the A/F ratios calculated by the mass of delivered air to the A/F ratios calculated by

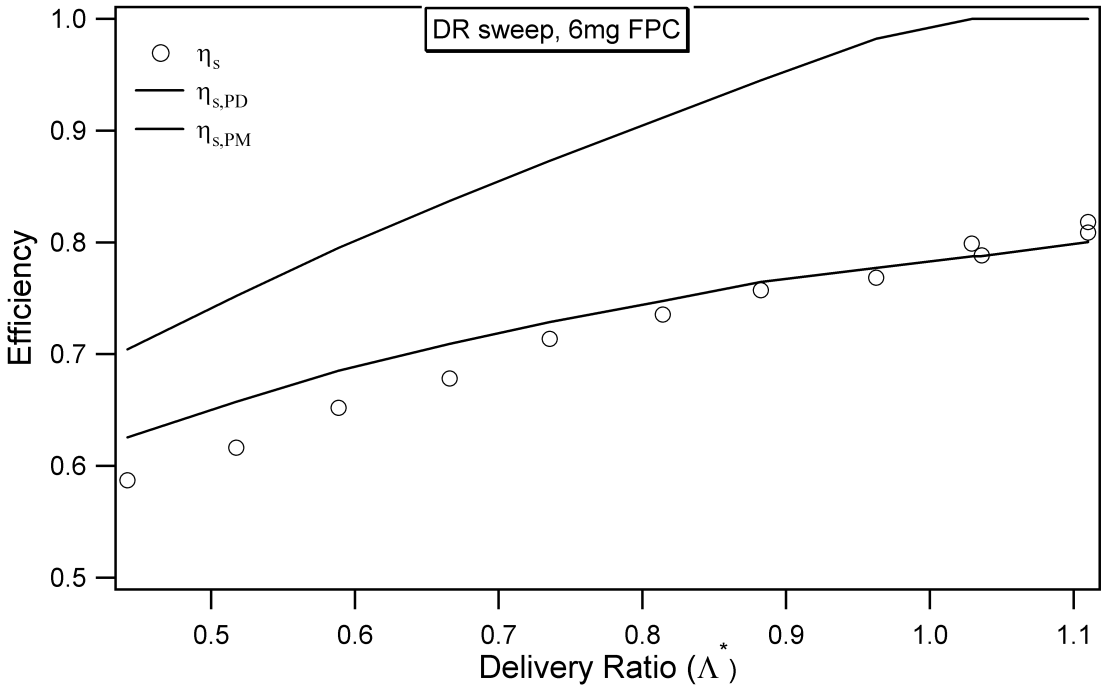

Figure 5.7: Scavenging efficiencies vs. delivery ratio for 6mg FPC

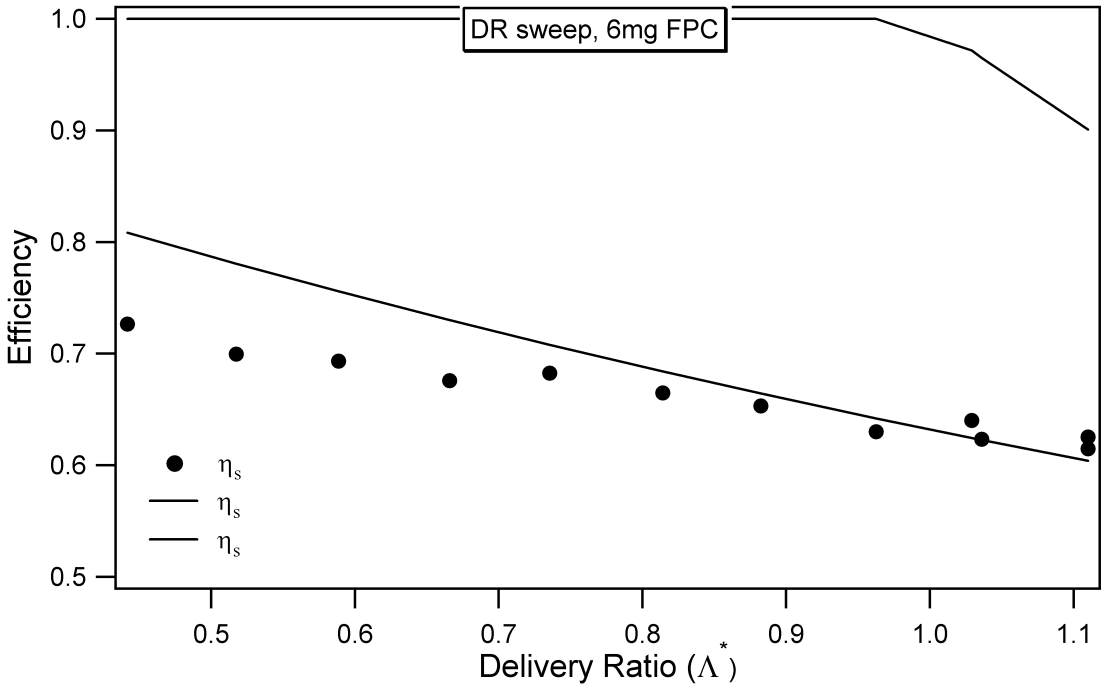

Figure 5.8: Trapping efficiencies vs. delivery ratio for 6mg FPC

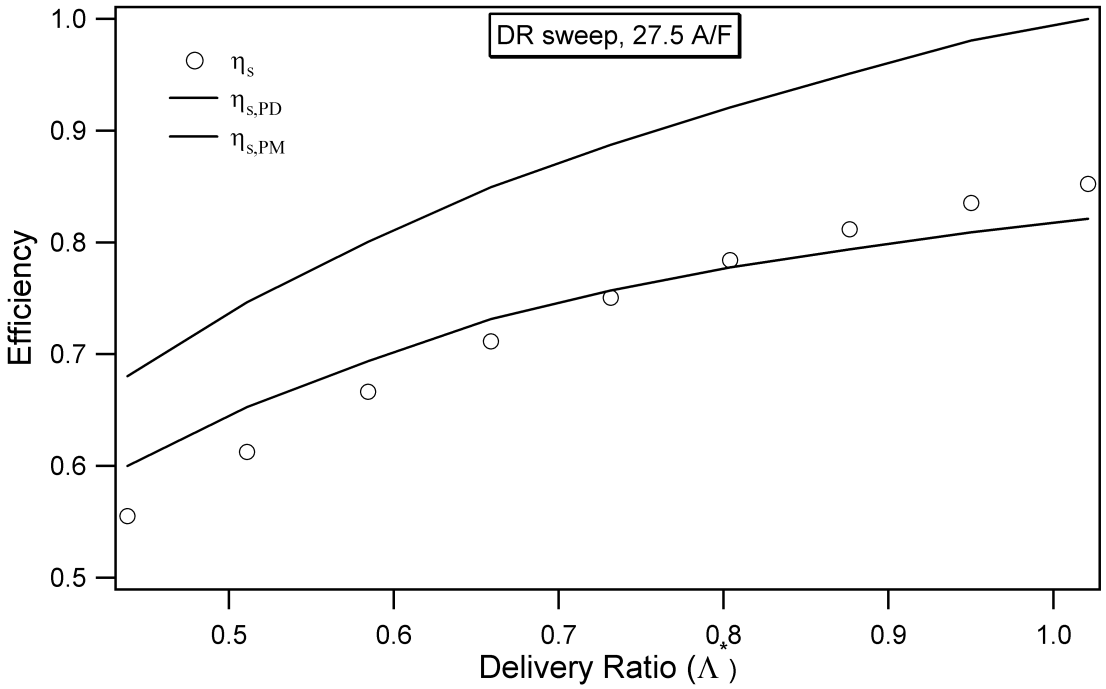

Figure 5.9: Scavenging efficiencies vs. delivery ratio for an A/F ratio of 27.5

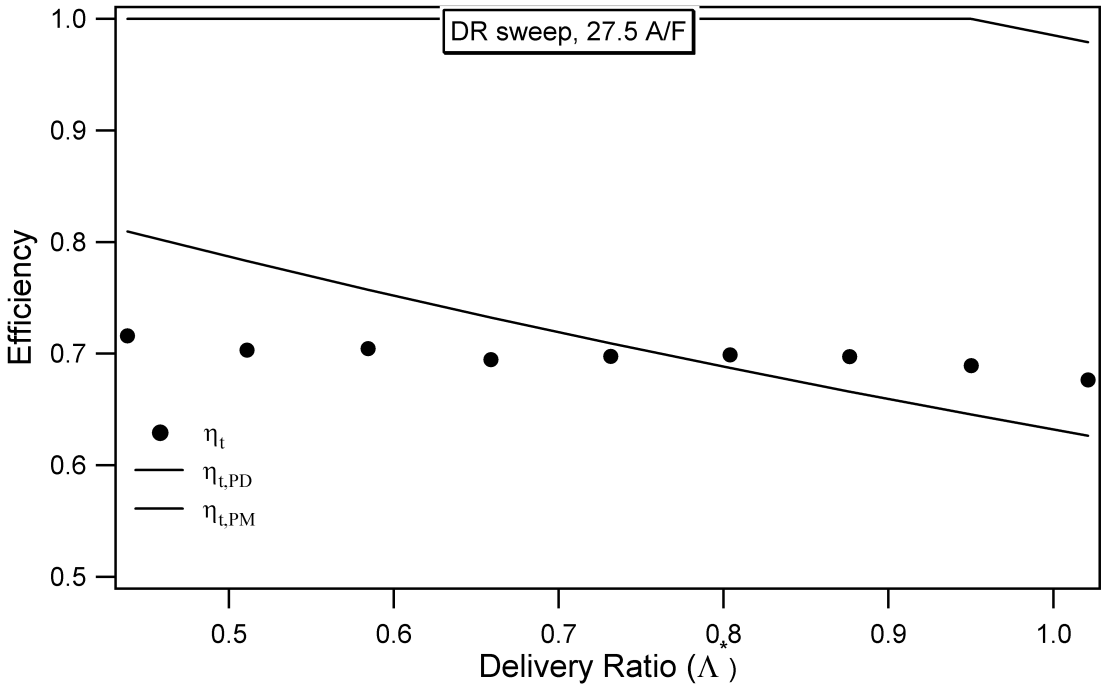

Figure 5.10: Trapping efficiencies vs. delivery ratio for an A/F ratio of 27.5

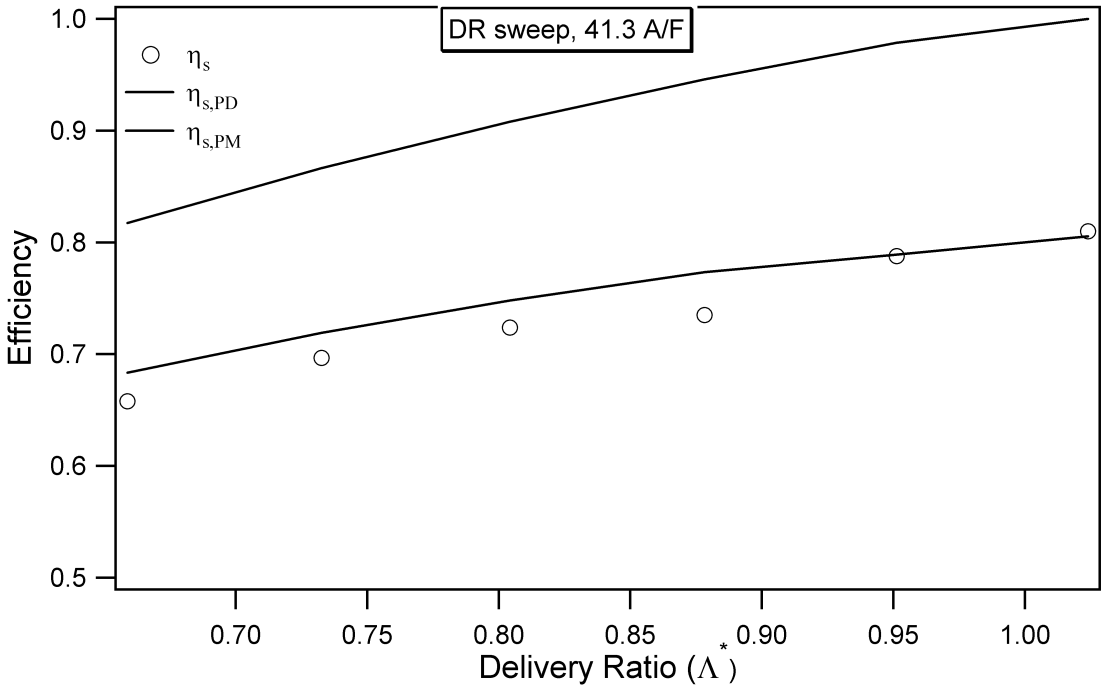

Figure 5.11: Scavenging efficiencies vs. delivery ratio for an A/F ratio of 41.3

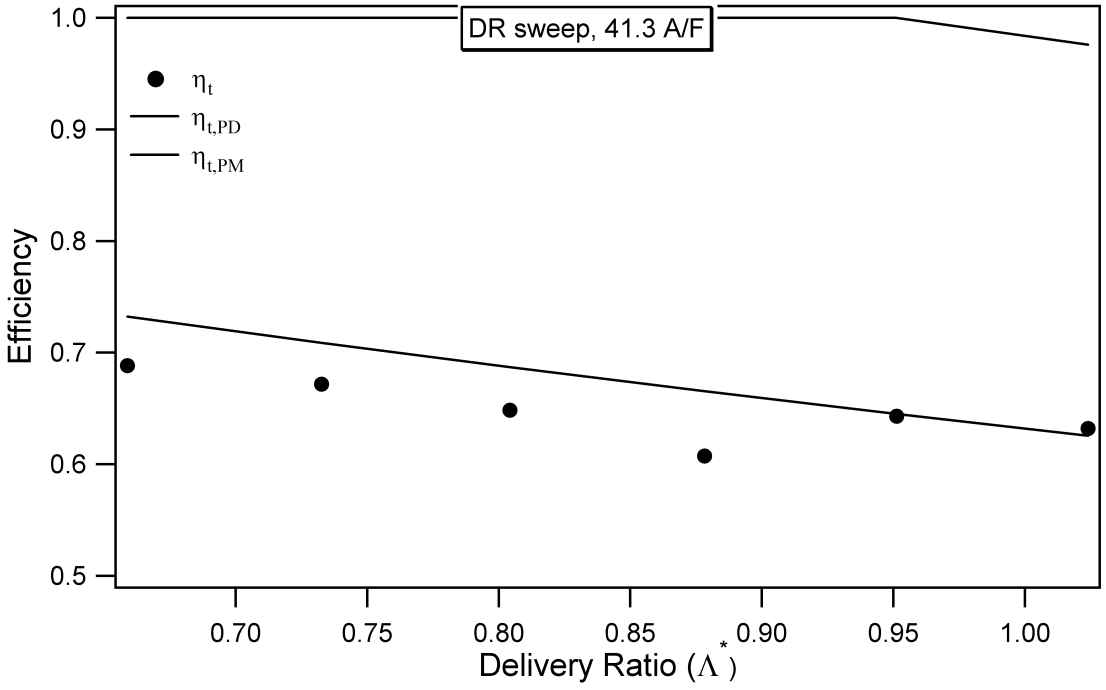

Figure 5.12: Trapping efficiencies vs. delivery ratio for an A/F ratio of 41.3

the trapped mass. The concentration of CO in the exhaust is shown, because it it generally a good indicator of changes in A/F ratio. Also, the trapped oxygen to fuel ratio is shown, because the measured A/F ratio is based on the trapped mass, which generally has a lower concentration of oxygen than air.

Comparing Figures 5.9 to 5.13 or 5.11 to 5.14 shows a correlation between trapping efficiency and A/F ratio calculated using the trapped mass. This is because, for a constant ratio of delivered air to delivered fuel, an increase in measured A/F ratio means a greater percent of the delivered charge is retained.

Another parameter of interest, and an indicator of the scavenging performance, is the trapped mass. A comparison of the calculated trapped mass for the constant A/F ratio tests is shown in Figure 5.15. The higher density of the fresh charge, as compared to the residual charge, leads to larger trapped mass at higher delivery ratios.

The final constant delivery ratio test was performed with the spark timing and fuel injection parameters controlled by the ECU map, based on the throttle position. The scavenging and trapping efficiencies for this test, as well as the perfect mixing and perfect displacement models for scavenging efficiency are shown in Figure 5.16.

The ECU map held the A/F ratio near to 21 for most of the test, except at low delivery ratio. At the lower delivery ratios the fuel was being injected earlier, so combustion was more stratified and the overall mixture could be leaner while maintaining a low COV of IMEP. With the exception of the point at $\Lambda^* = 0.59$, values of η_s and η_t are similar to the 27.5 A/F ratio test (Figure 5.9). The values of η_s and η_t at $\Lambda^* = 0.59$ derived using the sampled concentration of O_2 correlate with those calculated using CO_2, suggesting that this point is not erroneous.

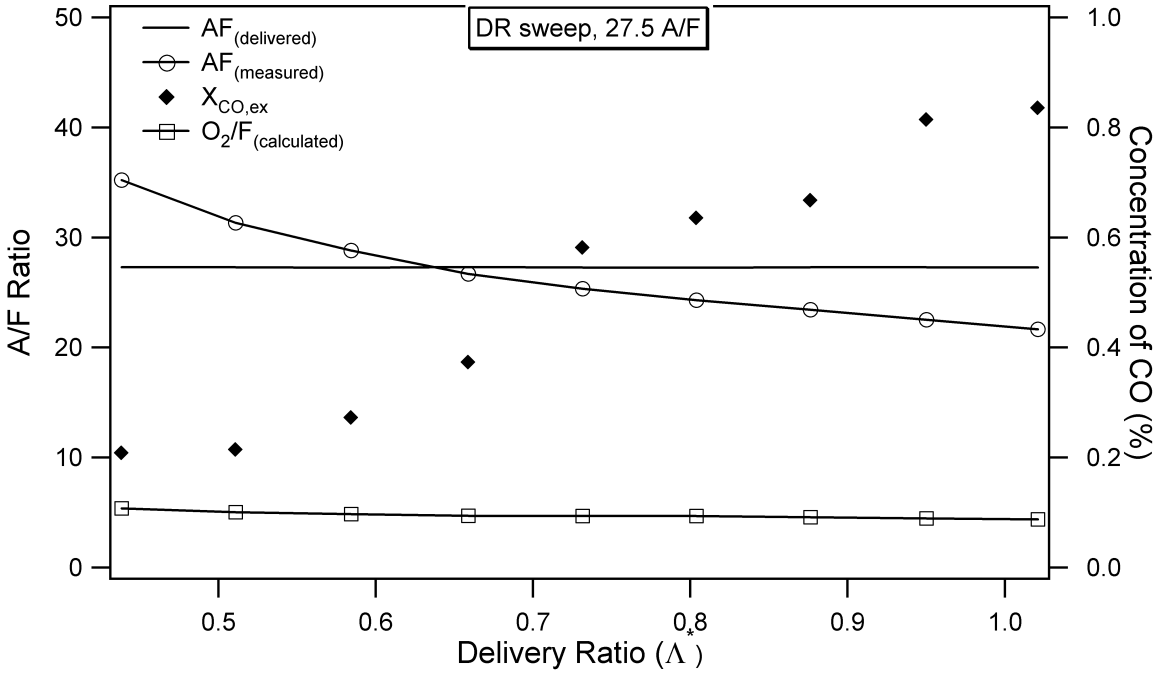

Figure 5.13: Delivered versus 'measured' A/F ratio for the 27.5 A/F ratio tests.

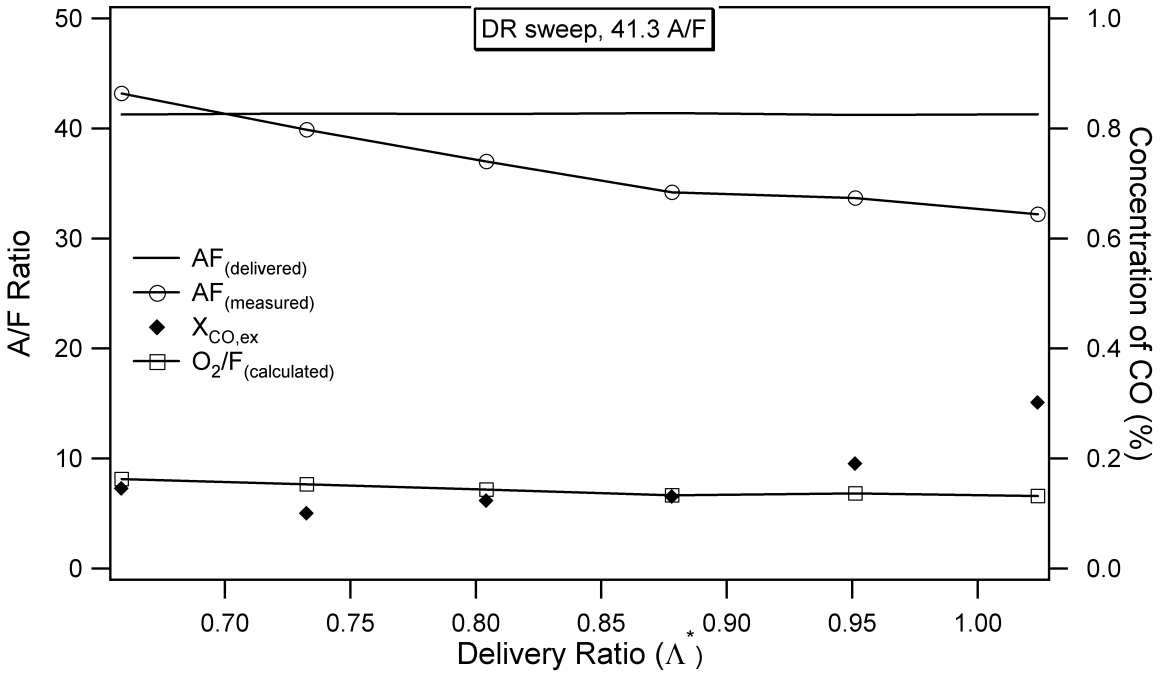

Figure 5.14: Delivered versus 'measured' A/F ratio for the 41.3 A/F ratio tests.

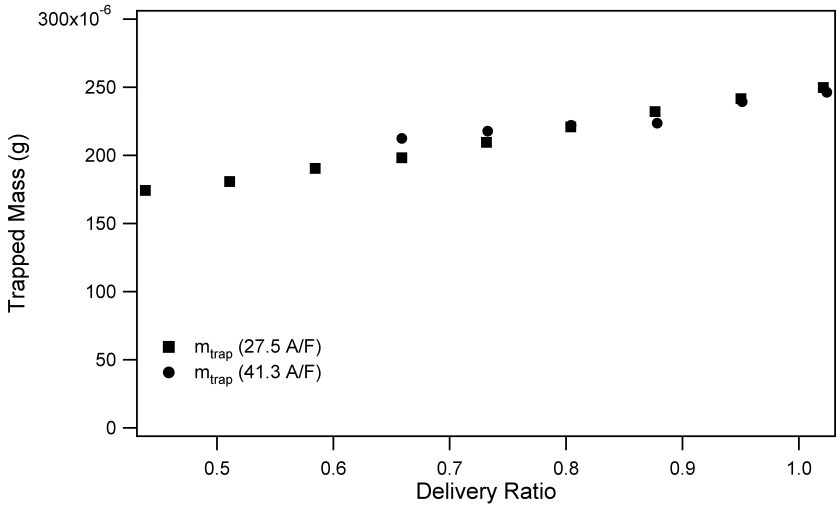

Figure 5.15: Calculated trapped mass vs. Λ^* for constant A/F ratio tests.

5.5.1.2 Variable A/F Ratio

Two sets of experiments were run varying A/F ratio while keeping Λ^* constant. Some adjustment of the exhaust backpressure and intake throttle were usually necessary to maintain Λ^* when changing running conditions. Figures 5.17 - 5.20 show the scavenging and trapping efficiencies and the corresponding perfect mixing and displacement models.

The calculated Λ^* was almost constant, because the intake temperature was approximated as 40°C. The slight downward trend of η_s with increasing A/F ratio may be simply an effect of the decreasing exhaust temperature. With accurate intake temperature, a better assessment could be made of this data.

5.5.1.3 Variable Speed

Two sets of experiments were run at variable speed, with Λ^* and delivered A/F ratio held constant. Figures 5.21 - 5.24 show the calculated scavenging and trapping efficiencies and the perfect mixing and the corresponding perfect displacement models.

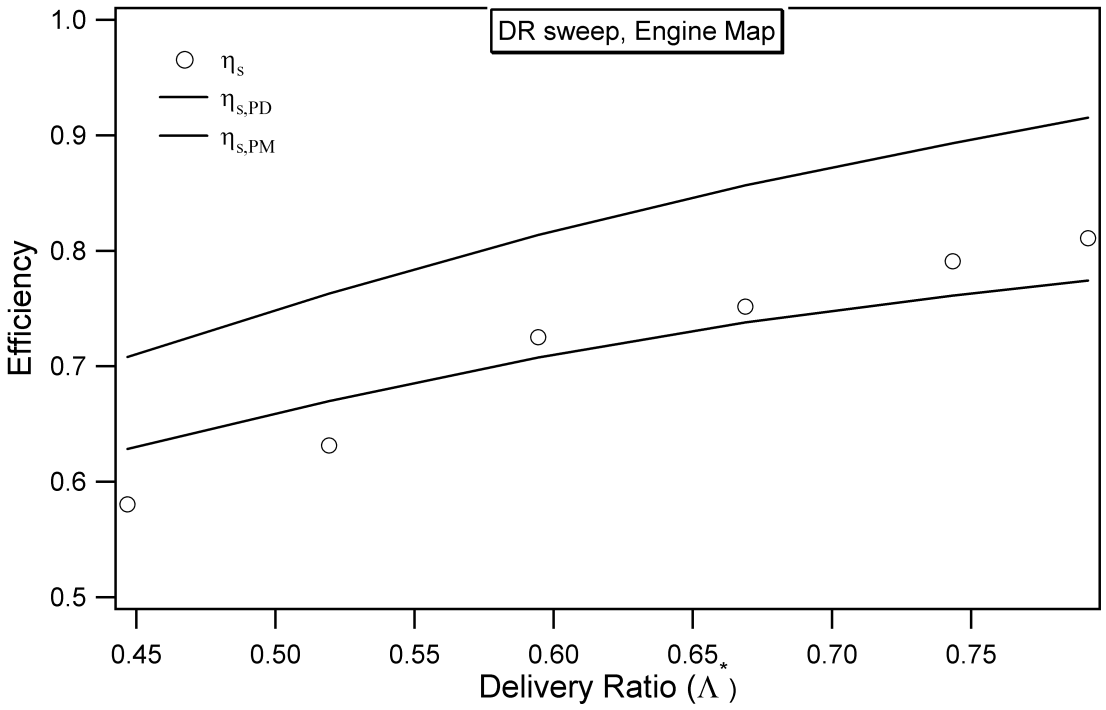

Figure 5.16: Scavenging and trapping efficiencies vs. delivery ratio with fuel delivery controlled by the engine map.

There is very little difference in η_s and η_t over the range of speeds tested. Cylinder temperature fluctuates slightly with speed changes, and this seems to correlate with the changes in scavenging and trapping efficiency.

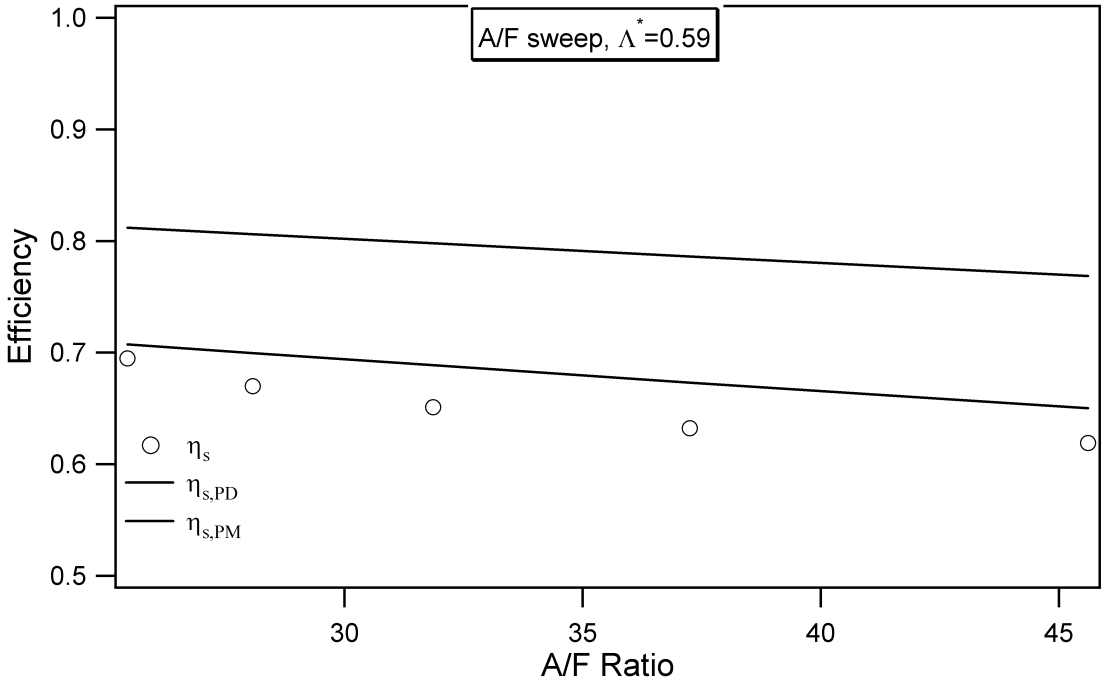

Figure 5.17: Scavenging efficiencies vs. A/F ratio for Λ^* of 0.59

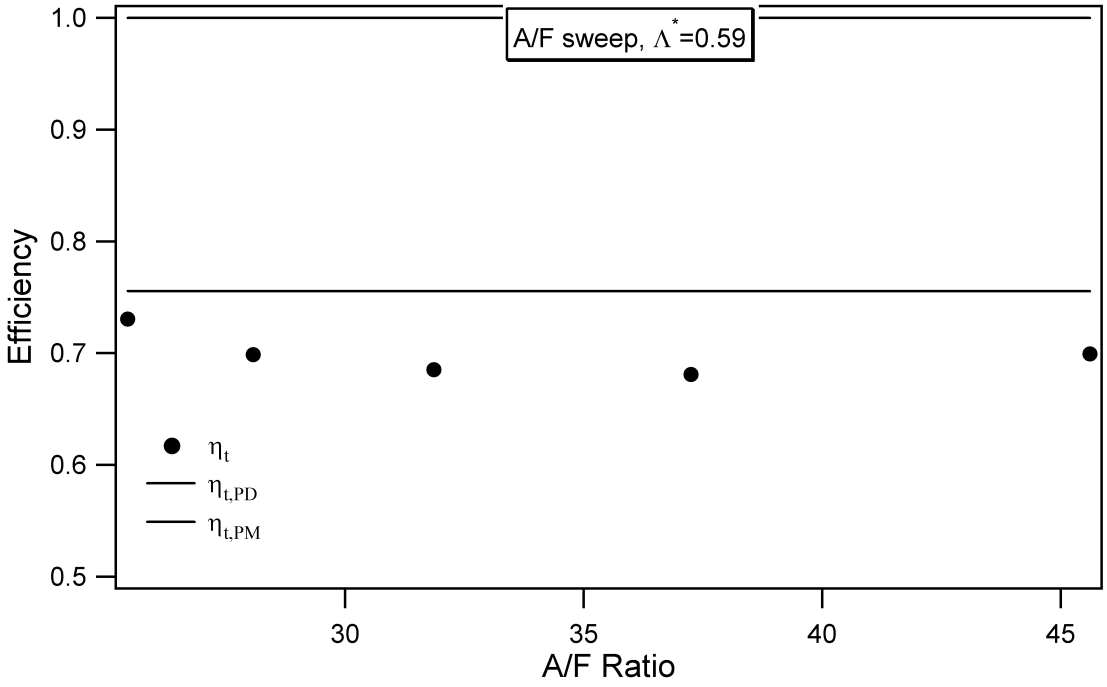

Figure 5.18: Trapping efficiencies vs. A/F ratio for Λ^* of 0.59

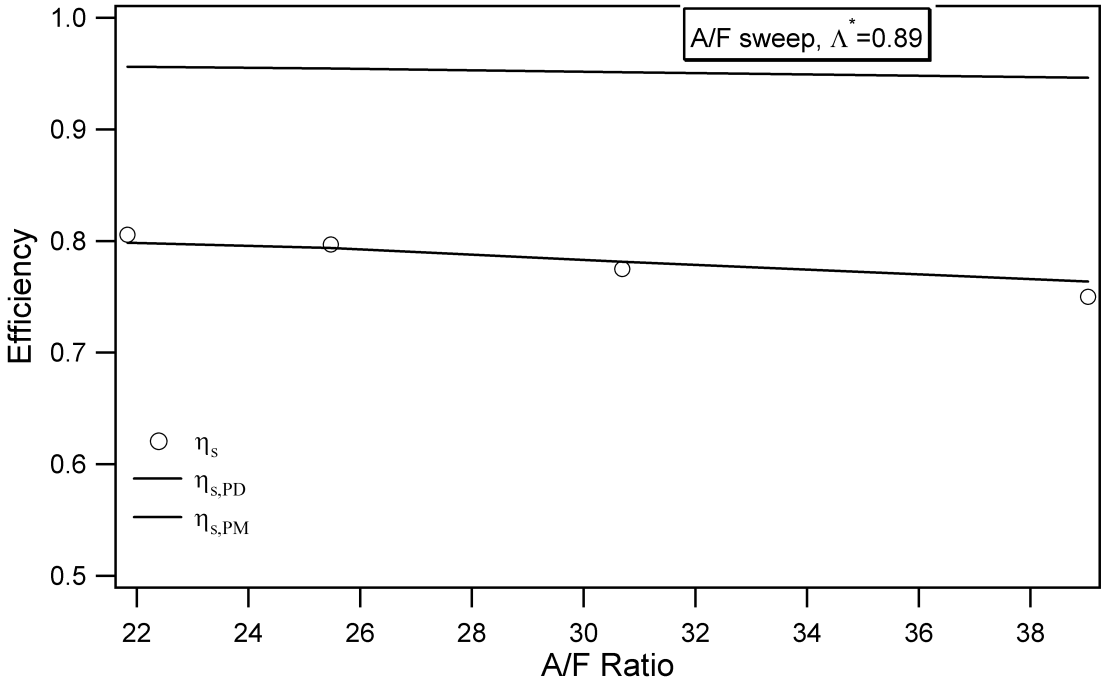

Figure 5.19: Scavenging efficiencies vs. A/F ratio for Λ^* of 0.89

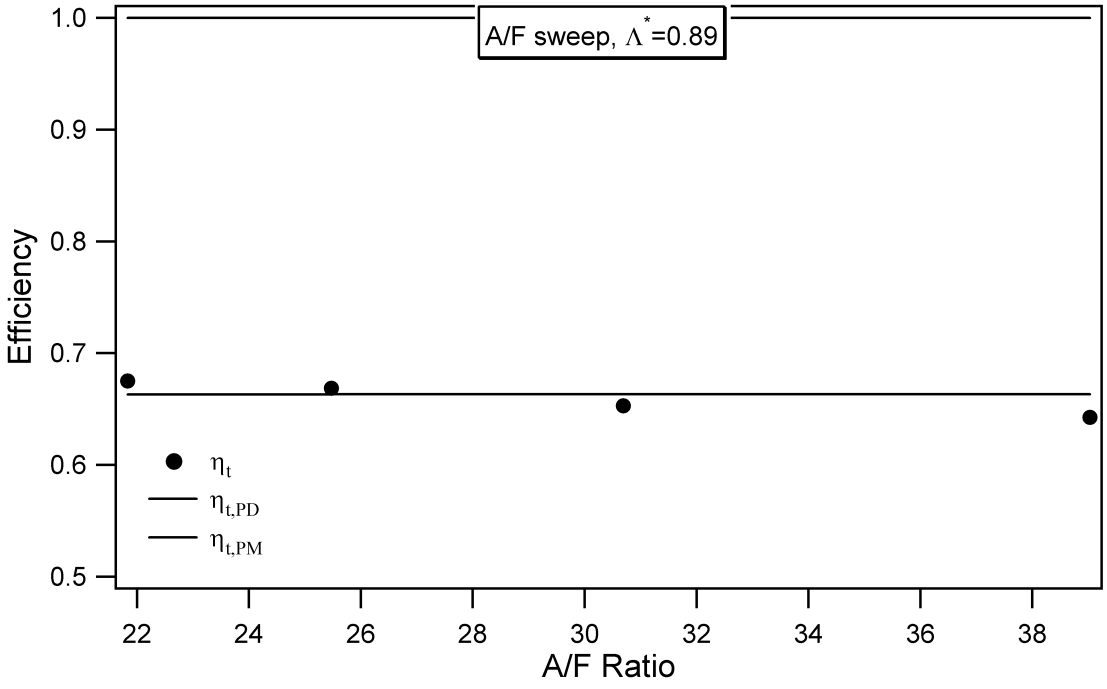

Figure 5.20: Trapping efficiencies vs. A/F ratio for Λ^* of 0.89

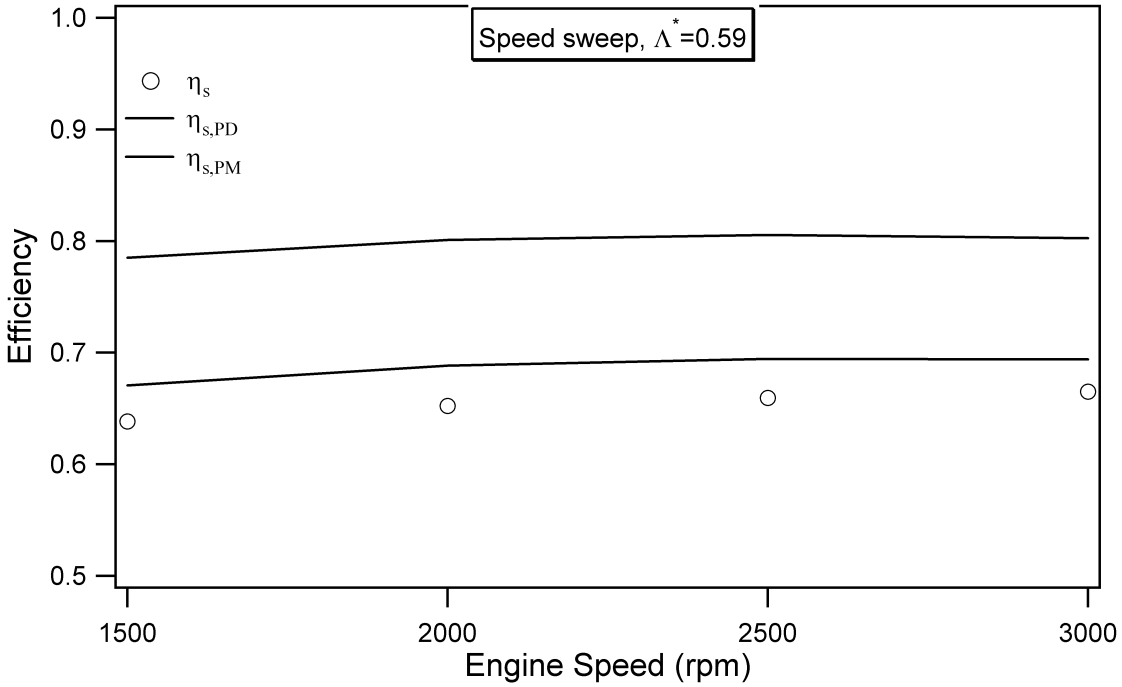

Figure 5.21: Scavenging efficiencies vs. speed for Λ^* of 0.59

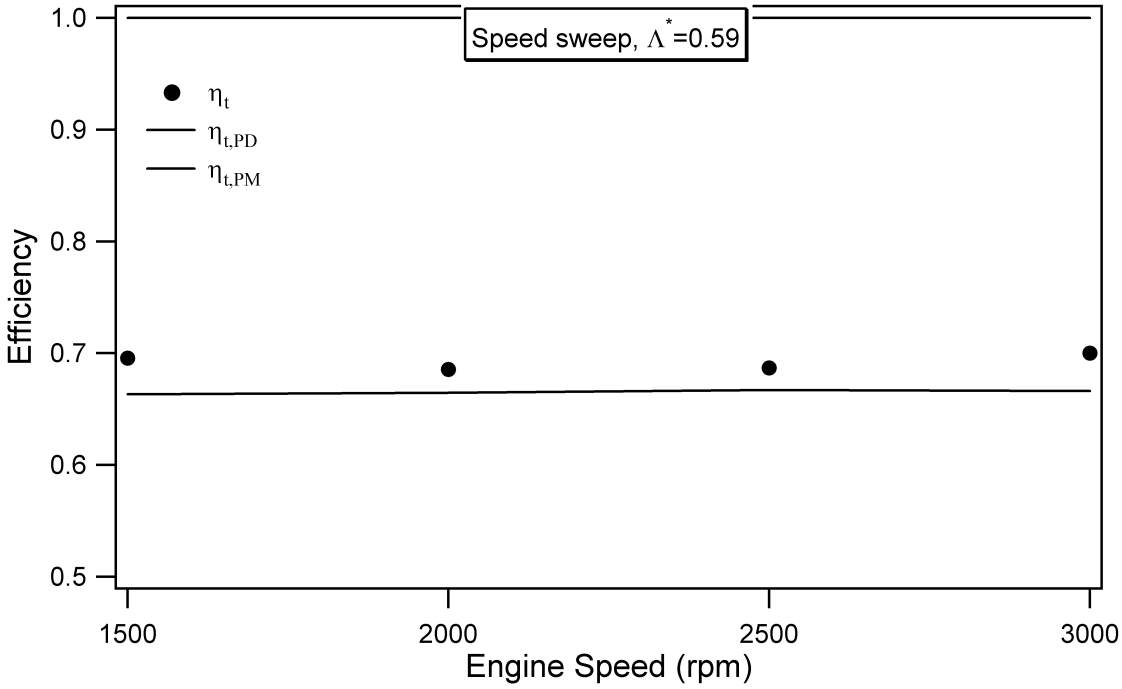

Figure 5.22: Trapping efficiencies vs. speed for Λ^* of 0.59

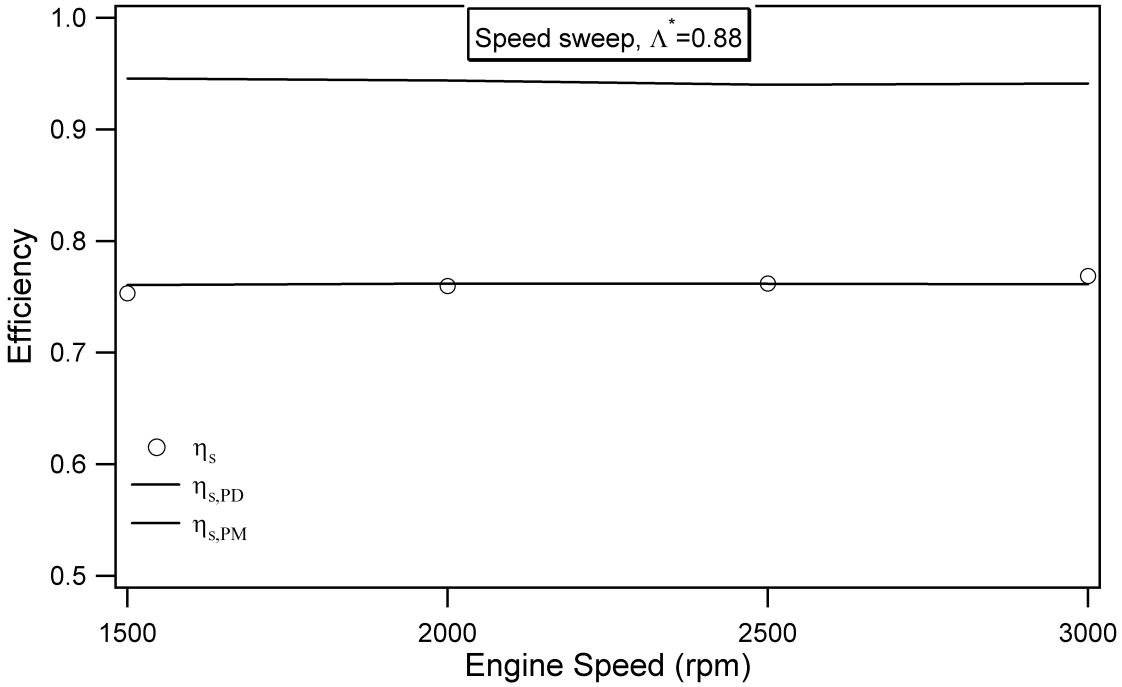

Figure 5.23: Scavenging efficiencies vs. speed for Λ^* of 0.88

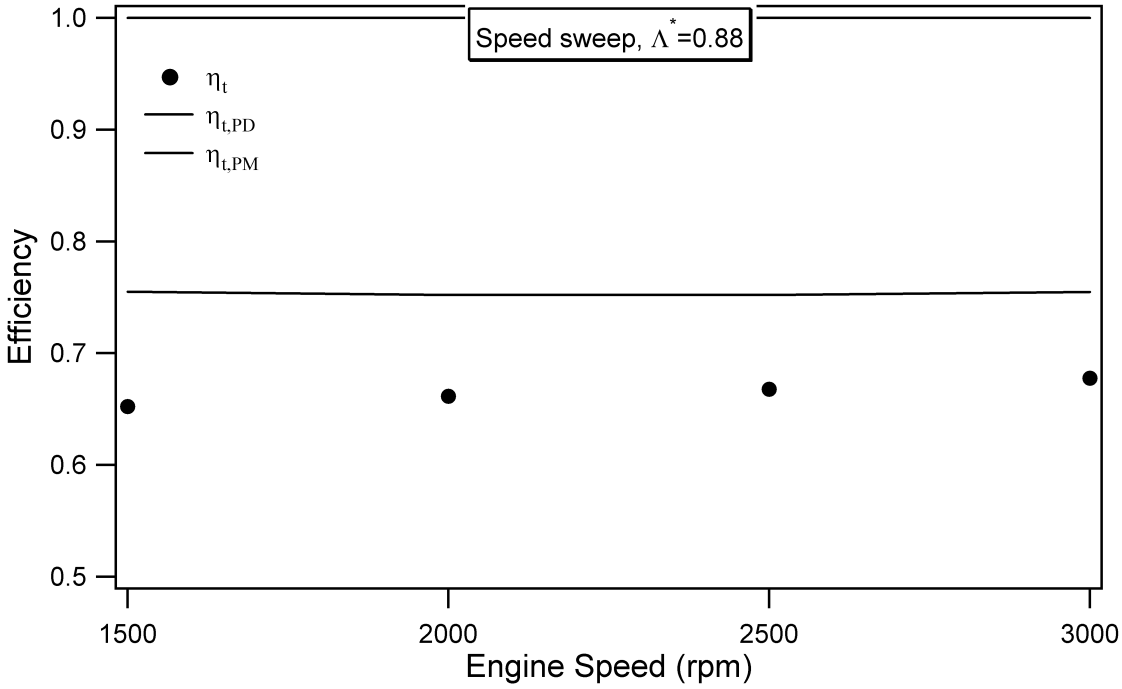

Figure 5.24: Trapping efficiencies vs. speed for Λ^* of 0.88

Chapter 6

Conclusions and Recommendations

6.1 Overview

The purpose of this research was to measure the scavenging process in a two-stroke direct-injection engine by sampling the pre-combustion trapped charge. The measured parameters necessary to solve to scavenging equations were: the concentration of either oxygen or carbon dioxide in the unburned charge, the air and fuel mass flow rates, and the temperatures of the intake air and combustion residual. The scavenging equations included: a dilution equation, which related the unburned concentration to the product concentration through the scavenging efficiency; a combustion chemistry equation, which compared the unburned concentration to the product concentration by assuming stoichiometric combustion; a trapped mass calculation, which derived the trapped mass based on density and scavenging efficiency; and a dry-to-wet conversion equation, which corrected the emissions values measured dry to true concentrations. The outputs from the scavenging equations included the scavenging and trapping efficiencies, the mass trapped in the cylinder before combustion, and the concentration of the combustion products.

The data gathering process was greatly simplified by sampling only the unburned gas, because it is difficult to get a sample that is representative of the cylinder contents during the short period after combustion and before exhaust port opening. A large sample was required to characterize the cylinder contents, partly due to the stratified-charge combustion conditions at which the direct-injected two-stroke engine runs.

6.2 Summary of Results

A valve capable of sampling a large portion of the pre-combustion gases, between exhaust port closing and exhaust port opening, during an unfired cycle that was non-intrusive to the scavenging and combustion processes during the normal cycles was developed. The valve was characterized by determining the effective area of the valve over the entire range of lift, as well as by directly measuring the sampled mass flow rate from a running engine. The valve was found to sample approximately 33% of the cylinder mass at 3000 RPM. The valve had excellent durability, a low leak rate, and required no additional cooling. Sampling occurred during a programmed dead cycle, after 20 fired cycles.

The scavenging equations solved equally well using both O_2 and CO_2. There were unsolved emission sampling problems with NO_x, which theoretically should have yielded similar results to CO_2. Carbon monoxide in the unburned sample was not a useful quantity, because production of CO continued long after the completion of combustion. Analysis of the scavenging parameters using two different constituent gases yielded almost identical results, suggesting that the sample size was adequate to overcome stratification in the cylinder. Experiments were performed to quantify the constituents of the unburned gas under different running conditions.

The experimental matrix included tests for variable delivery ratio with fuel injected

per cycle or air/fuel (A/F) ratio held constant, as well as a variable delivery ratio test in which the fueling parameters were chosen by the engine controller based on the throttle angle. All three sets of tests showed that scavenging efficiency increased and trapping efficiency decrease with increasing delivery ratio (Λ^*). In all the tests, the scavenging efficiency and trapping efficiency were close to the non-isothermal perfect mixing model.

Experiments were also performed at variable A/F ratio and constant delivery ratio. The results of these tests showed a slight decrease in scavenging efficiency with increased A/F ratio, however, the trend was too slight to be considered conclusive. Again, the scavenging and trapping efficiencies were near to the perfect mixing model.

The final set of experiments were performed at constant delivery ratio and A/F ratio with variable speed. The results showed that the scavenging efficiency increased slightly as engine speed increased, while trapping efficiency stayed constant.

6.3 Recommendations

To further verify the validity of the scavenging and trapping efficiency, and trapped mass calculations, samples should be taken after combustion and before exhaust port opening and used to calculate scavenging and trapping efficiency directly (see Section 2.3.4).

To increase the accuracy of the equations, the pressure in-cylinder should be studied to determine whether it is valid to assume that pressure is atmospheric during the scavenging period. Also, a more rigorous analysis of the combustion chemistry, especially the inclusion of CO, could increase accuracy.

The correlation between efficiencies calculated using O_2 and CO_2 was very good. Because of this, it would be possible to implement an inexpensive and portable wide-range oxygen sensor, instead of a complete emissions bench, for data collection in future tests.

After processing the constant A/F ratio data, it was discovered that a constant delivered A/F ratio did not necessarily mean that the in-cylinder ratio of trapped mass to fuel mass, or the ratio of oxygen to fuel were constant. Future experiments should be performed in which these parameters are calculated during the test runs based on the operating data, and held constant.

References

[1] T. Asanuma and S. Yanagihara. Gas sampling valve for measuring scavenging efficiency in high-speed two-stroke engines. *SAE Paper*, 70:420–433, 1962.

[2] R.S. Benson. A new gas dynamic model for the gas exchange process in two-stroke loop and cross scavenged engines. *Int. J. Mech. Sci*, 19:693–711, 1977.

[3] D.M. Bevan. Characterization of the scavenging efficiency in a direct-injection two-stroke engine. Master's thesis, Department of Mechanical Engineering, University of Wisconsin - Madison, 2000.

[4] G.P. Blair. The correlation of theory and experiment for scavenging flow in two-stroke cycle engines. *SAE Paper*, 881265, 1988.

[5] G.P. Blair. *Design and Simulation of Two-Stroke Engines*. Society of Automotive Engineers, Warrendale, PA, 1996.

[6] G.P. Blair and M.C. Ashe. The unsteady gas exchange characteristics of a two-cycle engine. *SAE Paper*, 760644, 1976.

[7] Richard R. Booy. "Evaluating Scavenging Efficiency of Two-Stroke Cycle Gasoline Engines". *SAE Paper*, 670029, 1967.

[8] T.D. Fansler and D.T. French. The scaveging flow field in a crankcase compression two-stroke engine - a three dimensional laser velocimetry survey. *SAE Paper*, 920417, 1992.

[9] R.W. Fox and A.T. McDonald. *Introduction to Fluid Mechanics*. John Wiley and Sons, Inc., New York, 1992.

[10] J.B. Ghandhi. Measurement of the scavenging efficiency of a direct-injection engine. Unpublished, 1998.

[11] J.B. Ghandhi and Martin J.K. Velocity field characteristics in motored two-stoke ported engines. *SAE Paper*, 920419, 1992.

[12] J.B. Ghandhi and S.L. Miller. Comparison of motored and fired velocities in a two stroke engine. *SAE Paper*, 982012, 1998.

[13] J.B. Heywood. *Internal Combustion Engine Fundamentals*. McGraw-Hill, New York, 1988.

[14] H.S. Hilbert and R.E. Falco. Measurements of flows during scavenging in a two-stroke engine. *SAE Paper*, 910671, 1991.

[15] B. Hopkinson. "The Charging of Two-Cycle Internal Combustion Engines". *Trans. NE Coast Instn. Engrs. Shipbuilders*, 30:433–462, 1914.

[16] E.W. Huber. Measuring the trapping efficiency of internal combustion engines through continuous exhaust gas analysis. *SAE Paper*, 710144, 1971.

[17] E. Hudak. Time-resolved exhaust measurement of a two-stroke direct -injection engine. Master's thesis, Department of Mechanical Engineering, University of Wisconsin - Madison, 1998.

[18] S. Isigami, Y. Tanaka, and M. Tamari. "The Trapping Efficiency Measurement of Two Stroke Cycle Diesel Engine by Tracer Gas Method". *Bulletin of JSME*, 6:524–531, 1963.

[19] A. Jante. "Scavenging and Other Problems of Two-Stroke Cycle Spark-Ignition Engines". *SAE*, 680468, 1968.

[20] R.G. Kenny. *Scavenging Flow in Small Two-Stroke Cycle Engines*. PhD thesis, The Queen's University of Belfast, 1980.

[21] P.C. Miles, R.M. Green, and P.O. Witze. In-cylinder gas velocity measurements comparing crankcase and blower scavenging in a fired two-stroke engine. *SAE Paper*, 940401, 1994.

[22] T. Ohira, Y. Ikeda, K Kakemizu, and T. Nakajima. In-cylinder flow measurement and its application for cyclic variation analysis in a two-stroke engine. *SAE Paper*, 950224, 1995.

[23] T. Oka and S. Ishihara. "Relation Between Scavenging Flow and Its Efficiency of a Two-Stroke Cycle Engine". *Bulletin of JSME*, 14:257–267, 1971.

[24] W. Rizk. "Experimental Studies of the Mixing Processes and Flow Configurations in Two-Cycle Engine Scavenging". *Proc. I. Mech. E.*, 172:417, 1958.

[25] SAE. *SAE Handbook, Volume 2: Parts and Components, Standards Development Program*. Society of Automotive Engineers, Warrendale, PA, 1999.

[26] D.S. Sanborn, G.P. Blair, R.G. Kenny, and A.H. Kingsbury. "Experimental Assessment of Scavenging Efficiency of Two-Stroke Cycle Engines". *SAE Paper*, 800975, 1980.

[27] D.S. Sanborn and W.M. Roeder. "Single Cycle Simulation Simplifies Scavenging Study". *SAE Paper*, 850175, 1985.

[28] E. Sher. Scavenging the two-stroke engine. *Prog. Energy Combust. Sci.*, 16:95–124, 1990.

[29] M. E. G. Sweeny, R. G. Kenny, G. B. G. Swann, and G. P. Blair. "Single Cycle Gas Testing Method for Two-Stroke Engine Scavenging". *SAE*, 850178, 1985.

[30] B.J. Tobis, Meyer R., J. Yang, D.D. Brehob, and R.W. Anderson. Scavenging of a firing two-stroke spark-ingnition engine. *SAE Paper*, 940393, 1994.

APPENDICIES

Appendix A

Equation Derivations

A.1 Dilution

The mole fraction of O_2 and CO_2 in the exhaust can be written as:

$$X_{O_2,ex} = \frac{n_{air,ex}}{n_{air,ex}+n_{prod,ex}} X_{O_2,air} + \frac{n_{prod,ex}}{n_{air,ex}+n_{prod,ex}} X_{O_2,prod}$$

$$X_{CO_2,ex} = \frac{n_{prod,ex}}{n_{air,ex}+n_{prod,ex}} X_{CO_2,prod}$$

mass balance of the products:

$$m_{prod,total} = m_{air,ret} + m_{prod,ret} + m_f = m_{prod,ex} + m_{prod,ret}$$

assuming $MW_{air} \approx MW_{prod}$:

$$n_{prod,ex} = n_{air,ret} + n_f \frac{MW_f}{MW_{air}}$$

and substitute the mole balance:

$$n_{air,del} = n_{air,ret} + n_{air,ex}$$

into the second dilution equation:

$$\begin{aligned}\frac{n_{prod,ex}}{n_{air,ex}+n_{prod,ex}}X_{CO_2,prod} &= \frac{n_{air,ret}+n_f\frac{MW_f}{MW_{air}}}{n_{air,del}+n_f\frac{MW_f}{MW_{air}}}X_{CO_2,prod}\\ &= \frac{\frac{n_{air,ret}}{n_{air,del}}+\frac{n_f}{n_{air,del}}\frac{MW_f}{MW_{air}}}{1+\frac{n_f}{n_{air,del}}\frac{MW_f}{MW_{air}}}X_{CO_2,prod}\\ &= \frac{\eta_t+\phi_{del}}{1+\phi_{del}}X_{CO_2,prod}\end{aligned}$$

For O_2 and CO_2 exhaust concentrations:

$$X_{O_2,ex} = \frac{1-\eta_t}{1+\phi_{del}}X_{O_2,air}+\frac{\eta_t+\phi_{del}}{1+\phi_{del}}X_{O_2,prod} \quad \text{(A.1)}$$

$$X_{CO_2,ex} = \frac{\eta_t+\phi_{del}}{1+\phi_{del}}X_{CO_2,prod} \quad \text{(A.2)}$$

A.2 Combustion Chemistry

Overall Mass Balance:

$$m_{air,del}+m_f = m_{prod}$$

Ideal Combustion Process:

$$CH_n+\left(1+\frac{n}{4}\right)(O_2+3.76\cdot N_2)\rightarrow CO_2+\frac{n}{2}H_2O+3.76\left(1+\frac{n}{4}\right)N_2$$

$$\begin{aligned}n_f \equiv n_{CH_n} &= \frac{m_f}{MW_{CH_n}}\\ m_{CO_2,formed} &= n_f\cdot MW_{CO_2} = m_{CO_2,f}\\ m_{O_2,consumed} &= n_f\left(1+\frac{n}{4}\right)MW_{O_2} = m_{O_2,c}\end{aligned}$$

$$m_{CO_2,u}+m_{CO_2,f} = m_{CO_2,p}$$

where $m_{CO_2,f}$, $m_{CO_2,u}$, and $m_{CO_2,p}$ are the mass of the CO_2 in the fuel, unburned charge, and products, respectively. Dividing by trapped mass:

$$\frac{m_{CO_2,u}}{m_{tr}} + \frac{m_{CO_2,f}}{m_{tr}} = \frac{m_{CO_2,p}}{m_{tr}} = \frac{m_{CO_2,p}}{m_{prod}} \frac{m_{prod}}{m_{tr}}$$

and convert to molar quantities:

$$\frac{n_{CO_2,u} \cdot MW_{CO_2}}{n_{tr} \cdot MW_{mix,u}} + \frac{n_{CO_2,f} \cdot MW_{CO_2}}{n_{tr} \cdot MW_{mix,u}} = \frac{n_{CO_2,p} \cdot MW_{CO_2}}{n_{prod} \cdot MW_{prod}} \frac{m_{prod}}{m_{tr}}$$

Assuming $MW_{mix,u} \approx MW_{mix,p} \approx MW_{air}$:

$$X_{CO_2,u} + \frac{n_{CO_2,f}}{n_{tr}} = X_{CO_2,p} \frac{m_{prod}}{m_{tr}} = X_{CO_2,p} \frac{m_{tr} + m_f}{m_{tr}}$$

And also assuming $n_{CO_2,f} = n_f$:

$$X_{CO_2,u} + \frac{m_f}{m_{tr}} \frac{MW_{air}}{MW_{CH_n}} = X_{CO_2,p} \frac{m_{tr} + m_f}{m_{tr}} \tag{A.3}$$

Likewise for O_2: (A.4)

$$X_{O_2,u} + \frac{m_f \left(1 + \frac{n}{4}\right)}{m_{tr}} \frac{MW_{air}}{MW_{CH_n}} = X_{O_2,p} \frac{m_{tr} + m_f}{m_{tr}} \tag{A.5}$$

A.3 Trapped Mass Calculation

The trapped mass is composed of the retained portion of the intake charge ($m_{air,ret}$), and the retained portion of the products ($m_{prod,ret}$):

$$m_{tr} = m_{air,ret} + m_{prod,ret}$$

$$m_{tr} = \rho_{del} \cdot V_{air,ret} + \rho_{res} \left(V_{EPC} - V_{air,ret}\right)$$

also:

$$\eta_s = \frac{m_{air,ret}}{m_{tr}} = \frac{\rho_{del} \cdot V_{air,ret}}{m_{tr}} \Rightarrow V_{air,ret} = \frac{\eta_s \cdot m_{tr}}{\rho_{del}}$$

where $V_{air,ret}$ is the volume of air retained, V_{EPC} is the cylinder volume at exhaust port closing, m_{tr} is the total trapped mass, and ρ_{del} and ρ_{res} are the densities of the delivered charge and the combustion products, respectively. It follows that:

$$m_{tr} = \eta_s \cdot m_{tr} + \rho_{res} \cdot V_{EPC} - \eta_s \cdot m_{tr} \frac{\rho_{prod}}{\rho_{del}}$$
$$m_{tr} \left[1 - \eta_s \left(1 - \frac{\rho_{res}}{\rho_{del}} \right) \right] = \rho_{res} \cdot V_{EPC}$$

and isolating m_{tr} gives:

$$m_{tr} = \frac{\rho_{res} \cdot V_{EPC}}{1 - \eta_s \left(1 - \frac{\rho_{res}}{\rho_{del}} \right)} \tag{A.6}$$

A.4 Perfect Displacement and Perfect Mixing

A.4.1 Perfect Displacement

For $\Lambda^* < 1$:

$$\eta_s = \frac{\rho_{del} \cdot V_{del}}{\rho_{del} \cdot V_{del} + \rho_{res} \cdot V_{res}}$$

where:

$$V_{EPC} = V_{del} + V_{res}$$

yields:

$$\begin{aligned} \eta_s &= \frac{\rho_{del} \cdot V_{del}}{\rho_{del} \cdot V_{del} + \rho_{res} (V_{EPC} - V_{del})} \\ &= \frac{1}{1 + \frac{\rho_{res}}{\rho_{del}} \frac{V_{EPC} - V_{del}}{V_{del}}} \\ &= \frac{1}{1 + \frac{\rho_{res}}{\rho_{del}} \left(\frac{V_{EPC}}{V_{del}} - 1 \right)} \end{aligned}$$

Also:

$$\begin{aligned}\frac{V_{EPC}}{V_{del}} &= \frac{\rho_{del}\cdot V_{EPC}}{\rho_{del}\cdot V_{del}} \\ &= \frac{\frac{1}{\Lambda^*}m_{air,del}}{\rho_{del}\cdot V_{del}} = \frac{\frac{1}{\Lambda^*}\rho_{del}\cdot V_{del}}{\rho_{del}\cdot V_{del}} \\ &= \frac{1}{\Lambda^*}\end{aligned}$$

So:

$$\eta_s = \frac{1}{1+\frac{\rho_{res}}{\rho_{del}}\left(\frac{V_{EPC}}{V_{del}}-1\right)} \tag{A.7}$$

$$\eta_t = 1 \tag{A.8}$$

For $\Lambda^* > 1$:

$$\eta_s = 1 \tag{A.9}$$

$$\eta_t = \frac{m_{air,ret}}{m_{air,del}} = \frac{\rho_{del}\cdot V_{EPC}}{m_{air,del}} = \frac{1}{\Lambda^*} \tag{A.10}$$

A.4.2 Perfect Mixing

M = trapped mass T = temperature of trapped mass

1st Law:

$$\frac{d}{dt}(M\cdot C_v\cdot T) = \dot{m}_i C_{p,i}\cdot T_i - \dot{m}_e\cdot C_{p,e}\cdot T_e \tag{A.11}$$

Ideal Gas:

$$P\cdot V = m\cdot R\cdot T \quad \rightarrow \quad \frac{d}{dt}(P\cdot V) = \frac{d}{dt}(m\cdot R\cdot T)$$

Assuming constant P and V:

$$\frac{d}{dt}(m\cdot R\cdot T) = 0$$

also:

$$M\frac{dT}{dt}+T\frac{dM}{dt}=0 \tag{A.12}$$

Using A.11 and assuming $C_{p,i}=C_{p,e}$:

$$\dot{m}_i\cdot T_i-\dot{m}_e\cdot T_e=0 \quad \rightarrow \quad \dot{m}_e=\dot{m}_i\left(\frac{T_i}{T_e}\right)$$

Mass:

$$\frac{dM}{dt}=\dot{m}_i-\dot{m}_e=\dot{m}_i\left(1-\frac{T_i}{T_e}\right)$$

From A.12

$$T-\frac{M}{T}\frac{dT}{dt}=\dot{m}_i\left(1-\frac{T_i}{T}\right)$$

$$\dot{m}_i=-\frac{M\frac{dT}{dt}}{T\left(1-\frac{T_i}{T}\right)}=-\frac{M\frac{dT}{dt}}{T-T_i} \tag{A.13}$$

Also:

$$M=\frac{P\cdot V}{R\cdot T}\rightarrow\frac{M(t)}{M_{EPC}}=\frac{P\cdot V}{R\cdot T(t)}\frac{R\cdot T_{EPC}}{P\cdot V}=\frac{T_{EPC}}{T(t)}$$

$$M(t)=M_{EPC}\frac{T_{EPC}}{T(t)}$$

From A.13:

$$\dot{m}_i=-M_{EPC}\cdot T_{EPC}\frac{\frac{dT}{dt}}{T\,(T-T_i)}$$

or:

$$\int_0^{(\Lambda^*\cdot\rho_{del}\cdot V_{EPC})}dm_i=-M_{EPC}\cdot T_{EPC}\int_{T_{blow}}^{T_{EPC}}\frac{dT}{T\,(T-T_i)}$$

$$M_{air,del}=\Lambda^*\cdot\rho_{del}\cdot V_{EPC}=-M_{EPC}\cdot T_{EPC}\int_{T_{blow}}^{T_{EPC}}\frac{dT}{T\,(T-T_i)}$$

Also:

$$\int\frac{dx}{x(bx+a)}=\frac{-1}{a}\ln\frac{bx+a}{x}$$

$$x=T \quad ; \quad b=1 \quad ; \quad a=-T_i$$

By definition $M_{EPC} = m_{tr}$:

$$\begin{aligned}
-\frac{m_{air,del}}{m_{tr}}\frac{1}{T_{EPC}} &= \left[\frac{1}{T_i}\ln\frac{T-T_i}{T}\right]_{T_{blow}}^{T_{EPC}} \\
-\frac{m_{air,del}}{m_{tr}}\frac{T_i}{T_{EPC}} &= \ln\left(\frac{T_{EPC}-T_i}{T_{EPC}}\right) - \ln\left(\frac{T_{blow}-T_I}{T_{blow}}\right) \\
-\frac{m_{air,del}}{m_{tr}}\frac{T_i}{T_{EPC}} &= \ln\left(\frac{T_{EPC}-T_i}{T_{EPC}}\frac{T_{blow}}{T_{blow}-T_i}\right)
\end{aligned} \tag{A.14}$$

Define:

$$\begin{aligned}
\mu \equiv \frac{m_{tr}}{\rho_{del}\cdot V_{EPC}} \quad \tilde{\rho} &\equiv \frac{\rho_{blow}}{\rho_i} \\
\exp\left(-\frac{\Lambda^*}{\mu}\frac{T_i}{T_{EPC}}\right) &= \frac{1-\frac{T_i}{T_{EPC}}}{1-\frac{T_i}{T_{blow}}} \\
\exp\left(-\frac{\Lambda^*}{\mu}\frac{\tilde{\rho}}{1+\eta_s(\tilde{\rho}-1)}\right) &= \frac{1-\eta_s}{1+\eta_s(\tilde{\rho}-1)}
\end{aligned} \tag{A.15}$$

Also:

$$\mu = \frac{\tilde{\rho}}{1-\eta_s(1-\tilde{\rho})}$$

$$\begin{aligned}
T_{EPC} &= \eta_s\cdot T_i + (1-\eta_s)T_{blow} \\
\frac{T_{EPC}}{T_i} &= \eta_s + (1-\eta_s)\frac{T_{blow}}{T_i} \quad \left(\frac{T_{blow}}{T_i} = \frac{\rho_i}{\rho_{blow}} = \frac{\rho_{del}}{\rho_{res}}\right) \\
&= \eta_s + (1-\eta_s)\frac{\rho_{del}}{\rho_{res}} \\
&= \eta_s + \frac{1}{\tilde{\rho}}(1-\eta_s) = \frac{(\tilde{\rho}-1)\eta_s + 1}{\tilde{\rho}}
\end{aligned}$$

$$\frac{T_i}{T_{EPC}} = \frac{\tilde{\rho}}{1-(1-\tilde{\rho})\eta_s} \tag{A.16}$$

$$
\begin{aligned}
-\frac{m_{air,del}}{m_{tr}}\frac{T_i}{T_{EPC}} &= \ln\left(\frac{T_{EPC}-T_i}{T_{EPC}}\frac{T_{blow}}{T_{blow}-T_i}\right) \\
\exp\left[-\frac{m_{air,del}}{\rho_{del}\cdot V_{EPC}}\frac{\rho_{del}\cdot V_{EPC}}{m_{tr}}\frac{\tilde{\rho}}{1-(1-\tilde{\rho})\eta_s}\right] &= \left(1-\frac{\tilde{\rho}}{1-(1-\tilde{\rho})\eta_s}\right)\left(\frac{1}{1-\frac{\rho_{res}}{\rho_{del}}}\right) \\
\exp\left[-\frac{\Lambda^*}{\mu}\frac{\tilde{\rho}}{1-(1-\tilde{\rho})\eta_s}\right] &= \frac{1-(1-\tilde{\rho})\eta_s-\tilde{\rho}}{1-(1-\tilde{\rho})\eta_s}\frac{1}{1-\tilde{\rho}}
\end{aligned}
$$

$$
m_{tr} = \frac{\rho_{res}\cdot V_{EPC}}{1-\eta_s\left(1-\frac{\rho_{res}}{\rho_{del}}\right)}
$$

$$
\mu \equiv \frac{m_{tr}}{\rho_{del}\cdot V_{EPC}} = \frac{\frac{\rho_{res}}{\rho_{del}}}{1-\eta_s\left(1-\frac{\rho_{res}}{\rho_{del}}\right)} = \frac{\tilde{\rho}}{1-\eta_s(1-\tilde{\rho})}
$$

$$
\begin{aligned}
\exp\left[-\Lambda^*\right] &= \frac{(1-\tilde{\rho})(1-\eta_s)}{1-(1-\tilde{\rho})\eta_s}\frac{1}{1-\tilde{\rho}} \\
&= \frac{1-\eta_s}{1-(1-\tilde{\rho})\eta_s} \\
\exp\left[\Lambda^*\right]-(1-\tilde{\rho})\exp(-\Lambda^*)\eta_s &= 1-\eta_s \\
\eta_s\left[1-(1-\tilde{\rho})\exp(-\Lambda^*)\right] &= 1-\exp(-\Lambda^*)
\end{aligned}
$$

$$
\eta_s = \frac{1-\exp(-\Lambda^*)}{1-(1-\tilde{\rho})\exp(-\Lambda^*)} \tag{A.17}
$$

Appendix B

Raw Data

Description of Test:														
Date	Ambient Temp (ºC)		Ambient Pressure (kPa)		Humidity	Coolant Temp		P_abs (psi)		Data Taker				
29.05.02	21.8		99.2		74%	48		14.25		H. Zach Foudray				
Notes:														
12 CA deg per 1ms at 2000rpm. A "u" or "s" at the end of a Hi-Techniques file indicates a test run that unsampled (meaning emissions measurements are taken from the exhaust) or sampled(emissions measurements taken from the cylinder), respectively.														
Run Number		**4**		**3**		**1**		**5**		**2**				
Time		1036	1043	1009	1022	915	925	1055	1104	944	955			
Hi-Techniques File		z_AF_conDR_5-29_4				z_AF_conDR_5-29_1								
Injector		orbital		orbital		orbital		orbital		orbital				
Spark Plug Type	Champion	RC10ECC		RC10ECC		RC10ECC		RC10ECC		RC10ECC				
Spark Plug Projection	mm	12		12		12		12		12				
Engine Speed	RPM	2000	2000	2000	2000	2000	2000	2000	2000	2000	2000			
Orifice Upstream Press	kPa	267.6	267.6	267.5	267.4	267.6	267.5	267.6	267.5	267.4	267.8			
Orifice Size	#	4		4		4		4		4				
Intake Air Flowrate	kg/hr	21.80	21.80	21.79	21.78	21.80	21.79	21.80	21.79	21.78	21.81			
Delivery Ratio		0.4003	0.4003	0.4001	0.4000	0.4003	0.4001	0.4003	0.4001	0.4000	0.4006			
Measured A/F Ratio		40.4	40.4	34.6	34.6	30.3	30.3	26.9	26.9	24.2	20.7			
Throttle Position (TPS)	%	22.0	21.8	22.1	21.7	21.79	21.79	21.7	21.3	21	20.89			
Inlet Surge Tank Press	kPa	99.2	99.2	99.2	99.2	99.2	99.3	99.2	99.2	99.3	99.2			
Exh Surge Tank Press	kPa	99.2	99.2	99.2	99.2	99.2	99.3	99.2	99.2	99.3	99.2			
Exhaust Back-Pressure	kPa	0.0	0.0	0.0	0	0	0	0.0	0	0.0	0			
Oil Flowrate	kg/hr of fuel	0.542	0.541	0.635	0.635	0.717	0.718	0.813	0.813	0.893	0.892			
Ignition Timing (actual	ºBTDC	41.000		40.563		40.000		38.500		37.875				
SOA Timing	ºBTDC	64.188		69.563		72.000		73.313		75.625				
EOA Timing	ºBTDC	34		34		34		34		34				
Fuel Pressure	psi	95		95		95		95		95				
Fuel/cycle	mg	4.50		5.25		6		6.75		7.5				
NOx (dry)	ppm	210.29	86.97	437.85	156.7	550.27	150.28	552.56	128.6	557.72	118.66			
CO2 (dry)	%	5.348	2.795	6.593	3.224	7.491	3.459	8.150	3.598	8.635	3.524			
CO (dry)	%	0.191	0.097	0.126	0.112	0.169	0.214	0.477	0.500	0.969	0.794			
O2 (dry)	%	13.312	16.908	11.692	16.200	10.326	15.724	9.259	15.303	8.103	15.152			
Engine Load	N-m	4.700	3.710	7.020	5.780	8.460	7.260	9.780	8.810	10.960	9.850			
Fuel Flowrate	mg/s	150	150	175	175	200	200	225	225	250	250			
Exhaust Gas	ºC	310.0	296.0	374.0	357.0	431.0	415.0	480.0	460.0	529.0	503.0			
Emissions Sample	ºC	80.5	56.9	85.8	58.6	63.2	40.9	86.6	59.4	82.2	58.5			
Sample After Ice	ºC	11.8		11.4	9.6	11.1	10.9	11.6	10.2	10.4	9.6			
Valve Body Temp	ºC	48.7		50.2	74.1	47.7	66.1	51.8	73.3	51.3	76.5			
COV of IMEP	%	7.63	13.57	3.44	14.69	2.94	15.98	4.06	16.34	3.93	17.06			
IMEP	kPa	169.00	165.00	205.00	198.00	236.00	226.00	248.00	242.00	270.00	262.00			
Peak Cyl. Pres.	MPa	2.36	2.32	2.67	2.56	2.82	2.71	2.86	2.77	3.00	2.88			
Location of PCP	°ATDC	6.0	5.0	5.0	5.0	4.0	5.0	5.0	5.0	4.0	4.0			
Sample Flow	#													
Demand	%	31.7	31.3	32	30.8	31.2	31.2	30.6	28.6	27.7	26.9			
DemandBaro	%	31.82	31.42	32.12	30.92	31.32	31.32	30.71	28.71	27.80	27.00			

Description of Test:														
Date	Ambient Temp (ºC)		Ambient Pressure (kPa)		Humidity	Coolant Temp		P_abs (psi)		Data Taker				
07.05.02	22.9		100		49%	48		14.3		H. Zach Foudray				
Notes:														
12 CA deg per 1ms at 2000rpm. A "u" or "s" at the end of a Hi-Techniques file indicates a test run that unsampled (meaning emissions measurements are taken from the exhaust) or sampled(emissions measurements taken from the cylinder), respectively.														
Run Number		**3**		**2**		**4**		**1**						
Time		1159	1208	1136	1148	1228	1235	1108	1119					
Hi-Techniques File		z_AF_conDR_4						z_AF_conDR_1						
Injector		orbital		orbital		orbital		orbital						
Spark Plug Type	Champion	RC10ECC		RC10ECC		RC10ECC		RC10ECC						
Spark Plug Projection	mm	12		12		12		12						
Engine Speed	RPM	2000	2000	2000	2000	2000	2000	2000	2000					
Orifice Upstream Press	kPa	407.5	407.5	407.5	407.5	407.5	407.8	407.8	407.7					
Orifice Size	#	4		4		4		4						
Intake Air Flowrate	kg/hr	32.79	32.79	32.79	32.79	32.79	32.82	32.82	32.81					
Delivery Ratio		0.5996	0.5996	0.5996	0.5996	0.5996	0.6000	0.6000	0.5999					
Measured A/F Ratio		45.5	45.5	36.4	36.4	30.4	30.4	26.0	26.0					
Throttle Position (TPS)	%	36.0	36.6	35.3	35.6	37	36.7	36.6	36.2					
Inlet Surge Tank Press	kPa	100.1	100.1	100.1	100.1	100.1	100	100.0	100					
Exh Surge Tank Press	kPa	100.0	100.1	100.0	100.1	100	100	100.0	99.9					
Exhaust Back-Pressure	kPa	0.0	0.0	0.0	0	0	0	0.0	0					
Oil Flowrate	kg/hr of fuel	0.722	0.723	0.900	0.901	1.082	1.083	1.266	1.267					
Ignition Timing (actual)	ºBTDC	40.000		37.813		36.000		34.000						
SOA Timing	ºBTDC	72.000		75.875		79.000		87.563						
EOA Timing	ºBTDC	34		34		34		35						
Fuel Pressure	psi	95	95	95	95	95	95	95	95					
Fuel/cycle	mg	6.00		7.50		9		10.5						
NOx (dry)	ppm	849.97	278.60	1063.69	292.16	1205.9	298.85	1337.83	256.73					
CO2 (dry)	%	4.889	1.754	6.049	1.930	7.001	2.028	7.832	2.230					
CO (dry)	%	0.099	0.048	0.207	0.096	0.468	0.204	0.869	0.426					
O2 (dry)	%	14.066	18.564	12.643	18.289	10.848	18.037	9.244	17.375					
Engine Load	N-m	8.670	7.540	12.070	11.050	15.210	14.100	17.960	16.570					
Fuel Flowrate	mg/s	200	200	250	250	300	300	350	350					
Exhaust Gas	ºC	361.0	347.0	443.0	422.0	514.0	490.0	546.0	526.0					
Emissions Sample	ºC	96.0	63.7	92.0	58.5	97.4	66.0	76.5	53.0					
Sample After Ice	ºC	8.3	8.4	7.6	7.6	9.9	9.1	8.3	6.8					
Valve Body Temp	ºC	51.4	63.8	51.3	65.3	53.6	70.4	53.2	76.0					
COV of IMEP	%	3.26	15.21	7.54	17.15	12.21	18.37	3.59	18.57					
IMEP	kPa	223.00	214.00	277.00	272.00	320.00	313.00	368.00	358.00					
Peak Cyl. Pres.	MPa	3.01	2.89	3.22	3.14	3.36	3.28	3.71	3.60					
Location of PCP	ºATDC	3.0	3.0	4.0	4.0	4.0	4.0	3.0	3.0					
Sample Flow	#													
Demand	%	57.5	58.6	50.1	56.8	59.4	58.8	58.7	57.8					
DemandBaro	%	58.22	59.34	50.73	57.52	60.15	59.54	59.33	58.42					

Description of Test:																				
Date	Ambient Temp (ºC)		Ambient Pressure (kP		Humidity	Coolant Temp		P_abs (psi)		Data Taker										
24.04.02	23		98.7		43%	48		14.2		H. Zach Foudray										
Notes:																				
12 CA deg per 1ms at 2000rpm. A "u" or "s" at the end of a Hi-Techniques file indicates a test run that unsampled (meaning emissions measurements are taken from the exhaust) or sampled(emissions measurements taken from the cylinder), respectively.																				
Run Number		8		3		7		1		2		9		6		4		5		
Time		1338	1346	1147	1154	1318	1326	1105	1111	1125	1132	1357	1405	1254	1301	1207	1215	1233	1240	
Hi-Techniques File		z_tas_conAF_4-25_8						z_tas_conAF_4-24_1												
Injector		orbital		orbital		orbital		orbital		orbital		orbital		orbital		orbital		orbital		
Spark Plug Type	Champion	RC10ECC		RC10ECC		RC10ECC		RC10ECC		RC10ECC		RC10ECC		RC10ECC		RC10ECC		RC10ECC		
Spark Plug Projection	mm	12		12		12		12		12		12		12		12		12		
Engine Speed	RPM	2000	2000	2000	2000	2000	2000	2000	2000	2000	2000	2000	2000	2000	2000	2000	2000	2000	2000	
Orifice Upstream Press	kPa	196.7	196.7	230.7	230.7	265.3	265.3	300.3	300.4	334.5	334.5	368.7	368.7	402.7	402.7	437.5	437.5	216.7	216.7	
Orifice Size	#	4		4		4		4		4		4		4		4		5		
Intake Air Flowrate	kg/hr	16.22	16.22	18.90	18.90	21.62	21.62	24.37	24.38	27.06	27.06	29.74	29.74	32.42	32.42	35.15	35.15	37.78	37.78	
Delivery Ratio		0.3007	0.3007	0.3502	0.3502	0.4006	0.4006	0.4516	0.4517	0.5014	0.5014	0.5512	0.5512	0.6007	0.6007	0.6514	0.6514	0.7002	0.7002	
Measured A/F Ratio		27.5	27.5	27.5	27.5	27.4	27.4	27.5	27.5	27.5	27.5	27.4	27.4	27.5	27.5	27.5	27.5	27.5	27.5	
Throttle Position (TPS)	%	15.6	15.4	18.4	18.4	20.6	21	24.17	24	27.2	27.2	31.4	31.19	37.2	36.9	44.8	43.8	63.9	59.5	
Inlet Surge Tank Press	kPa	98.6	98.6	98.7	98.7	98.5	98.5	98.8	98.8	98.7	98.8	98.6	98.6	98.6	98.5	98.7	98.6	98.6	98.6	
Exh Surge Tank Press	kPa	98.6	98.6	98.7	98.7	98.45	98.5	98.8	98.8	98.6	98.7	98.6	98.5	98.5	98.5	98.6	98.5	98.5	98.5	
Exhaust Back-Pressure	kPa	0.0	0.0	0.0	0	0	0	0.0	0	0		0.0	0	0.0	0	0	0	0	0	
Oil Flowrate	kg/hr of fuel	0.590	0.590	0.685	0.685	0.786	0.786	0.888	0.888	0.980	0.980	1.081	1.082	1.175	1.175	1.280	1.281	1.373	1.373	
Ignition Timing (actual)	ºBTDC	40.813		40.000		38.750		37.813		37.375		35.750		34.875		34.000		32.500		
SOA Timing	ºBTDC	67.188		71.875		73.125		75.375		79.250		81.688		85.625		89.125		94.375		
EOA Timing	ºBTDC	34		34		34		34		34		34		34		35		35		
Fuel Pressure	psi	95	95	95	95	95	95	95	95	95	95	95	95	95	95	95	95	95	95	
Fuel/cycle	mg	4.95		5.77		6.61		7.43		8.27		9.09		9.9		10.73		11.54		
NOx (dry)	ppm	101.31	36.20	335.34	93.15	578.7	141.38	842.96	198.38	1173.34	275.44	1324.38	293.02	1511.4	262.19	1521.73	220.92	1454.96	246.97	
CO2 (dry)	%	8.237	4.723	8.318	4.165	8.235	3.566	8.105	3.104	7.798	2.668	7.735	2.296	7.550	2.000	7.387	1.765	7.174	1.608	
CO (dry)	%	0.208	0.177	0.214	0.232	0.272	0.278	0.373	0.337	0.581	0.335	0.635	0.309	0.667	0.302	0.814	0.334	0.835	0.277	
O2 (dry)	%	9.416	14.417	9.320	15.079	9.243	15.789	9.426	16.464	9.565	17.185	9.585	17.872	9.656	18.023	9.881	18.275	9.639	18.643	
Engine Load	N-m	6.940	5.880	8.940	7.990	10.780	9.690	12.110	10.820	13.480	12.400	15.800	14.290	17.330	15.880	18.640	17.210	20.880	19.400	
Fuel Flowrate	mg/s	164	164	191	191	219	219	246	246	273	273	301	301	328	328	355	355	382	382	
Exhaust Gas	ºC	369.0	346.0	427.0	415.0	472.0	459.0	521.0	501.0	540.0	519.0	548.0	523.0	540.0	519.0	533.0	508.0	517.0	500.0	
Emissions Sample	ºC	88.1	58.8	86.8	54.4	94.2	63.4	65.0	40.5	87.2	53.0	84.4	61.0	91.5	64.8	95.6	60.6	61.1	60.4	
Sample After Ice	ºC	9.6	8.6	9.1	7.7	9.7	9.4	9.1	7.4	8.4	7.5	10.1	8.0	10.2	9.6	9.2	8.4	14.5	9.6	
Valve Body Temp	ºC	49.3	65.4	49.8	69.5	52.0	69.8	48.8	71.9	52.7	70.6	54.3	69.6	56.2	73.3	55.7	77.8	56.5	75.9	
COV of IMEP	%	5.87	15.47	3.73	14.61	3.03	16.12	3.66	16.93	3.71	17.32	3.40	17.74	3.29	18.43	3.02	18.82	3.01	18.36	
IMEP		176.00	169.00	207.00	203.00	242.00	234.00	272.00	264.00	295.00	286.00	322.00	311.00	354.00	342.00	380.00	366.00	413.00	396.00	
Peak Cyl. Pres.	MPa	2.17	2.09	2.66	2.60	2.89	2.80	3.10	3.01	3.30	3.20	3.45	3.33	3.61	3.50	3.76	3.64	3.85	3.65	
Location of PCP	°ATDC	9.0	8.0	6.0	5.0	5.0	5.0	4.0	4.0	3.0	3.0	3.0	3.0	3.0	3.0	4.0	3.0	4.0	5.0	
Sample Flow	#																			
Demand	%	14	13.1	22.8	22.8	26.9	27.7	35.1	35	37	37	42.1	41.9	59.5	59.2	65	63.9	82.1	79.3	
DemandBaro	%	13.98	13.08	22.77	22.77	26.87	27.67	35.06	34.96	36.96	36.96	42.05	41.85	59.44	59.14	64.93	63.83	82.01	79.22	

Description of Test:														
Date	Ambient Temp (ºC)		Ambient Pressure (kI		Humidity	Coolant Temp		P_abs (psi)		Data Taker				
01.05.02	23.1		98.9		34%	48		14.2		H. Zach Foudray				
Notes:														
12 CA deg per 1ms at 2000rpm. A "u" or "s" at the end of a Hi-Techniques file indicates a test run that unsampled (meaning emissions measurements are taken from the exhaust) or sampled(emissions measurements taken from the cylinder), respectively.														
Run Number		**2**		**1**		**6**		**5**		**3**		**4**		
Time		1115	1121	1047	1057	1242	1248	1225	1233	1133	1142	1159	1206	
Hi-Techniques File		z_highAF_5-1_2		z_highAF_5-1_1					?				?	
Injector		orbital		orbital		orbital		orbital		orbital		orbital		
Spark Plug Type	Champion	RC10ECC		RC10ECC		RC10ECC		RC10ECC		RC10ECC		RC10ECC		
Spark Plug Projection	mm	12		12		12		12		12		12		
Engine Speed	RPM	2000	2000	2000	2000	2000	2000	2000	2000	2000	2000	2000	2000	
Orifice Upstream Press	kPa	300.3	300.1	335.0	334.7	368.8	368.8	403.6	404.0	438.0	437.6	217.4	217.5	
Orifice Size	#	4		4		4		4		4		5		
Intake Air Flowrate	kg/hr	24.37	24.35	27.10	27.07	29.75	29.75	32.49	32.52	35.19	35.16	37.90	37.92	
Delivery Ratio		0.4508	0.4505	0.5013	0.5008	0.5504	0.5504	0.6010	0.6016	0.6510	0.6504	0.7011	0.7015	
Measured A/F Ratio		41.3	41.2	41.4	41.3	41.3	41.3	41.4	41.4	41.2	41.2	41.3	41.3	
Throttle Position (TPS)	%	24.77	24.77	28.1	28	31.8	31.8	36.3	36.3	45.1	44.4	56.4	54.5	
Inlet Surge Tank Press	kPa	98.9	98.8	98.9	98.8	98.8	98.8	98.9	98.8	98.8	98.9	98.8	98.8	
Exh Surge Tank Press	kPa	98.9	98.8	98.9	98.8	98.8	98.8	98.8	98.8	98.8	98.9	98.8	98.8	
Exhaust Back-Pressure	kPa	0.0	0	0	0	0.0	0	0.0	0	0	0	0	0	
Oil Flowrate	kg/hr of fuel	0.583	0.582	0.655	0.657	0.721	0.721	0.785	0.796	0.853	0.860	0.860	0.917	
Ignition Timing (actual)	ºBTDC	40.750		40.188		40.000		38.875		38.000		37.750		
SOA Timing	ºBTDC	67.500		71.313		72.000		72.938		74.125		68.313		
EOA Timing	ºBTDC	34		34		34		34		34		34		
Fuel Pressure	psi	95		95		95		95		95		95		
Fuel/cycle	mg	4.92		5.46		6		6.54		7.11		7.65		
NOx (dry)	ppm	406.02	158.1	703.04	258.83	832.44	275.65	963.75	309.93	979.43	264.14	731.24	154.68	
CO2 (dry)	%	5.295	2.487	5.425	2.247	5.409	2.118	5.361	2.161	5.311	1.636	5.058	1.485	
CO (dry)	%	0.145	0.071	0.100	0.055	0.123	0.083	0.130	0.115	0.190	0.085	0.301	0.155	
O2 (dry)	%	13.513	17.432	13.342	17.754	13.361	17.936	13.368	17.969	13.405	18.664	13.664	18.802	
Engine Load	N-m	6.530	5.470	7.980	6.890	9.270	7.980	10.300	9.180	11.590	10.300	12.510	11.190	
Fuel Flowrate	mg/s	164	164	182	182	200	200	218	218	237	237	255	255	
Exhaust Gas	ºC	334.0	320.0	366.0	351.0	389.0	378.0	401.0	380.0	408.0	391.0	409.0	394.0	
Emissions Sample	ºC	62.5	43.7	52.5	38.6	85.8	58.1	79.1	55.6	73.8	49.7	75.5	55.0	
Sample After Ice	ºC	10.3	8.7	8.6	7.8	10.1	8.6	9.6	8.1	10.5	8.6	11.4	8.7	
Valve Body Temp	ºC	47.1	65.0	47.2	68.4	52.4	66.7	54.2	76.2	50.9	69.2	50.6	83.0	
COV of IMEP	%	3.95	14.09	3.11	14.80	3.09	15.24	3.14	16.05	3.95	16.67	4.99	17.31	
IMEP		179.00	174.00	208.00	199.00	224.00	214.00	245.00	235.00	264.00	258.00	277.00	265.00	
Peak Cyl. Pres.	MPa	2.60	2.51	2.84	2.75	2.96	2.84	3.08	2.96	3.13	3.08	3.12	2.97	
Location of PCP	ºATDC	5.0	4.0	4.0	4.0	3.0	3.0	3.0	3.0	4.0	4.0	4.0	4.0	
Sample Flow	#													
Demand	%	35.5	35.5	37.7	37.6	42.6	42.5	58.1	58.1	65.5	64.3	77	75	
DemandBaro	%	35.50	35.50	37.70	37.60	42.60	42.50	58.10	58.10	65.50	64.30	77.00	75.00	

Description of Test:														
Date	Ambient Temp (ºC)		Ambient Pressure (kPa)		Humidity	Coolant Temp		P_abs (psi)		Data Taker				
01.04.02	22.4		99.3		19%	48		14.25		H. Zach Foudray				
Notes:														
12 CA deg per 1ms at 2000rpm. A "u" or "s" at the end of a Hi-Techniques file indicates a test run that unsampled (meaning emissions measurements are taken from the exhaust) or sampled(emissions measurements taken from the cylinder), respectively.														
Run Number		**1**		**4**		**3**		**2**		**6**		**5**		
Time		1212	1220	1310	1318	1248	1301	1233	1240	1341	1346	1326	1334	
Hi-Techniques File		z_tas_4-1_1												
Injector		orbital		orbital		orbital		orbital		orbital		orbital		
Spark Plug Type	Champion	RC10ECC		RC10ECC		RC10ECC		RC10ECC		RC10ECC		RC10ECC		
Spark Plug Projection	mm	12		12		12		12		12		12		
Engine Speed	RPM	2000	2000	2000	2000	2000	2000	2000	2000	2000	2000	2000	2000	
Orifice Upstream Press	kPa	198.2	198.3	267.3	267.1	336.5	336.2	405.6	405.4	218.4	218.4	236.4	236.7	
Orifice Size	#	4		4		4		4		5		5		
Intake Air Flowrate	kg/hr	16.34	16.35	21.77	21.76	27.21	27.19	32.64	32.63	38.07	38.07	41.07	41.12	
Delivery Ratio		0.3004	0.3006	0.4002	0.4000	0.5002	0.4998	0.6001	0.5998	0.6997	0.6997	0.7550	0.7559	
Measured A/F Ratio		22.8	22.8	30.4	30.4	38.0	38.0	45.6	45.5	53.1	53.1	57.3	57.4	
Throttle Position (TPS)	%	18.0	18.0	24.8	24.62	31.3	31	40.1	39.2	56	54	100	77	
Inlet Surge Tank Press	kPa	99.4	99.4	99.3	99.3	99.4	99.3	99.4	99.4	99.3	99.3	99.2	99.3	
Exh Surge Tank Press	kPa	99.3	99.3	99.3	99.3	99.35	99.3	99.3	99.3	99.2	99.3	99.1	99.3	
Exhaust Back-Pressure	kPa	0.0	0.0	0.0	0	0	0	0	0	0	0	0	0	
Oil Flowrate	kg/hr of fuel	0.726	0.726	0.729	0.73	0.729	0.728	0.728	0.728	0.73	0.73	0.73	0.729	
Ignition Timing (actual)	ºBTDC	40		40		40		40		40		40		
SOA Timing	ºBTDC	72		72		72		72		72		72		
EOA Timing	ºBTDC	34		34		34		34		34		34		
Fuel Pressure	psi	95		95		95		95		95		95		
Fuel/cycle	mg	6.00		6.00		6		6		6		6		
NOx (dry)	ppm	67.85	25.75	503.79	135.04	698.88	220.07	705.01	217.23	774.16	241.62	706.53	203.3	
CO2 (dry)	%	9.844	5.172	7.588	3.417	5.938	2.280	4.869	1.683	4.076	1.219	3.716	1.045	
CO (dry)	%	0.555	0.565	0.166	0.161	0.147	0.081	0.147	0.069	0.118	0.041	0.122	0.036	
O2 (dry)	%	6.989	12.899	10.501	15.678	12.772	17.345	14.266	18.278	15.343	18.949	15.852	19.266	
Engine Load	N-m	9.230	8.850	9.750	9.070	9.350	8.730	9.210	8.220	8.880	8.170	8.810	7.980	
Fuel Flowrate	mg/s	199	199	199	199	199	199	199	199	199	199	199	199	
Exhaust Gas	ºC	458.0	446.0	432.0	418.0	405.0	391.0	377.0	362.0	329.0	318.0	314.0	300.0	
Emissions Sample	ºC	71.0	41.0	82.8	53.0	74.2	49.2	71.7	46.0	84.0	55.9	80.0	54.0	
Sample After Ice	ºC	8.9	9.8	11.0	12.2	10.5	12.3	10.2	10.6	10.8	10.4	11.3	11.7	
Valve Body Temp	ºC	45.7	63.4	51.9	65.3	50.7	65.1	49.4	59.0	51.2	59.9	51.0	60.7	
COV of IMEP	%	4.37	12.02	3.43	11.61	3.51	12.92	3.52	12.96	3.52	11.87	3.56	12.88	
IMEP		208.00	205.00	221.00	219.00	224.00	219.00	228.00	220.00	225.00	219.00	227.00	217.00	
Peak Cyl. Pres.	MPa	2.28	2.21	2.79	2.75	2.90	2.84	2.97	2.89	3.00	2.91	3.02	2.92	
Location of PCP	ºATDC	10.0	11.0	5.0	5.0	4.0	4.0	4.0	4.0	4.0	4.0	4.0	4.0	
Sample Flow	#													
Demand	%	22.2	22.3	35.5	35.4	42	41.6	61.1	60.6	76.3	73.9	100	87.8	
DemandBaro	%	22.33	22.43	35.70	35.60	42.24	41.84	61.45	60.95	76.74	74.33	100.00	88.31	

Description of Test:													
Date	Ambient Temp (ºC)		Ambient Pressure (kPa)		Humidity	Coolant Temp		P_abs (psi)		Data Taker			
03.04.02	24.3		100.6		20%	48		14.4		H. Zach Foudray			
Notes:													
12 CA deg per 1ms at 2000rpm. A "u" or "s" at the end of a Hi-Techniques file indicates a test run that unsampled (meaning emissions measurements are taken from the exhaust) or sampled(emissions measurements taken from the cylinder), respectively.													
Run Number		**2**		**4**		**3**		**5**		**1**		**6**	
Time		1432	1438	1500	1507	1446	1452	1515	1523	1414	1422	1534	1542
Hi-Techniques File		z_tas_4-3_2								z_tas_4-3_1			
Injector		orbital		orbital		orbital		orbital		orbital		orbital	
Spark Plug Type	Champion	RC10ECC		RC10ECC		RC10ECC		RC10ECC		RC10ECC		RC10ECC	
Spark Plug Projection	mm	12		12		12		12		12		12	
Engine Speed	RPM	2000	2000	2000	2000	2000	2000	2000	2000	2000	2000	2000	2000
Orifice Upstream Press	kPa	233.8	233.7	303.6	303.6	373.5	373.5	443.3	443.4	220.0	220.3	236.4	236.4
Orifice Size	#	4		4		4		4		5		5	
Intake Air Flowrate	kg/hr	19.14	19.13	24.63	24.63	30.12	30.12	35.61	35.62	38.33	38.38	41.07	41.07
Delivery Ratio		0.3495	0.3494	0.4497	0.4497	0.5500	0.5500	0.6502	0.6504	0.7000	0.7009	0.7500	0.7500
Measured A/F Ratio		26.7	26.7	34.4	34.4	42.0	42.0	49.7	49.7	53.5	53.6	57.3	57.3
Throttle Position (TPS)	%	21.3	21.3	27.8	27.5	34.5	34.2	47.1	44.6	53.3	53	75.6	64.8
Inlet Surge Tank Press	kPa	100.5	100.5	100.5	100.6	100.5	100.5	100.6	100.6	100.5	100.5	100.5	100.5
Exh Surge Tank Press	kPa	100.5	100.5	100.5	100.6	100.4	100.45	100.6	100.6	100.5	100.5	100.45	100.45
Exhaust Back-Pressure	kPa	0.0	0.0	0.0	0	0	0	0	0	0	0	0	0
Oil Flowrate	kg/hr of fuel	0.728	0.728	0.729	0.729	0.728	0.728	0.729	0.729	0.726	0.727	0.729	0.729
Ignition Timing (actual)	ºBTDC	40		40		40		40		40		40	
SOA Timing	ºBTDC	72		72		72		72		72		72	
EOA Timing	ºBTDC	34		34		34		34		34		34	
Fuel Pressure	psi	95		95		95		95		95		95	
Fuel/cycle	mg	6.00		6.00		6		6		6		6	
NOx (dry)	ppm	254.20	57.62	644.58	196.16	777.62	243.36	757.02	239.31	683.32	212.48	686.81	201.37
CO2 (dry)	%	8.698	4.253	6.739	2.861	5.382	1.954	4.478	1.525	4.078	1.310	3.795	1.119
CO (dry)	%	0.210	0.224	0.126	0.097	0.117	0.059	0.116	0.051	0.120	0.044	0.118	0.037
O2 (dry)	%	9.106	14.601	11.710	16.568	13.744	17.771	14.760	18.555	15.586	18.978	15.728	19.172
Engine Load	N-m	9.450	8.930	9.570	8.820	9.200	8.520	8.990	8.000	8.370	7.700	8.520	7.850
Fuel Flowrate	mg/s	199	199	199	199	199	199	199	199	199	199	199	199
Exhaust Gas	ºC	437.0	427.0	413.0	402.0	384.0	371.0	344.0	331.0	320.0	309.0	306.0	294.0
Emissions Sample	ºC	100.7	60.7	86.8	60.9	93.3	60.6	85.8	59.8	75.0	52.0	78.6	57.7
Sample After Ice	ºC	7.5	9.3	8.5	9.8	8.1	8.9	8.7	9.3	9.0	8.9	9.3	9.3
Valve Body Temp	ºC	49.2	56.6	50.6	55.7	50.7	56.9	50.5	62.8	46.3	60.0	49.9	60.7
COV of IMEP	%	2.84	12.35	2.92	11.74	3.20	12.72	3.27	11.91	3.39	11.95	3.54	11.87
IMEP		219.00	214.00	225.00	220.00	227.00	211.00	228.00	220.00	226.00	222.00	224.00	217.00
Peak Cyl. Pres.	MPa	2.65	2.59	2.88	2.83	2.96	2.89	3.01	2.93	2.99	2.93	3.02	2.96
Location of PCP	ºATDC	7.0	7.0	4.0	5.0	4.0	4.0	4.0	4.0	4.0	4.0	4.0	3.0
Sample Flow	#												
Demand	%	28.6	28.6	37.4	37.2	46.2	45.7	66.7	65	72.7	72	87.3	82.6
DemandBaro	%	29.10	29.10	38.05	37.85	47.01	46.50	67.87	66.14	73.97	73.36	88.83	84.05

Description of Test:														
Date	Ambient Temp (ºC)		Ambient Pressure (kPa)		Humidity	Coolant Temp		P_abs (psi)		Data Taker				
03.04.02	23.3		100.6		24%	48		14.4		H. Zach Foudray				
Notes:														
12 CA deg per 1ms at 2000rpm. A "u" or "s" at the end of a Hi-Techniques file indicates a test run that unsampled (meaning emissions measurements are taken from the exhaust) or sampled(emissions measurements taken from the cylinder), respectively.														
Run Number		**3**		**5**		**2**		**1**		**4**		**6**		
Time		1204	1210	1245	1253	1144	1152	1116	1130	1225	1231	1307	1314	
Hi-Techniques File							z_tas_map_4-3_1							
Injector		orbital		orbital		orbital		orbital		orbital		orbital		
Spark Plug Type	Champion	RC10ECC		RC10ECC		RC10ECC		RC10ECC		RC10ECC		RC10ECC		
Spark Plug Projection	mm	12		12		12		12		12		12		
Engine Speed	RPM	2000	2000	2000	2000	2000	2000	2000	2000	2000	2000	2000	2000	
Orifice Upstream Press	kPa	200.6	200.0	234.7	235.0	270.0	270.1	305.0	304.8	340.1	340.0	363.0	262.9	
Orifice Size	#	4		4		4		4		4		4		
Intake Air Flowrate	kg/hr	16.53	16.48	19.21	19.24	21.99	21.99	24.74	24.72	27.50	27.49	29.30	21.43	
Delivery Ratio		0.3009	0.3000	0.3496	0.3501	0.4001	0.4003	0.4502	0.4499	0.5004	0.5003	0.5332	0.3900	
Measured A/F Ratio		24.0	24.0	24.4	24.4	20.5	20.5	21.4	21.4	21.5	21.5	21.1	15.5	
Throttle Position (TPS)	%	18.4	18.4	21.0	21	23.8	23.6	27	26.8	30.5	30.5	33.3	33.2	
Inlet Surge Tank Press	kPa	100.5	100.4	100.5	100.55	100.5	100.5	100.6	100.6	100.5	100.5	100.5	100.5	
Exh Surge Tank Press	kPa	100.5	100.5	100.5	100.6	100.4	100.5	100.6	100.5	100.4	100.4	100.4	100.4	
Exhaust Back-Pressure	kPa	0.0	0.0	0.0	0	0	0	0.0	0	0	0	0	0	
Oil Flowrate	kg/hr of fuel	0.687	0.688	0.786	0.787	1.065	1.064	1.149	1.148	1.271	1.271	1.388	1.387	
Ignition Timing (actual)	ºBTDC	40.000		38.750		35.938		34.938		34.000		32.250		
SOA Timing	ºBTDC	72.063		73.063		81.750		84.188		89.125		94.500		
EOA Timing	ºBTDC	34		34		34		34		35		35		
Fuel Pressure	psi	95		95		95		95		95		95		
Fuel/cycle	mg	5.77		6.60		9.01		9.68		10.71		11.62		
NOx (dry)	ppm	95.42	31.15	225.82	54.5	409.68	81.82	674.15	118.91	867.19	130.94	958.28	135.92	
CO2 (dry)	%	9.671	5.147	9.230	4.441	8.924	3.473	8.722	3.121	8.582	2.581	8.707	2.383	
CO (dry)	%	0.322	0.352	0.494	0.431	2.566	1.631	2.170	1.273	2.347	1.207	2.287	1.249	
O2 (dry)	%	7.604	13.297	8.085	14.203	6.650	14.473	7.307	15.241	7.334	16.095	7.196	16.381	
Engine Load	N-m	9.640	8.870	11.240	10.610	14.700	13.900	16.160	15.300	17.610	16.880	19.780	18.650	
Fuel Flowrate	mg/s	191	191	219	219	298	298	321	321	355	355	385	385	
Exhaust Gas	ºC	450.0	438.0	484.0	473.0	557.0	547.0	571.0	562.0	579.0	570.0	579.0	565.0	
Emissions Sample	ºC	104.2	60.3	105.4	64.0	100.3	54.7	93.4	47.6	105.0	64.0	108.5	66.5	
Sample After Ice	ºC	8.3	9.3	8.3	9.6	7.6	8.8	6.9	8.7	8.2	9.9	8.9	9.8	
Valve Body Temp	ºC	48.9	61.3	51.1	59.8	52.8	64.6	50.5	69.9	53.7	66.3	54.6	65.2	
COV of IMEP	%	3.38	11.68	3.13	13.47	3.51	14.68	3.19	14.01	2.79	15.28	2.83	14.51	
IMEP		210.00	201.00	242.00	237.00	296.00	288.00	323.00	317.00	348.00	345.00	383.00	373.00	
Peak Cyl. Pres.	MPa	2.27	2.19	2.67	2.60	3.16	3.13	3.42	3.36	3.64	3.56	3.80	3.70	
Location of PCP	ºATDC	10.0	11.0	8.0	8.0	6.0	5.0	4.0	4.0	3.0	3.0	3.0	3.0	
Sample Flow	#													
Demand	%	22.9	22.9	27.6	27.6	34.9	34.8	36.9	36.8	41.2	41.2	44.3	44	
DemandBaro	%	23.28	23.38	28.05	28.05	35.47	35.37	37.51	37.41	41.88	41.88	45.03	44.73	

Description	Compare the B119 emissions bench with the FT-IR in B127.												
of Test:													
Date	Ambient Temp (ºC)		Ambient Pressure (kP		Humidity	Coolant Temp		P_abs (psi)		Data Taker			
29.05.02	23.4		99.1		74%	48		14.25		H. Zach Foudray			
Notes:													
12 CA deg per 1ms at 2000rpm. A "u" or "s" at the end of a Hi-Techniques file indicates a test run that unsampled (meaning emissions measurements are taken from the exhaust) or sampled(emissions measurements taken from the cylinder), respectively.													
Run Number		1		3		4		2					
Time		1345	1400	1440	1451	1503	1514	1415	1425				
Hi-Techniques File	z_varRPM_0.4DR_1												
Injector		orbital		orbital		orbital		orbital					
Spark Plug Type	Champion	RC10ECC		RC10ECC		RC10ECC		RC10ECC					
Spark Plug Projection	mm	12		12		12		12					
Engine Speed	RPM	1500	1500	2000	2000	2500	2500	3000	3000				
Orifice Upstream Pres	kPa	196.9	196.8	266.0	265.8	335.0	334.9	403.5	403.3				
Orifice Size	#	4		4		4		4					
Intake Air Flowrate	kg/hr	16.24	16.23	21.67	21.66	27.10	27.09	32.48	32.46				
Delivery Ratio		0.4002	0.4000	0.4005	0.4002	0.4006	0.4005	0.4002	0.4000				
Measured A/F Ratio		30.1	30.1	30.1	30.1	30.1	30.1	30.1	30.1				
Throttle Position (TPS	%	16.9	16.8	21.2	21.34	25.8	25.1	24.8	24.4				
Inlet Surge Tank Pres	kPa	99.1	99.1	99.1	99.1	99.1	99.1	99.1	99.1				
Exh Surge Tank Pres	kPa	99.1	99.1	99.1	99.1	99.1	99.1	99.1	99.2				
Exhaust Back-Pressu	kPa	0.0	0.0	0.0	0	0.0	0	0.0	0				
Oil Flowrate	g/hr of fuel	0.544	0.544	0.726	0.726	0.898	0.898	1.076	1.076				
Ignition Timing (actua	ºBTDC	40.000		40.000		42.000		43.000					
SOA Timing	ºBTDC	72.000		72.000		81.250		90.500					
EOA Timing	ºBTDC	34		34		36		34					
Fuel Pressure	psi	95		95		95		95					
Fuel/cycle	mg	6.00	6.00	6.00	6.00	6.00	6.00	6.00	6.00				
NOx (dry)	ppm	909.16	x	567.57	164.37	663.85	202.67	678.32	187.66				
CO2 (dry)	%	7.767	3.561	7.571	3.468	7.635	3.387	7.609	3.269				
CO (dry)	%	0.098	0.096	0.157	0.202	0.102	0.098	0.085	0.070				
O2 (dry)	%	10.039	15.748	10.337	15.899	10.305	16.092	10.352	16.270				
Engine Load	N-m	7.890	7.030	9.160	7.960	10.320	9.180	10.890	9.700				
Fuel Flowrate	mg/s	150	150	200	200	250	250	300	300				
Exhaust Gas	ºC	375.0	361.0	427.0	410.0	449.0	432.0	458.0	440.0				
Emissions Sample	ºC	58.2	39.8	85.3	58.4	89.5	61.0	80.8	53.2				
Sample After Ice	ºC	10.3	9.3	10.6	10.6	10.9	9.3	10.0	8.1				
Intake Air (Reeds)	ºC	43.1	44.6	47.3	47.3	47.3	47.2	43.2	43.4				
Intake Air (Boost Por	ºC	131.2	129.9	143	141.4	153.3	151	158.5	156.6				
Valve Body Temp	ºC	48.0	67.8	51.6	69.8	52.8	74.0	52.2	80.2				
COV of IMEP	%	2.84	14.75	3.25	15.77	3.01	16.02	3.02	16.67				
IMEP		226.00	218.00	237.00	226.00	247.00	238.00	255.00	244.00				
Peak Cyl. Pres.	MPa	3.00	2.87	2.81	2.68	2.97	2.86	3.01	2.88				
Location of PCP	ºATDC	3.0	3.0	5.0	5.0	5.0	5.0	6.0	6.0				
Sample Flow	#												
Demand	%	19	18.7	28.1	29	36.6	36.1	36.2	35.8				
DemandBaro	%	19.05	18.75	28.18	29.08	36.70	36.20	36.30	35.90				

Description	Compare the B119 emissions bench with the FT-IR in B127.												
of Test:													
Date	Ambient Temp (ºC)		Ambient Pressure (kP		Humidity	Coolant Temp		P_abs (psi)		Data Taker			
30.05.02	23.3		98.9		73%	48		14.2		H. Zach Foudray			
Notes:													
12 CA deg per 1ms at 2000rpm. A "u" or "s" at the end of a Hi-Techniques file indicates a test run that unsampled (meaning emissions measurements are taken from the exhaust) or sampled(emissions measurements taken from the cylinder), respectively.													
Run Number		4		2		1		3					
Time		1052	1102	958	1118	931	943	1024	1034				
Hi-Techniques File	z_varRPM_0.6DR_1												
Injector		orbital		orbital		orbital		orbital					
Spark Plug Type	Champion	RC10ECC		RC10ECC		RC10ECC		RC10ECC					
Spark Plug Projection	mm	12		12		12		12					
Engine Speed	RPM	1500	1500	2000	2000	2500	2500	3000	3000				
Orifice Upstream Pres	kPa	299.9	299.8	402.8	402.8	233.1	233.0	282.0	281.9				
Orifice Size	#	4		4		5		5					
Intake Air Flowrate	kg/hr	24.34	24.33	32.42	32.42	40.52	40.51	48.69	48.67				
Delivery Ratio		0.6007	0.6005	0.6003	0.6003	0.6001	0.5999	0.6009	0.6007				
Measured A/F Ratio		45.1	45.1	45.0	45.0	45.0	45.0	45.1	45.1				
Throttle Position (TPS	%	29.2	29.2	37.4	35.9	37.0	36.65	35.37	34.92				
Inlet Surge Tank Pres	kPa	98.9	98.8	98.9	98.9	98.9	98.9	98.9	98.9				
Exh Surge Tank Pres	kPa	98.9	98.9	98.9	98.9	98.9	98.9	98.9	99				
Exhaust Back-Pressu	kPa	0.0	0.0	0.0	0	0.0	0	0.0	0				
Oil Flowrate	g/hr of fuel	0.540	0.540	0.716	0.715	0.902	0.903	1.098	1.098				
Ignition Timing (actual	°BTDC	35.000		40.000		42.000		43.000					
SOA Timing	°BTDC	61.000		72.000		81.375		89.625					
EOA Timing	°BTDC	30		34		36		34					
Fuel Pressure	psi	95		95		95		95					
Fuel/cycle	mg	6.00	6.00	6.00	6.00	6.00	6.00	6.00	6.00				
NOx (dry)	ppm	876.92	272.93	896.71	259.78	865.93	271.3	688.12	206.86				
CO2 (dry)	%	5.000	1.723	4.944	1.656	4.948	1.625	4.812	1.554				
CO (dry)	%	0.108	0.058	0.097	0.062	0.085	0.034	0.098	0.037				
O2 (dry)	%	13.802	18.310	13.894	18.489	13.800	18.484	14.082	18.648				
Engine Load	N-m	7.900	6.680	8.610	6.840	9.570	8.450	10.360	9.280				
Fuel Flowrate	mg/s	150	150	200	200	250	250	300	300				
Exhaust Gas	°C	352.0	338.0	362.0	351.0	367.0	356.0	366.0	252.0				
Emissions Sample	°C	80.1	54.3	72.1	50.0	60.3	43.6	82.3	55.9				
Sample After Ice	°C	11.4	10.6	10.6	9.6	9.4	7.8	11.6	7.9				
Intake Air (Reeds)	°C	43.3	42.9	41.8	42.4	38.6	39.9	39.4	39.3				
Intake Air (Boost Port	°C	105	102	114.5	110.2	117	117.1	119.5	116				
Valve Body Temp	°C	49.9	66.5	50.6	68.1	47.7	72.1	51.4	72.7				
COV of IMEP	%	3.88	15.18	2.77	15.84	3.13	16.52	4.71	17.96				
IMEP		237.00	225.00	240.00	226.00	256.00	243.00	261.00	247.00				
Peak Cyl. Pres.	MPa	2.96	2.82	3.02	2.86	3.17	3.05	3.15	3.00				
Location of PCP	°ATDC	4.0	3.0	3.0	3.0	4.0	4.0	5.0	5.0				
Sample Flow	#												
Demand	%	39.4	39.4	59.6	57.2	59.4	58.9	57.5	56.9				
DemandBaro	%	39.43	39.43	59.65	57.25	59.45	58.95	57.55	56.95				

Appendix C

Valve Drawings

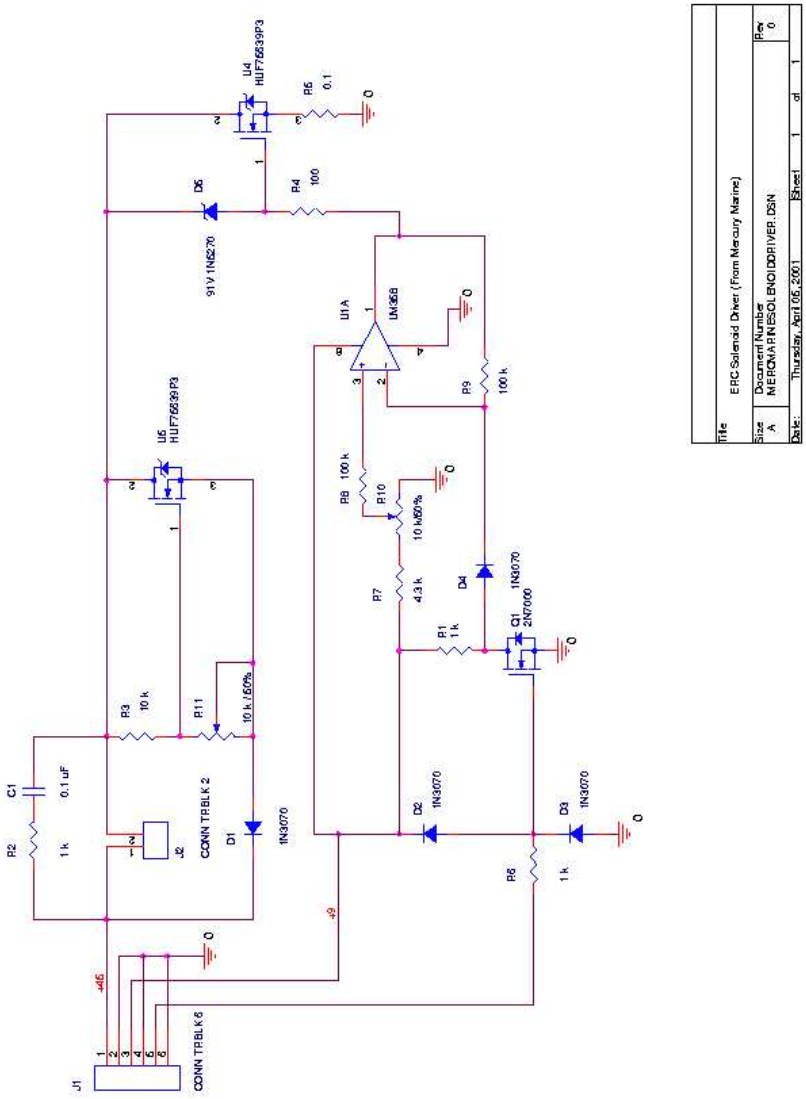
U4
HUF76639P3
R6
0.1
D5
91V1N5270
R4
100
U1:A
LM368
R9
100 k
U5
HUF76639P3
R8
100 k
R10
10 k/50%
R7
4.3 k
D4
1N3070
Q1
2N7000
R1
1 k
R3
10 k
R11
10 k/50%
C1
0.1 uF
R2
1 k
J2
CONN TRBLK 2
D1
1N3070
D2
1N3070
D3
1N3070
R5
1 k
J1
CONN TRBLK 6
Title
ERC Solenoid Driver (From Mercury Marine)
Size
A
Document Number
MERCMARINESOLENOIDDRIVER.DSN
Rev
0
Date:
Thursday, April 05, 2001
Sheet
1
of
1

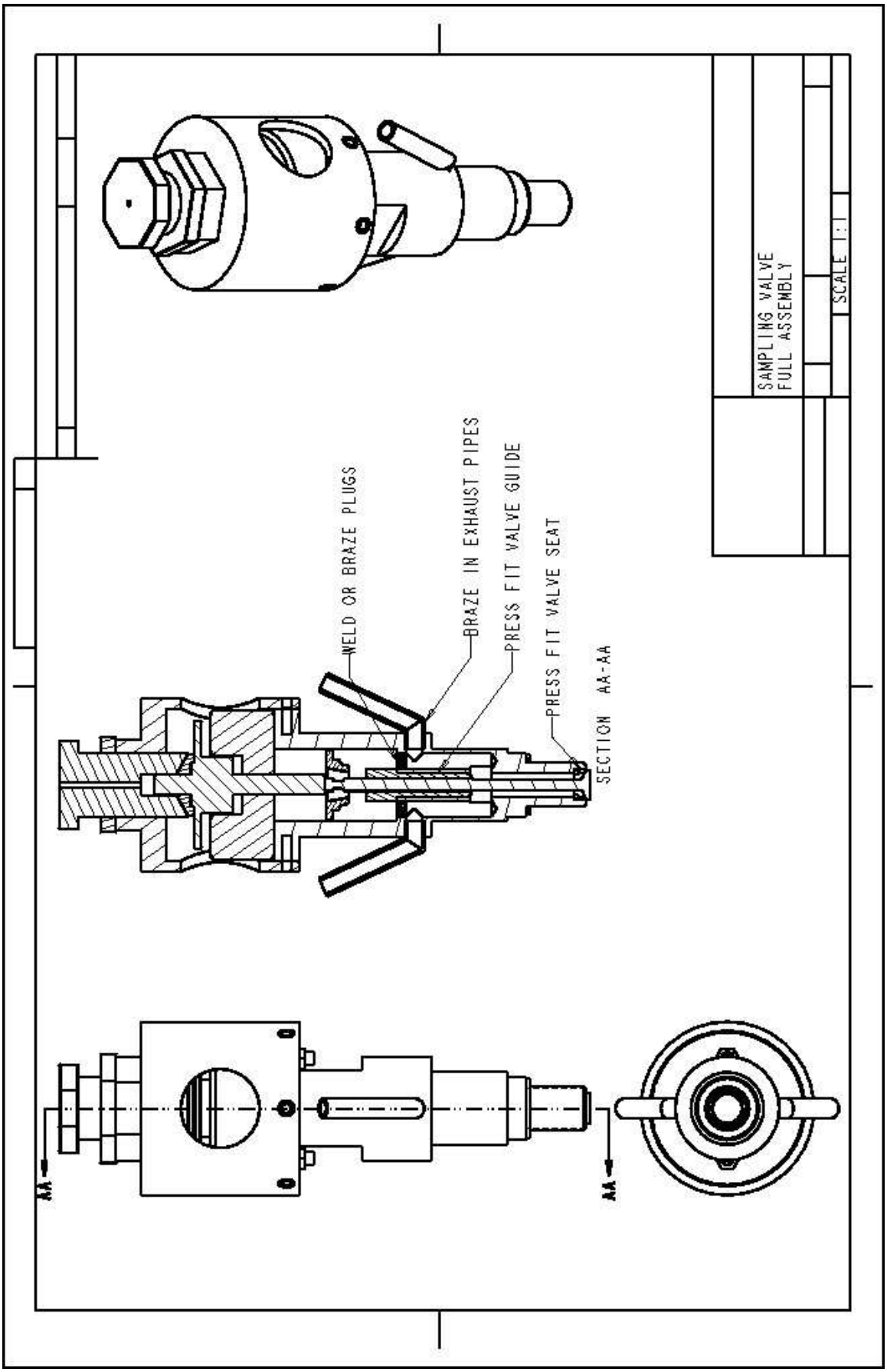
SAMPLING VALVE
FULL ASSEMBLY
SCALE 1:1
WELD OR BRAZE PLUGS
BRAZE IN EXHAUST PIPES
PRESS FIT VALVE GUIDE
PRESS FIT VALVE SEAT
SECTION AA-AA
AA
AA

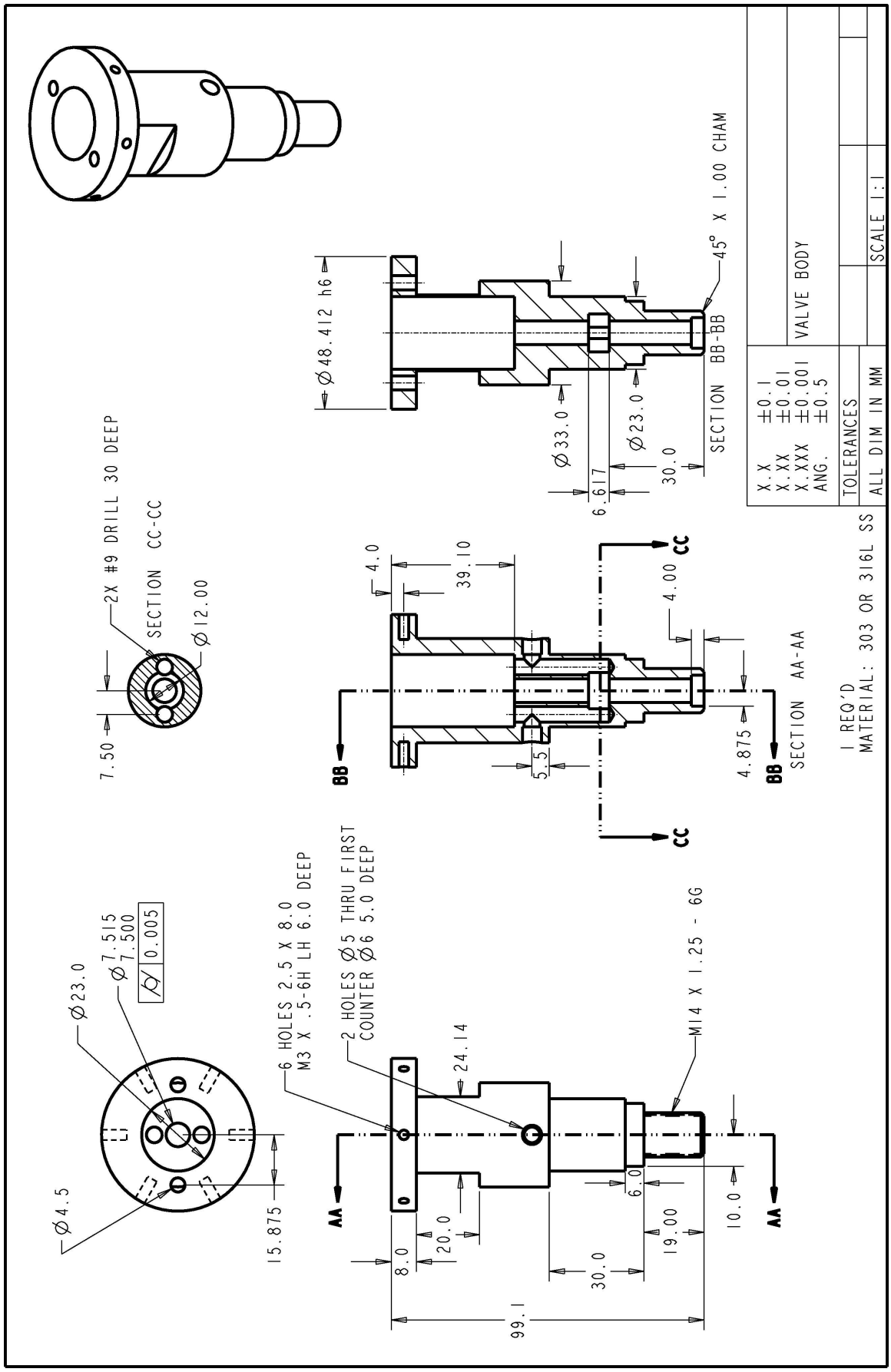
VALVE BODY
SCALE 1:1
TOLERANCES
X.X ±0.1
X.XX ±0.01
X.XXX ±0.001
ANG. ±0.5
ALL DIM IN MM
1 REQ'D
MATERIAL: 303 OR 316L SS
SECTION AA-AA
SECTION BB-BB
SECTION CC-CC
45° X 1.00 CHAM
2X #9 DRILL 30 DEEP
6 HOLES 2.5 X 8.0
M3 X .5-6H LH 6.0 DEEP
2 HOLES Ø5 THRU FIRST
COUNTER Ø6 5.0 DEEP
M14 X 1.25 - 6G
Ø48.412 h6
Ø33.0
Ø23.0
Ø12.00
Ø23.0
Ø7.515
7.500
0.005
Ø4.5
99.1
30.0
19.00
20.0
8.0
24.14
39.10
4.0
4.00
5.5
6.0
10.0
4.875
6.617
30.0
15.875
7.50

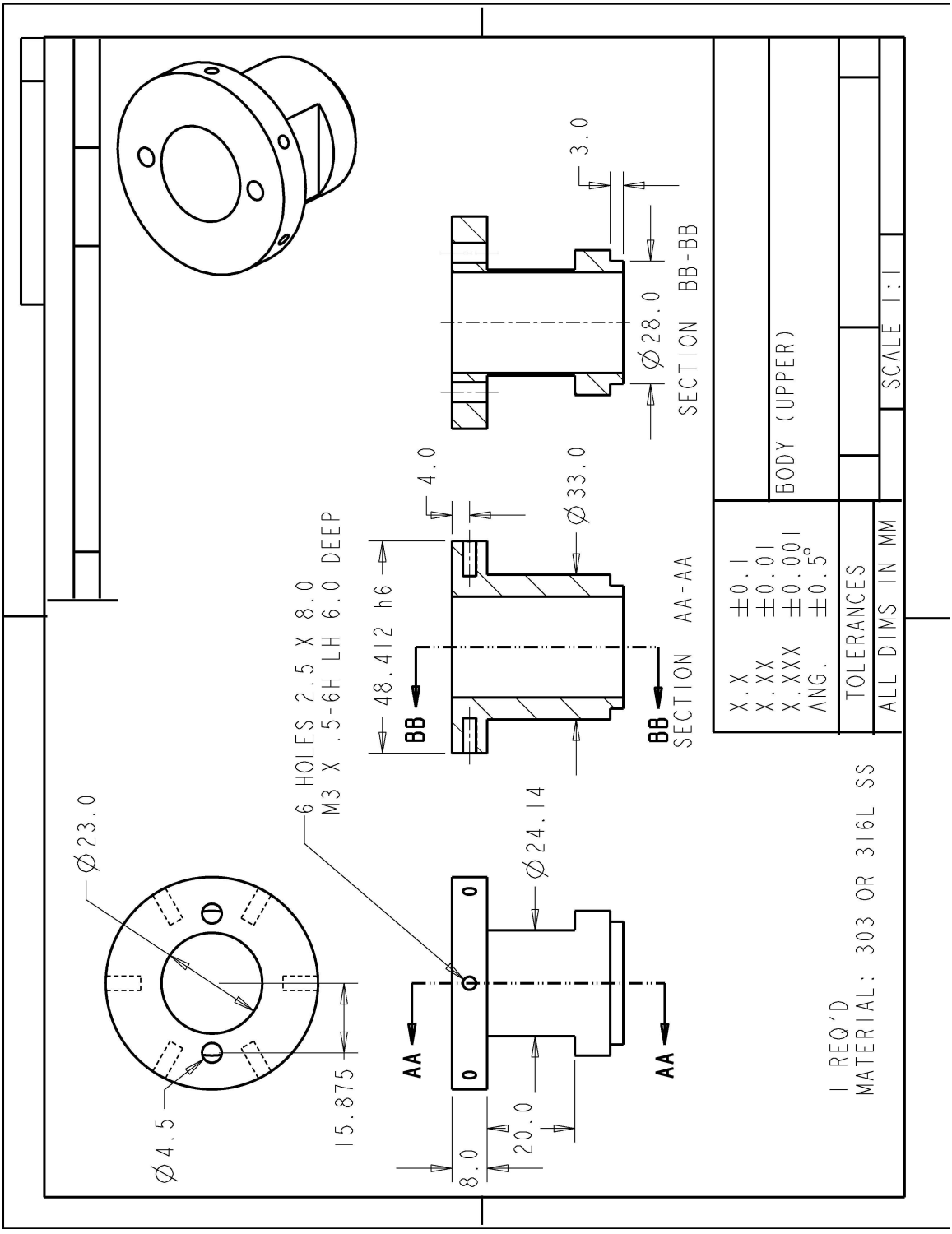
BODY (UPPER)
TOLERANCES
X.X ±0.1
X.XX ±0.01
X.XXX ±0.001
ANG. ±0.5°
ALL DIMS IN MM
SCALE 1:1
1 REQ'D
MATERIAL: 303 OR 316L SS
SECTION BB-BB
SECTION AA-AA
6 HOLES 2.5 X 8.0
M3 X .5-6H LH 6.0 DEEP
48.412 h6
Ø23.0
Ø4.5
15.875
Ø24.14
Ø33.0
Ø28.0
3.0
4.0
8.0
20.0
AA
BB

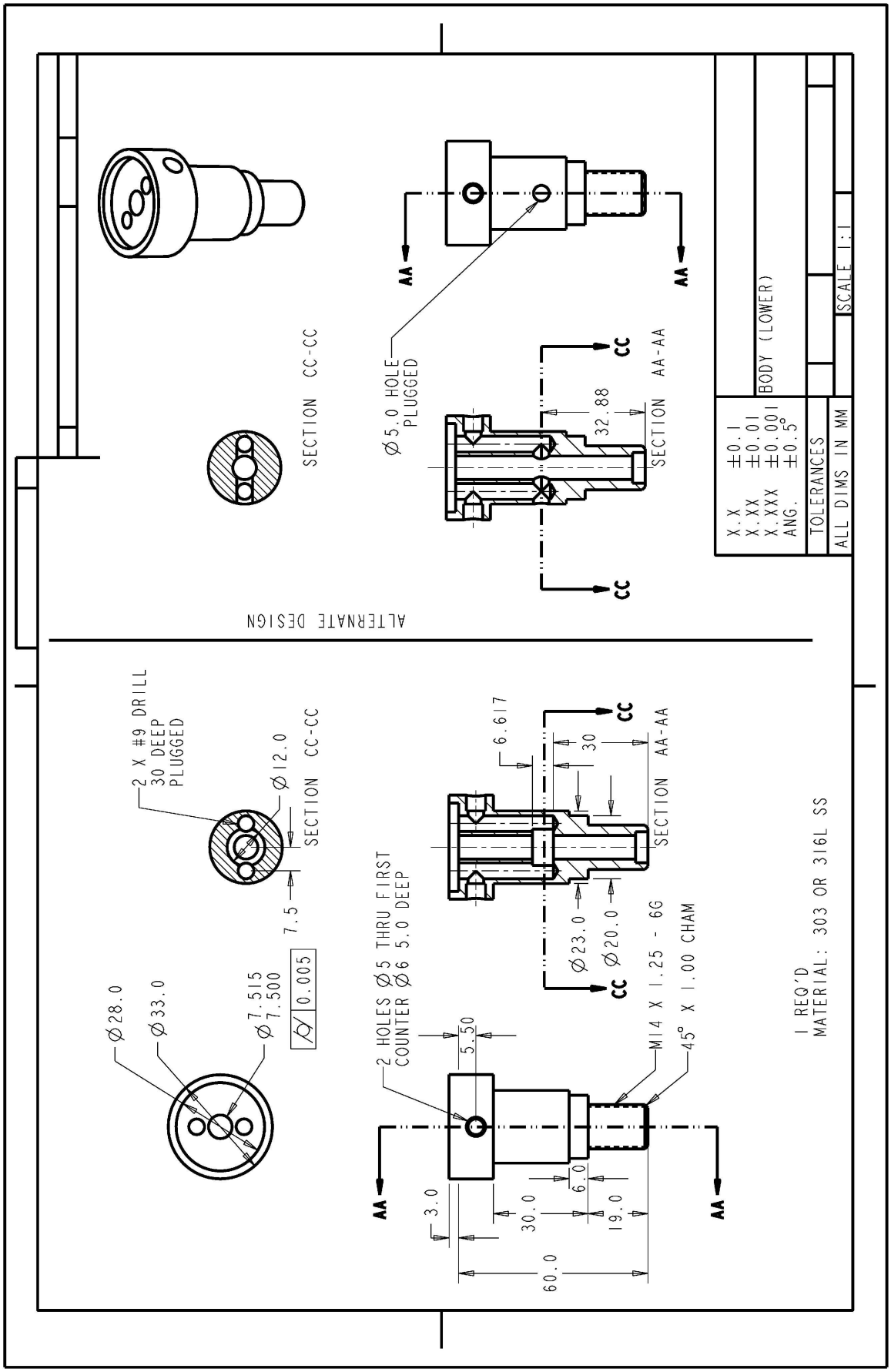
ALTERNATE DESIGN
SECTION CC-CC
Ø5.0 HOLE PLUGGED
32.88
SECTION AA-AA
BODY (LOWER)
SCALE 1:1
X.X ±0.1
X.XX ±0.01
X.XXX ±0.001
ANG. ±0.5°
TOLERANCES
ALL DIMS IN MM
2 X #9 DRILL 30 DEEP PLUGGED
Ø12.0
SECTION CC-CC
7.5
Ø28.0
Ø33.0
Ø7.515
7.500
0.005
2 HOLES Ø5 THRU FIRST COUNTER Ø6 5.0 DEEP
6.617
30
SECTION AA-AA
Ø23.0
Ø20.0
M14 X 1.25 - 6G
45° X 1.00 CHAM
5.50
3.0
30.0
6.0
19.0
60.0
1 REQ'D
MATERIAL: 303 OR 316L SS

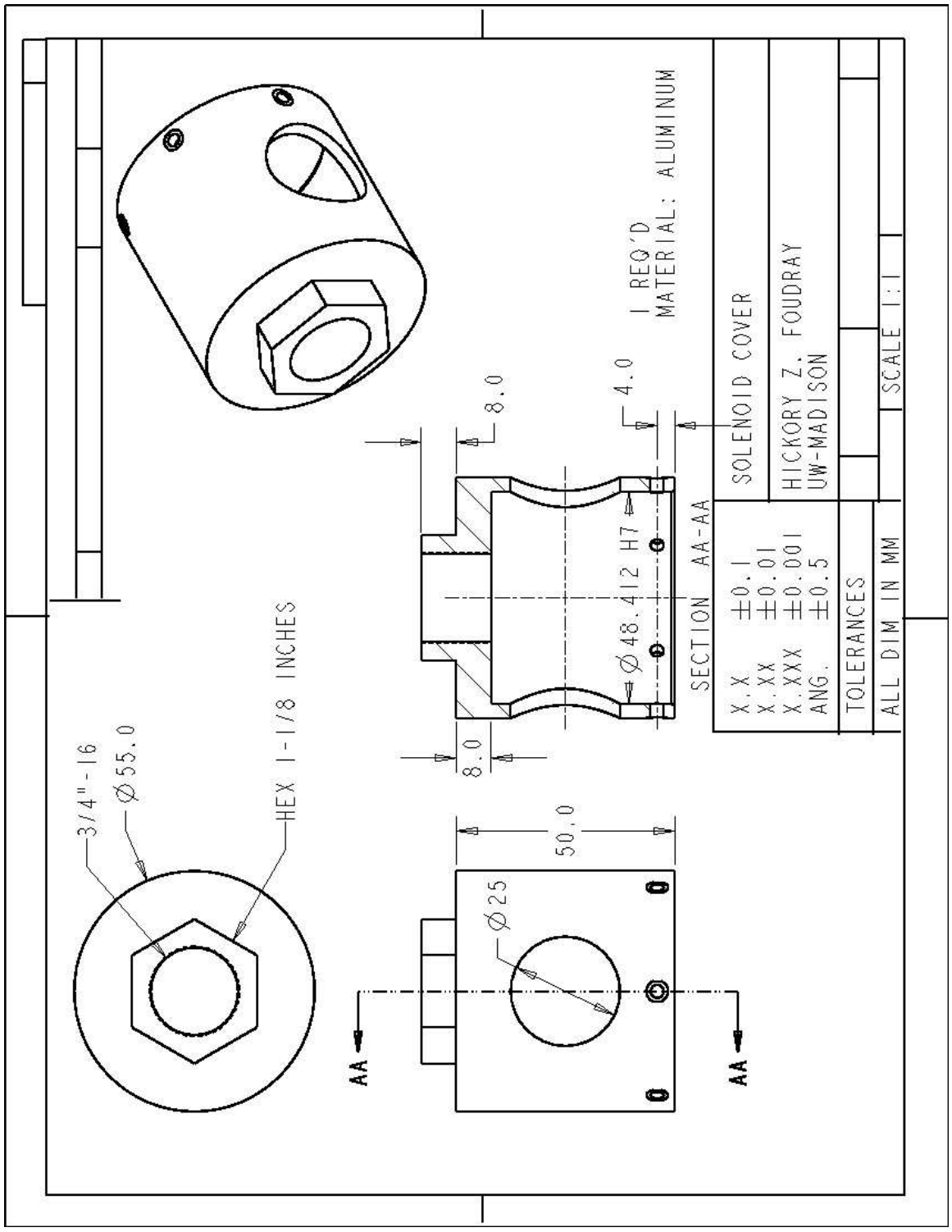
3/4"-16
Ø55.0
HEX 1-1/8 INCHES
AA
Ø25
50.0
8.0
8.0
4.0
Ø48.412 H7
SECTION AA-AA
1 REQ'D
MATERIAL: ALUMINUM
SOLENOID COVER
HICKORY Z. FOUDRAY
UW-MADISON
X.X ±0.1
X.XX ±0.01
X.XXX ±0.001
ANG. ±0.5
TOLERANCES
ALL DIM IN MM
SCALE 1:1

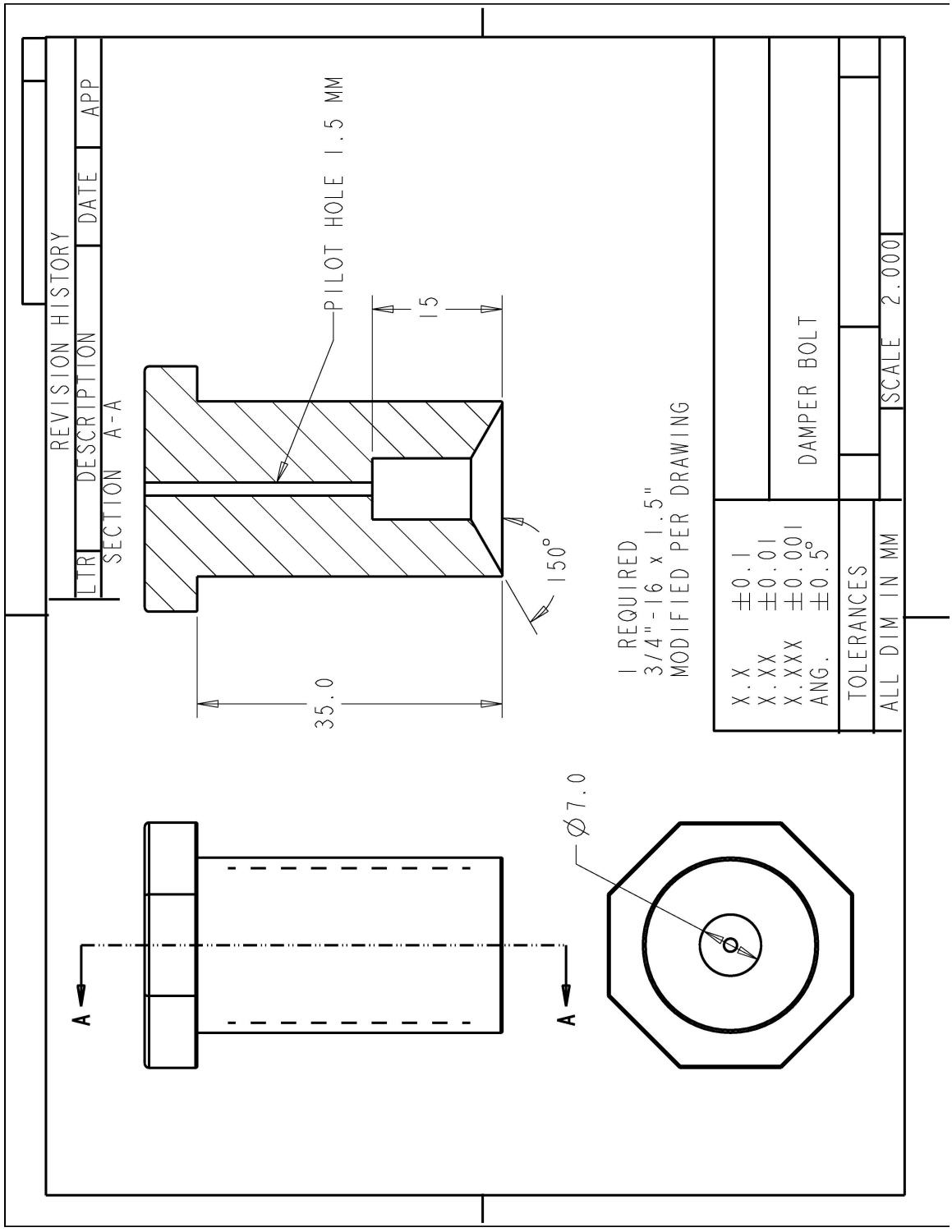
REVISION HISTORY
LTR
DESCRIPTION
DATE
APP
SECTION A-A
PILOT HOLE 1.5 MM
15
150°
35.0
1 REQUIRED
3/4"-16 x 1.5"
MODIFIED PER DRAWING
DAMPER BOLT
SCALE 2.000
X.X ±0.1
X.XX ±0.01
X.XXX ±0.001
ANG. ±0.5°
TOLERANCES
ALL DIM IN MM
Ø7.0
A
A

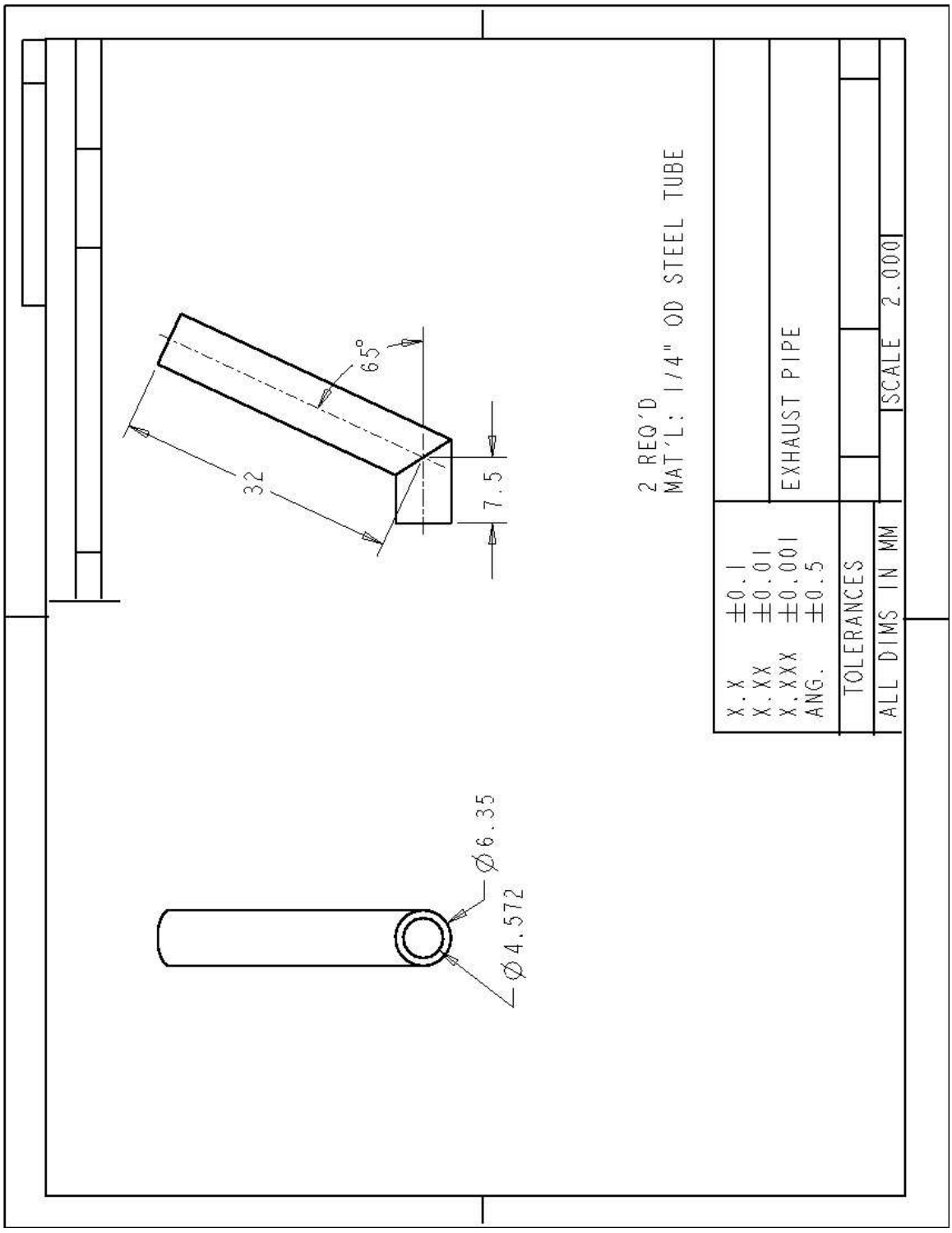
65°
32
7.5
Ø6.35
Ø4.572
2 REQ'D
MAT'L: 1/4" OD STEEL TUBE
EXHAUST PIPE
X.X ±0.1
X.XX ±0.01
X.XXX ±0.001
ANG. ±0.5
TOLERANCES
ALL DIMS IN MM
SCALE 2.000

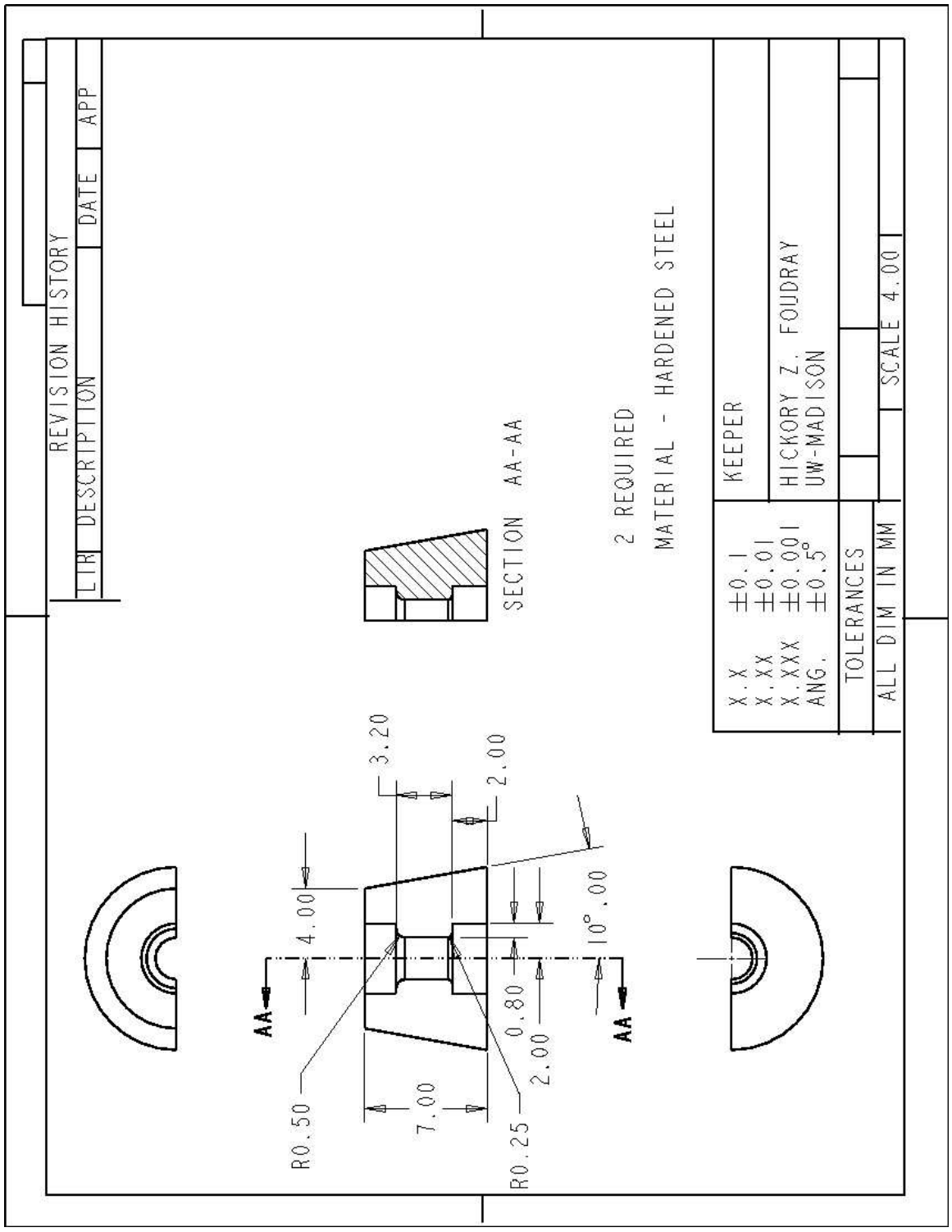
REVISION HISTORY
LTR
DESCRIPTION
DATE
APP
SECTION AA-AA
2 REQUIRED
MATERIAL - HARDENED STEEL
KEEPER
HICKORY Z. FOUDRAY
UW-MADISON
X.X ±0.1
X.XX ±0.01
X.XXX ±0.001
ANG. ±0.5°
TOLERANCES
ALL DIM IN MM
SCALE 4.00
3.20
2.00
4.00
10°.00
0.80
2.00
7.00
R0.50
R0.25
AA
AA

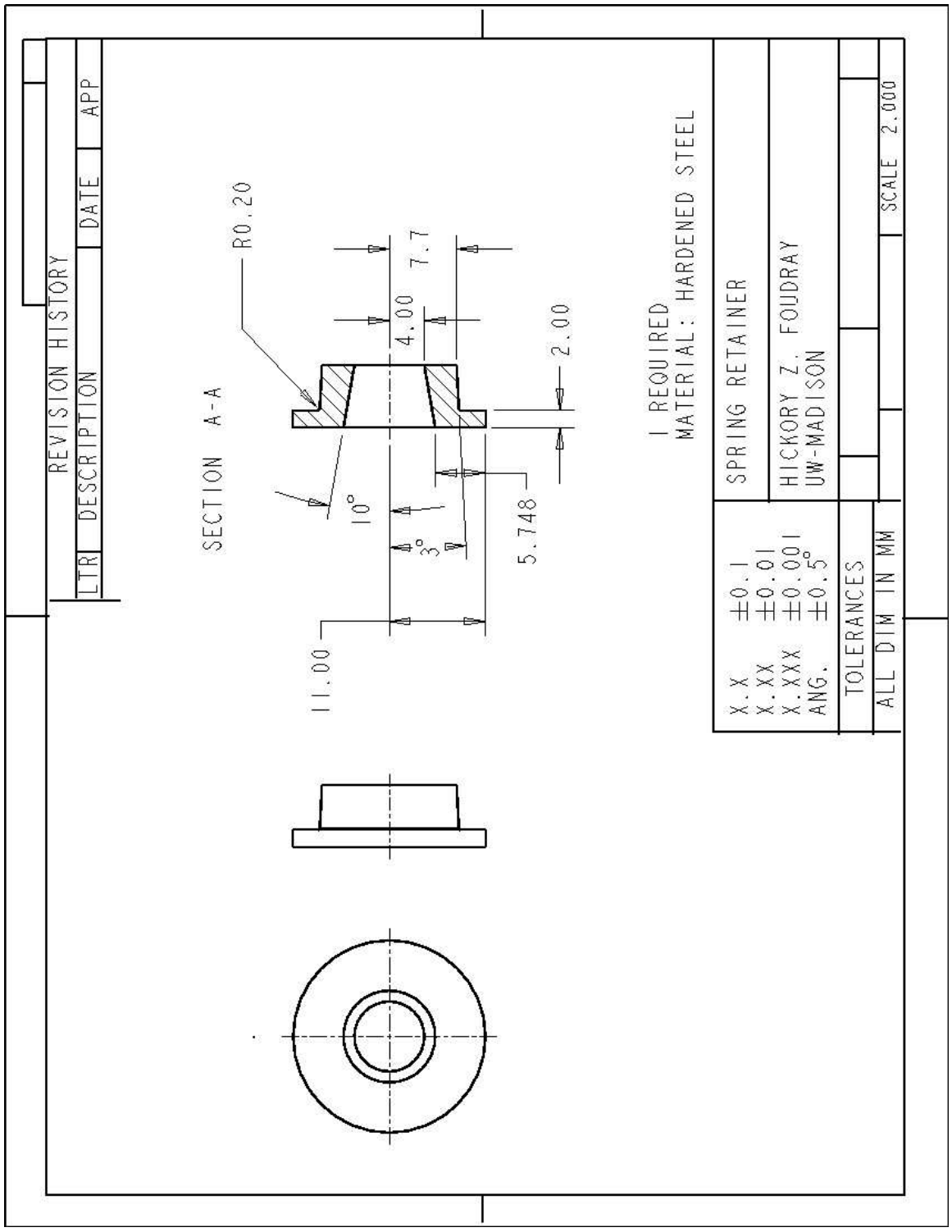
REVISION HISTORY
LTR
DESCRIPTION
DATE
APP
SECTION A-A
R0.20
4.00
7.7
2.00
10°
3°
5.748
11.00
1 REQUIRED
MATERIAL: HARDENED STEEL
SPRING RETAINER
HICKORY Z. FOUDRAY
UW-MADISON
X.X ±0.1
X.XX ±0.01
X.XXX ±0.001
ANG. ±0.5°
TOLERANCES
ALL DIM IN MM
SCALE 2.000

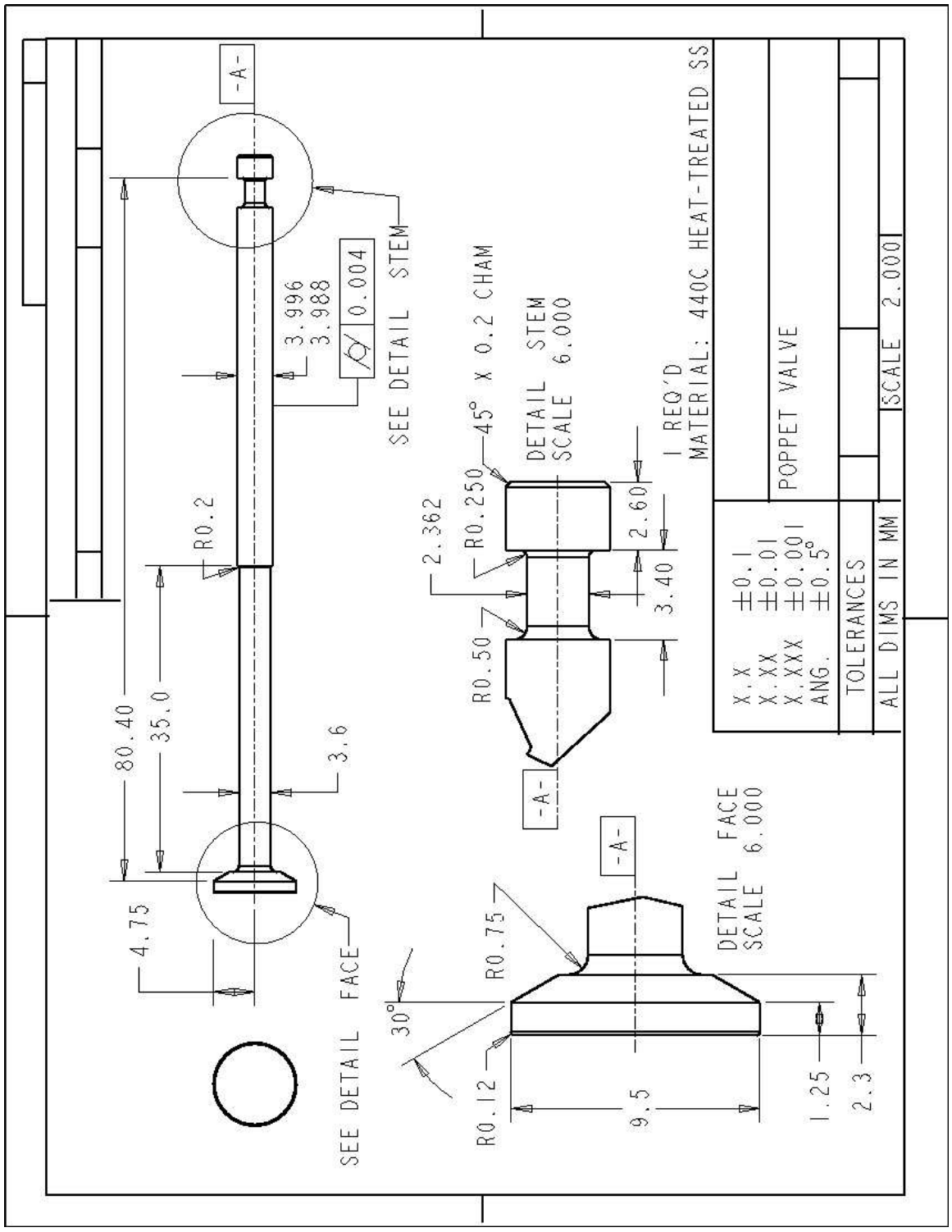
-A-
3.996
3.988
0.004
SEE DETAIL STEM
R0.2
80.40
35.0
3.6
4.75
SEE DETAIL FACE
45° X 0.2 CHAM
DETAIL STEM
SCALE 6.000
2.362
R0.250
2.60
3.40
R0.50
1 REQ'D
MATERIAL: 440C HEAT-TREATED SS
POPPET VALVE
X.X ±0.1
X.XX ±0.01
X.XXX ±0.001
ANG. ±0.5°
TOLERANCES
ALL DIMS IN MM
SCALE 2.000
DETAIL FACE
SCALE 6.000
R0.75
30°
R0.12
9.5
1.25
2.3

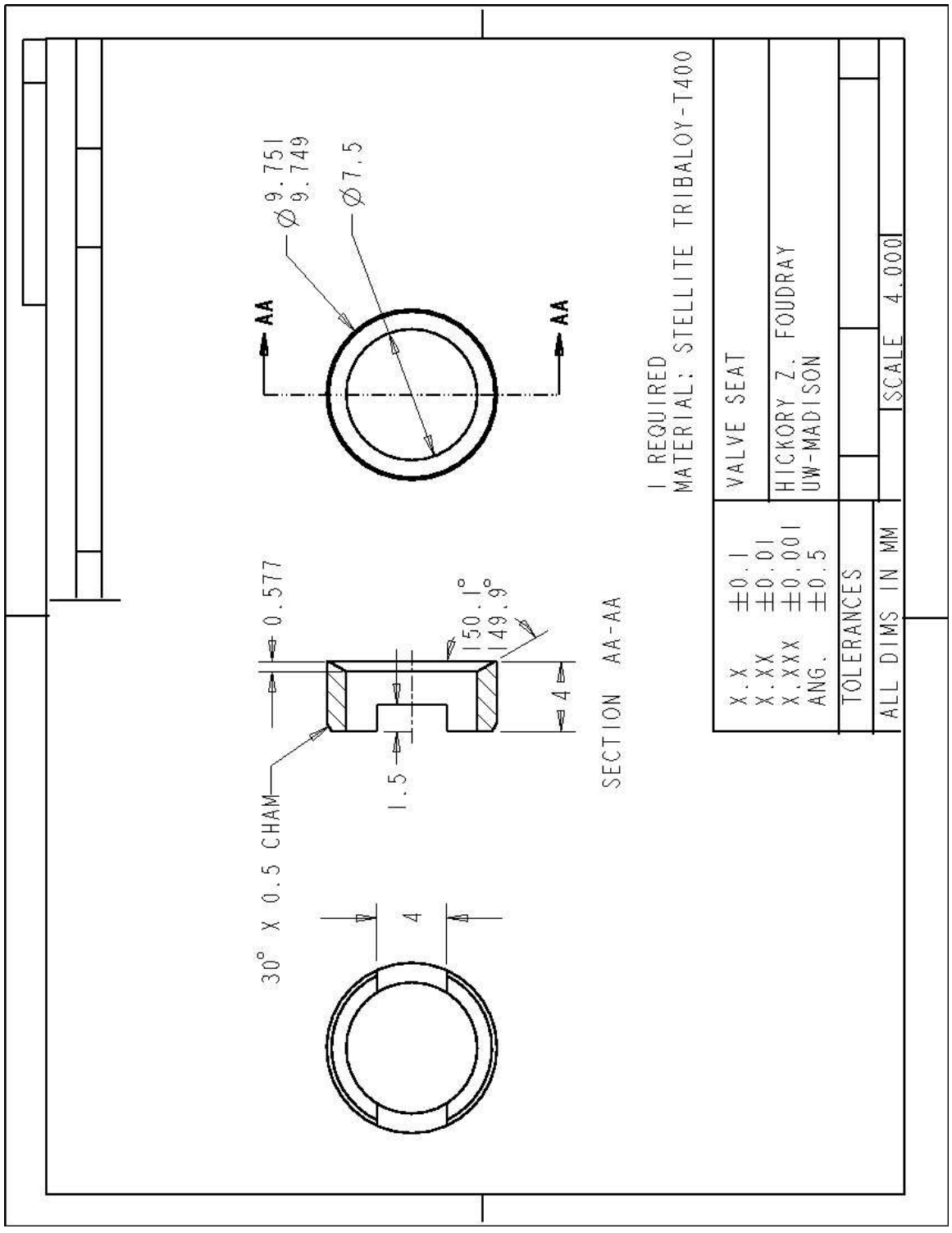
Ø 9.751
9.749
Ø7.5
AA
AA
0.577
150.1°
149.9°
4
1.5
30° X 0.5 CHAM
4
SECTION AA-AA
1 REQUIRED
MATERIAL: STELLITE TRIBALOY-T400
VALVE SEAT
HICKORY Z. FOUDRAY
UW-MADISON
X.X ±0.1
X.XX ±0.01
X.XXX ±0.001
ANG. ±0.5
TOLERANCES
ALL DIMS IN MM
SCALE 4.000

Appendix D

EES Program

```
MW_CHn=12+n;  MW_air=28.97;    MW_O2=32    "Molecular weights"
n=1.86;          M=MW_air/MW_CHn  "n=hydrogen/carbon ratio of fuel"
V_epc=2.73e-4 "[m3]"    "Volume at exhaust port closing"

DR_ref=Lookup('DR_sweep_27.5AF',run,'Delivery Ratio')     "Delivery ratio, standard definition"
P_atm = 101.5 "[kPa]"
Cp_air = SPECHEAT(AirH2O,T=T_air,P=P_atm,R=.01*lookup('DR_sweep_27.5AF',run,'Humidity'))
Cp_res = X_CO2_p*SPECHEAT(CO2,T=T_res)+X_O2_p*SPECHEAT(O2,T=T_res)+X_H2O_p*SPECHEAT(H2O,T=T_res) + (1-X_CO2_p - X_O2_p
                - X_H2O_p)*SPECHEAT(N2,T=T_res) "calculate the specific heat of the residual gas"
Cp_avg = (Cp_air+Cp_res)/2
X_H2O_p/X_CO2_p=n/2

" all data from test#1 DR_Sweep_constant_MAP_4-03-02"
x_CO2_u=Lookup('DR_sweep_27.5AF',run,'X_CO2_u')*.01*Ku; "measured unburned CO2"
x_CO2_ex=Lookup('DR_sweep_27.5AF',run,'X_CO2_ex')*.01/K2
x_O2_u=Lookup('DR_sweep_27.5AF',run,'X_O2_u')*.01*Ku;     x_O2_a=0.21;
x_O2_ex=Lookup('DR_sweep_27.5AF',run,'X_O2_ex')*.01/K2
T_ex=converttemp(C,K,lookup('DR_sweep_27.5AF',run,'T_ex')) "[K]"
T_air=converttemp(C,K,lookup('DR_sweep_27.5AF',run,'T_air')) "[K]"
{T_ex=437+273;       T_air=30+273}
T_ex = eta_s*T_res*(Cp_res/Cp_avg)+(1-eta_s)*T_air*(Cp_air/CP_avg)

Ku=1-(1-eta_s)*n*x_CO2_p/2;       K2=1.05;
m_f=Lookup('DR_sweep_27.5AF',run,'m_f')/1000000 "mass of fuel injected per cycle in kg"
m_air=Lookup('DR_sweep_27.5AF',run,'m_air')/(60*Lookup('DR_sweep_27.5AF',run,'RPM')) "[kg]" "mass of air delivered in kg"
phi_del=m_f/m_air;    AFdel=1/phi_del

rho_res=density(air,T=T_res,P=P_atm)
rho_del=density(air,T=T_air,P=P_atm)

{ // USING CO2 BALANCE//}
x_CO2_p=x_CO2_u/(1-eta_s) "Eq. 5"
x_CO2_u + M/m_tr\m_f = x_CO2_p*(1+1/m_tr\m_f) "Eq.3"

{ // TRAPPED MASS ESTIMATION //}
m_tr\m_f=(rho_res*V_epc/(1-eta_s*(1-rho_res/rho_del))) / m_f

{ // USING O2 BALANCE//}
x_o2_u-(1+n/4)*M/m_tr\m_fO2=x_o2_p*(1+1/m_tr\m_fO2)
x_o2_u=eta_sO2*x_O2_a+(1-eta_sO2)*x_O2_p
m_tr\m_fO2=rho_res*V_epc/(1-eta_sO2*(1-rho_res/rho_del)) / m_f
eta_trO2=m_tr\m_fO2*m_f*eta_sO2/m_air

{// FINAL CONDITIONS //}

TrappedMass=m_f*m_tr\m_f
eta_tr=m_tr\m_f*m_f*eta_s/m_air  "Definition of trapping efficiency"
TrappedAir=eta_s*TrappedMass
TrappedO2_air=TrappedAir*(x_O2_a*(MW_O2/MW_air))
TrappedO2_res=(1-eta_s)*TrappedMass*(x_O2_p*(MW_O2/MW_air))
TrappedO2=x_O2_u*(MW_O2/MW_air)*TrappedMass
TrappedAF_O2=(TrappedO2/m_f)/(x_O2_a*(MW_O2/MW_air))
```

```
TrappedAF_air=TrappedAir/m_f

{// CHECKS //}
{mole fraction of O2 in products}
x_o2_u-(1+n/4)*M/m_tr\m_f=x_o2_ps*(1+1/m_tr\m_f) "calculated based on stoichiometry"
x_o2_u=eta_s*x_O2_a+(1-eta_s)*x_O2_pd1 "calculated based on dilution method 1"
x_O2_ex=(eta_tr+phi_del)*x_O2_pd2/(1+phi_del)+(1-eta_tr)*x_O2_a/(1+phi_del)"calculated based on dilution method 2"
{mole fraction of CO2 in exhaust}
x_co2_exd1=(eta_tr+phi_del)*x_CO2_p/(1+phi_del) "calculated based on dilution method 2"
x_O2_exd2=(eta_tr+phi_del)*x_O2_p/(1+phi_del)+(1-eta_tr)*x_O2_a/(1+phi_del) "calculated based on dilution method 2"

P_sea=101.5 "[kPa]"
T_cyl = converttemp(K,C,P_sea*convert(kPa,Pa)*V_epc*MW_air/(R#*(rho_res*convert(kg/m3,g/m3)*V_epc/(1-eta_s*(1-rho_res/rho_del))))) "[C]"

lambda=m_air/(rho_del*V_epc);rho_tilde=rho_res/rho_del "Delivery Ratio"
eta_PD=1/(1+rho_tilde*(1/lambda-1)) "perfect displacement model of eta_s"
eta_PM=(1-exp(-lambda))/(1-(1-rho_tilde)*exp(-lambda)) "perfect mixing model of eta_s"

eta_t_PD=1/lambda "perfect displacement model of eta_t"
eta_t_PM=(eta_PM*rho_tilde)/(lambda*(1-eta_PM*(1-rho_tilde))) "perfect mixing model of eta_s"
O2\f = TrappedO2/m_f "ratio of trapped oxygen to fuel"
```